Energy & Environmental Science

REVIEW

View Article Online
View Journal | View Issue

Cite this: *Energy Environ. Sci.*, 2014, **7**, 2831

Photocatalytic organic pollutants degradation in metal–organic frameworks

Chong-Chen Wang,[ab] Jian-Rong Li,*[b] Xiu-Liang Lv,[b] Yan-Qiu Zhang[c] and Guangsheng Guo*[b]

Received 26th April 2014
Accepted 6th June 2014

DOI: 10.1039/c4ee01299b

www.rsc.org/ees

Efficient removal of organic pollutants from wastewater has become a hot research topic due to its ecological and environmental importance. Traditional water treatment methods such as adsorption, coagulation, and membrane separation suffer from high operating costs, and even generate secondary pollutants. Photocatalysis on semiconductor catalysts (TiO_2, ZnO, Fe_2O_3, CdS, GaP, and ZnS) has demonstrated efficiency in degrading a wide range of organic pollutants into biodegradable or less toxic organic compounds, as well as inorganic CO_2, H_2O, NO_3^-, PO_4^{3-}, and halide ions. However, the difficult post-separation, easy agglomeration, and low solar energy conversion efficiency of these inorganic catalysts limit their large scale applications. Exploitation of new catalysts has been attracting great attention in the related research communities. In the past two decades, a class of newly-developed inorganic–organic hybrid porous materials, namely metal–organic frameworks (MOFs) has generated rapid development due to their versatile applications such as in catalysis and separation. Recent research has showed that these materials, acting as catalysts, are quite effective in the photocatalytic degradation of organic pollutants. This review highlights research progress in the application of MOFs in this area. The reported examples are collected and analyzed; and the reaction mechanism, the influence of various factors on the catalytic performance, the involved challenges, and the prospect are discussed and estimated. It is clear that MOFs have a bright future in photocatalysis for pollutant degradation.

Broader context

On account of its ecological and environmental importance, removing organic pollutants with high toxicity and hard degradation properties from wastewater has been attracting a great deal of attention and becoming a hot research topic. Traditional methods such as adsorption and coagulation usually suffer from high operating costs and, worse still, generate other secondary pollutants in the process. Alternately, photocatalytic degradation has demonstrated green implementation and high efficiency, in which photocatalysis plays a crucial role. Metal–organic frameworks (MOFs), a class of newly-developed functional materials, have given rise to rapid development in the field of catalysis. A number of studies have shown that they are suitable materials for being the photocatalysts that function in the catalytic degradation of organic pollutants. In this review, we summarize research advances with regard to this topic, emphasizing the related catalytic reaction mechanisms, factors that affect the catalytic performances, and challenges involved in these studies. It is clear that MOFs have a promising future in this regard, and might become one of the most powerful photocatalysts that could help generate a green environment, thereby having a significant impact on environmental science.

1. Introduction

Industrial plants generate increasing amounts of wastewater, which often causes severe environmental problems. Wastewater produced in many industrial processes often contains organic compounds that are toxic and not amenable to direct biological treatment.[1–4] There are a huge number of different types of organic pollutants, including organic dyes, phenols, biphenyls, pesticides, fertilizers, hydrocarbons, plasticizers, detergents, oils, greases, pharmaceuticals, proteins, carbohydrates, and so on.[5] Each type of pollutant has a lot of varieties. Take organic dyes for example, there are more than 100 000 commercially available dyes, with over 7×10^5 t produced annually. These organic dyes are chemically stable and not very biodegradable in water, which makes them potentially harmful to the eco-environment.[6,7] One of the greatest environmental concerns with organic dyes is their absorption and reflection of sunlight entering the water, which further interferes with the growth of bacteria to a level sufficient to biologically degrade impurities in the water.[8] Organic pollutants in wastewater, being highly toxic

[a]*Key Laboratory of Urban Stormwater System and Water Environment (Ministry of Education), Beijing University of Civil Engineering and Architecture, Beijing, 100044, China*

[b]*Department of Chemistry and Chemical Engineering, College of Environmental and Energy Engineering, Beijing University of Technology, Beijing 100022, China. E-mail: jrli@bjut.edu.cn*

[c]*Beijing Climate Change Response Research and Education Center, Beijing University of Civil Engineering and Architecture, Beijing, 100044, China*

and difficult to degrade, have become one of the most serious global environmental issues today. Organic pollutants once released into the aquatic ecosystem can cause various environmental problems, such as clogging sewage treatment plants, adversely affecting aquatic biota, and increasing biochemical oxygen.[9,10] Therefore, an effective and economical technique needs to be developed to reduce the concentration of organic pollutants before releasing the wastewater into the aquatic environment. Currently, industrially available wastewater treatment technologies such as adsorption and coagulation merely concentrate or separate these pollutants from water, but does not completely "eliminate" or "destroy" them into biodegradable or less toxic organic compounds, as well as inorganic CO_2, H_2O, NO_3^-, PO_4^{3-} and halide ions.[11] Other water treatment methods, such as chemical and membrane technologies, usually involve high operating costs, and sometimes generate other toxic secondary pollutants.[12] For example, chlorination has been widely used in disinfection process, where the generated by-products are mutagenic and carcinogenic to human health.[13–16]

Guangsheng Guo obtained his Ph.D. degree from Beijing University of Chemical Technology. From 1986 to 2009, he was an assistant professor, associate professor, and professor at the same university. In 1995, he was also a visiting scholar at the Chinese University of Hong Kong, where he conducted profound research in the field of Higher Education. From 2010, he has been a full professor at Beijing University of Technology. His research interests focus on the preparation and application of nano-functional materials and applied laser-chemistry, as well as higher education management.

Chong-Chen Wang obtained his Ph.D. degree from Beijing University of Chemical Engineering. Since 2004, he has been an assistant professor, associate professor, and professor at Beijing University of Civil Engineering and Architecture. In 2014, he is also a visitor professor at Beijing University of Technology. His research interests focus on environmental remediation using new materials (such as MOFs) and new technologies.

Among various physical, chemical, and biological technologies used in pollution control, the advanced oxidation processes (AOPs), including the Fenton reaction, photocatalysis, sonolysis, ozonation, and combinations of these, are increasingly adopted in the destruction of organic contaminants, due to their high efficiency, simplicity, good reproducibility, and easy handling.[13,17] In general, the AOP involves *in situ* generation of highly reactive and nonselective chemical oxidants (*i.e.* H_2O_2, $^{\bullet}OH$, $^{\bullet}O_2^-$, O_3) to degrade persistent and nonbiodegradable organic substances.[13] The advantage of AOPs is to convert toxic organic compounds into less toxic ones. Under suitable conditions, it is possible to oxidize completely organic molecules to form CO_2 and H_2O. In AOPs, the heterogeneous photocatalysis by using semiconductor catalysts such as TiO_2, ZnO, Fe_2O_3, CdS, GaP, and ZnS has been demonstrated to be highly efficient in degrading a wide range of organic pollutants into easily biodegradable compounds or less toxic molecules, even eventually mineralizing them into innocuous CO_2 and H_2O.[13,18–27] Heterogeneous photocatalysis possesses some advantages, which has feasible applications in wastewater treatment, including (i) ambient operating temperature and pressure, (ii) complete mineralization of parents and their intermediate compounds without leaving secondary pollution, and (iii) low operating costs.[13] One typical drawback of photocatalysis is that the semiconductor photocatalysts that are normally used are not very photo-stable under the operating conditions. Usually, the illumination of these catalysts in aqueous media leads to their corrosion, which leads to the migration of metal ions into water, and finally the complete dissolution of the solid catalysts. For example, transition metal sulfides are highly unstable narrow band-gap semiconductors, and irradiation under light often leads to their dissolution. Other metal oxides, such as iron oxides with various stoichiometries, silver oxide, and copper oxides are also susceptible to photo corrosion. Among the explored semiconductor photocatalysts, TiO_2 is the most popular, due to its durability, low cost, low toxicity, superhydrophilicity, and remarkable chemical and photochemical

Jian-Rong "Jeff" Li obtained his Ph.D. degree in 2005 from Nankai University. Until 2007, he was an assistant professor at the same University. In 2004, he was also a research assistant at Hong Kong University of Science & Technology. From 2008 to 2009, he was a postdoctoral research associate, first at Miami University and later at Texas A&M University; from 2010 he was an assistant research scientist at the same university. Since 2011, he has been a full professor at Beijing University of Technology. His research interests focus on new porous materials for chemical engineering, energy and environmental science.

stability.[28–32] However, the application of a TiO_2 catalyst for wastewater treatment is also facing a series of technical challenges. Firstly, post-separation of the TiO_2 catalyst is difficult after water treatment, which obstructs practicality in industrial processes. Secondly, the fine particle size of the TiO_2, together with its large surface area-to-volume ratio and high surface energy leads to a strong tendency for catalyst agglomeration. Finally, the catalyst itself also shows some disadvantageous issues, like low photocurrent quantum yield due to electron–hole recombination and low solar energy utilization efficiency resulting from the narrow band gap ($E_g = 3.2$ eV). Consequently, it is of urgency to look for new photocatalysts with improved performances.[13]

Metal–organic frameworks (MOFs), a class of newly-developed inorganic–organic hybrid porous materials, have generated a rapid development due to their diverse and easily tailored structures,[33–38] as well as various potential applications, such as in catalysis,[39–42] separation,[43–48] gas storage,[41,49–52] carbon dioxide capture,[53–56] and so on.[33–38,43–46,57–60] MOFs are composed of metal-containing nodes connected by organic linkers through strong chemical bonds. Some MOFs behave as semiconductors when exposed to the light, implying that they are potentially useful as photocatalysts.[61] Recent research indeed not only demonstrated porous MOF materials to be a new class of photocatalyst, usable in catalytic degradation of organic pollutants under UV/visible/UV-visible irradiation, but also triggered an intense interest in exploring the application of MOFs as photocatalysts in other aspects.[62–72] Based on the richness of metal-containing nodes and organic bridging linkers, as well as the controllability of the synthesis, it is easy to construct MOFs with tailorable capacity to absorb light, thereby initiating desirable photocatalytic properties for specific applications in the degradation of organic pollutants. The study of the application of MOFs in this topic thus has a bright future, even though it has not been so widely explored to date, in contrast to the conventional photocatalysts of metal oxides and sulfides. Herein, we highlight the research progress of the application of MOFs in the photocatalytic degradation of organic pollutants. The reported examples are collected and analyzed, the reaction mechanism and the influence of various factors on the catalytic performances are discussed, and the challenges involved and future prospects are addressed.

2. Organic pollutant degradation in d-block metal based MOFs

Recently, much effort has been devoted to develop new photocatalytic materials based on MOFs, motivated largely by a demand to solve pollution problems, in view of their potential applications in the green degradation of organic pollutants.[74–78] It is clear that MOFs provide a unique opportunity for exploring new catalysts to achieve good performance towards organic pollutant degradation. Some organic pollutants treated in this review are listed in Table 1.

In the past decade, d-block transition metal MOFs have attracted intense interest, not only due to their significant contribution in numerous areas including magnetism,[78,79] catalysis,[80,81] gas separation,[47] drug delivery[82,83] and the embedding of nanoparticles,[41,84] but also due to their structural diversity and intriguing topologies.[85–87] Some MOFs constructed by transition metals, like Zn(II),[62,63,88,89] Cu(I)/Cu(II),[89,90] Cd(II),[89,90] Co(II)/Co(III),[63,89–94] and Fe(II)/Fe(III)[27,88,89] were examined as photocatalysts to degrade organic pollutants under UV, visible or UV-vis light. Table 2 lists some of these MOFs, which showed good photocatalytic performances for the degradation of organic pollutants.

MOF-5 (ref. 141) was first proposed to behave as a photocatalyst.[68] This MOF is composed of Zn_4O clusters located at the corners of the cubic framework structure, connected orthogonally by 1,4-bdc ligands. It was found that this MOF has a broad absorption band located in the range 500–840 nm, which can be assigned to delocalized electrons living on the microsecond time scale, and most probably occupying conduction bands (CB). The actual conduction band energy value was estimated to be 0.2 V *versus* NHE, with a band gap of 3.4 eV, as illustrated in Fig. 1a. It exhibited comparable activity in the degradation of phenol in aqueous solutions to that of the commercial TiO_2 (Degussa P-25) (Fig. 1b). The charge-separation state, with electrons in the conduction band and holes in the valence band (VB), made MOF-5 behave as an efficient photocatalyst. The possible mechanistic proposal, as illustrated in Fig. 1c, suggested that, just as in the case of TiO_2, the photodegradation of phenol might occur through a network of reactions, including initial formation of a radical cation by electron transfer from phenol to MOF-5 hole or the generation of oxygen active species by the reaction of the photoejected electrons with oxygen. The more efficient photocatalytic activity of MOF-5 with respect to the other photocatalysts would probably perform, depending on the light source. In particular, visible irradiation using filtered light (cut-off filter $\lambda > 380$ nm) would disfavor the activity of TiO_2 and ZnO due to their lack of absorption at wavelengths >350 nm, but the absorption spectrum of MOF-5 extends to 400 nm, which means MOF-5 could achieve better photocatalysis efficiency.

Furthermore, MOF-5 displayed reverse shape-selectivity towards different organic compounds, in which large phenolic molecules that cannot diffuse freely into the microspores of MOF-5 degraded significantly faster than the small ones that can access the interior of MOF-5, as found by Garcia and coworkers.[62,68] They studied the competitive photodegradation of 2,6-di-*tert*-butylphenol (DTBP) and phenol (P), in which DTBP was considerably bigger than the P molecule. When both compounds were independently irradiated under UV light in the presence of MOF-5, DTBP degraded at an initial rate comparable to that of P. The initial rate constants for the two systems (calculated as the slope of the time conversion plots at short irradiation times) gave a $k(\mathrm{DTBP})_{\mathrm{pure}}/k(\mathrm{P})_{\mathrm{pure}}$ ratio of 1.1. But, when a mixed solution containing both P and DTBP was irradiated in the presence of MOF-5, DTBP degraded with a rate constant ratio (*i.e.* $k(\mathrm{DTBP})_{\mathrm{mix}}/k(\mathrm{P})_{\mathrm{mix}}$ value) 4.42 fold higher with respect to P, implying a selective photodegradation of about 82% toward bigger DTBP with respect to P. Furthermore, about 50% phenol and 100% DTBP decomposed after 180 min

Table 1 The structure and nature of some organic pollutants

Dye name	Chemical structures	Ionicity	Size (nm^3)	Absorption λ_{max} (nm)
Orange G (OG)	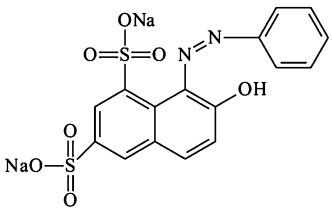	Anionic	1.62 × 0.94 × 0.29	484
Methyl Orange (MO)	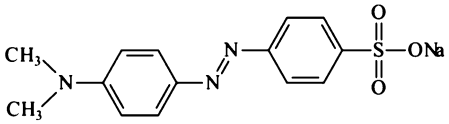	Anionic	1.54 × 0.48 × 0.28	467
Alizarin Red S (ARS)	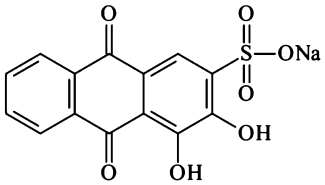	Anionic	1.17 × 0.57 × 0.23	428
Congo Red (CR)	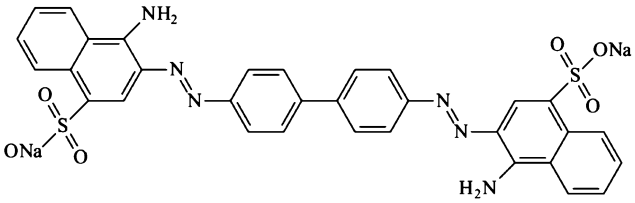	Anionic	2.61 × 0.86 × 0.39	493
Cresol Red (CRR)	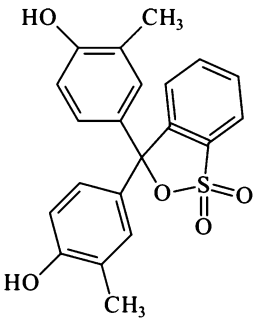	Anionic	1.01 × 1.13 × 0.31	435
Cotton Blue (CB)	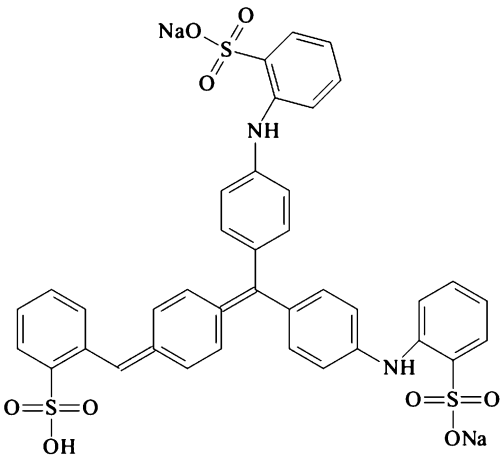	Anionic	1.98 × 1.17 × 0.34	595

Table 1 (*Contd.*)

Dye name	Chemical structures	Ionicity	Size (nm^3)	Absorption λ_{max} (nm)
Coomassie brilliant blue R-250 (CBB)	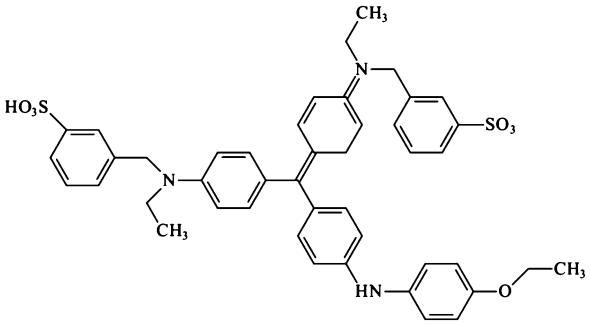	Anionic	2.23 × 1.21 × 0.41	555
Methylene Blue (MB)	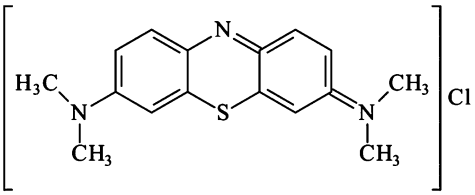	Cationic	1.38 × 0.64 × 0.21	672
Rhodamine Blue L (RBL)	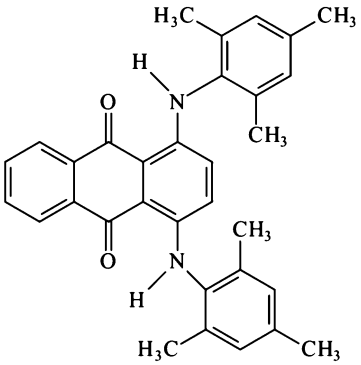	Cationic	1.78 × 1.12 × 0.43	610
Methyl Violet (MV)	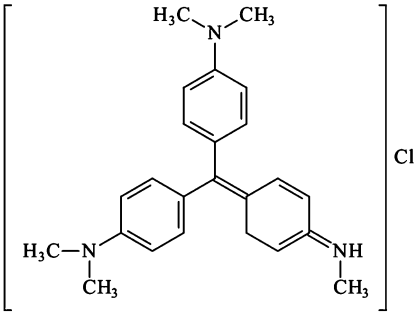	Cationic	1.42 × 1.01 × 0.22	585
Methyl Red (MR)	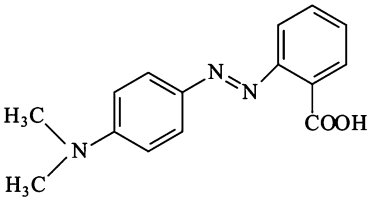	Cationic	1.50 × 0.41 × 0.23	436

Table 1 (*Contd.*)

Dye name	Chemical structures	Ionicity	Size (nm^3)	Absorption λ_{max} (nm)
Bismarck Brown R (BBR)	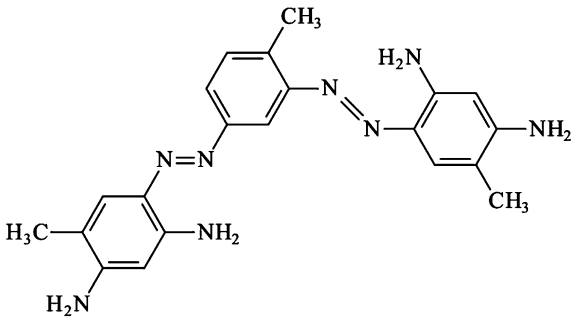	Cationic	2.21 × 0.39 × 0.20	520
Acid mordant navy blue RRN (RRN)	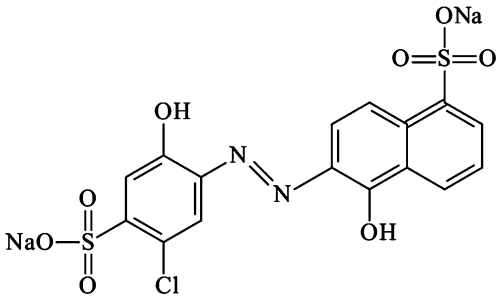	Anionic	2.35 × 0.87 × 5.58	597
Rhodamine B (RhB)	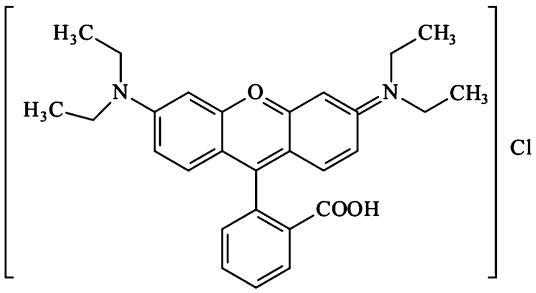	Cationic	1.56 × 1.35 × 0.42	552
Remazol Brilliant Blue R (RBBR)	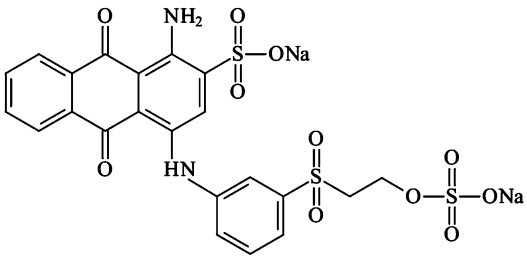	Anionic	1.57 × 1.16 × 0.53	591
Reactive Red X3B (X3B)	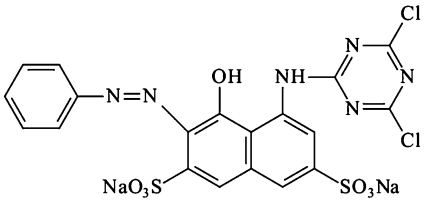	Anionic	1.53 × 1.32 × 0.45	511
Metanil Yellow (MY)	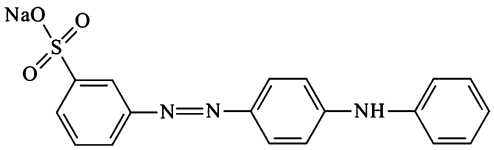	Anionic	1.62 × 0.78 × 0.30	414

Table 1 (*Contd.*)

Dye name	Chemical structures	Ionicity	Size (nm^3)	Absorption λ_{max} (nm)
2,6-Di-*tert*-butylphenol (DTBP)	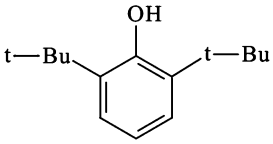	—	1.04 × 0.81 × 0.54	—
Phenol	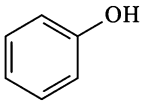	—	0.65 × 0.58 × 0.28	270
Thiophene		—	0.74 × 0.68 × 0.28	—

irradiation in the presence of MOF-5, as illustrated in Fig. 2. Clearly, MOF-5 displayed a reverse size-selective photocatalysis. These findings could be explained as follows: the smaller molecule P was able to diffuse freely into the interior of MOF-5, resulting in a lower degradation rate, while the large molecule DTBP remained on the external surface of the MOF-5, leading to a higher degradation rate. A similar situation could be found in the previous literatures on the titanosilicate ETS-10.[142,143]

Motivated by the discovery of MOF-5 as an efficient photocatalyst to degrade organic pollutants, Chen and co-workers explored a doubly interpenetrated porous MOF $[Zn_4O(2,6\text{-ndc})_3(DMF)_{1.5}(H_2O)_{0.5}]\cdot 4DMF\cdot 7.5H_2O$ (UTSA-38), with a band gap of 2.85 eV, which exhibited photocatalytic activity for the degradation of methyl orange (MO) in aqueous solution.[93] It was found that under the irradiation of visible light, the concentration of MO in water gradually decreased as a function of increasing time, suggesting detectable degradation of MO in the presence of the MOF catalyst. When UV light was utilized to initiate such a photocatalytic reaction, the decomposition of MO was significantly faster. MO could be completely decomposed into colorless small molecules in 120 min, indicating clearly that UV light was more efficient for this photocatalytic reaction than visible light, as illustrated in Fig. 3b. Furthermore, the UTSA-38 catalyst could be readily recovered from the reaction mixtures *via* simple filtration, and showed no obvious decay of catalytic efficiency even after recycling 7 times. The main pathways proposed for MO photodegradation by UTSA-38 under UV or visible light irradiation are shown in Fig. 3a. It was considered that the initial process of photocatalysis was the generation of electron–hole pairs in the UTSA-38. After absorption of energy equal to or greater than the band gap of the UTSA-38 ($h\nu \geq 2.85$ eV), the electrons (e^-) were excited from the valence band (VB) and entered into the conduction band (CB), leaving the holes (h^+) in the VB. The electrons and holes migrated to the surface of the UTSA-38, then the photoinduced energy transferred to the adsorbed species: electrons reduced the oxygen (O_2) to oxygen radicals ($^{\bullet}O_2^-$), and finally they transformed into hydroxyl radicals ($^{\bullet}OH$); in turn, holes oxidized the hydroxyl (H_2O) to hydroxyl radicals ($^{\bullet}OH$). Hydroxyl radicals ($^{\bullet}OH$) were capable of decomposing MO effectively.[144,145]

In order to clarify the relationship between degradation efficiency of different organic dyes and band gap values, Natarajan and co-workers used a series of MOFs, $[Co_2(4,4'\text{-bpy})](4,4'\text{-obb})_2$, $[Ni_2(4,4'\text{-bpy})_2](4,4'\text{-obb})_2\cdot H_2O$, and $[Zn_2(4,4'\text{-bpy})](4,4'\text{-obb})_2$ with band gap values of 3.11, 3.89 and 4.02 eV, respectively, to degrade different organic dyes, like orange G (OG), rhodamine B (RhB), remazol brilliant blue R (RBBR), and methylene blue (MB).[63] The Langmuir–Hinshelwood (L–H) kinetic has been successfully used for heterogeneous photocatalytic degradation to determine the relationship between the initial degradation rate and the initial concentration of the organic substrate,[146–148] which could be written as $r_0 = k_0C_0/(1 + K_0C_0)$, where r_0 was the initial rate, C_0 was the initial concentration of the dyes, k_0 was the kinetic rate constant, and parameter K_0 represented the equivalent adsorption coefficient. The values of k_0 and K_0 for the photocatalytic degradation of the four dyes in $[Co_2(4,4'\text{-bpy})](4,4'\text{-obb})_2$, $[Ni_2(4,4'\text{-bpy})_2](4,4'\text{-obb})_2\cdot H_2O$, and $[Zn_2(4,4'\text{-bpy})](4,4'\text{-obb})_2$ are listed in Table 3. It was found that all these reactions gave very small K_0 values. As the parameter K_0 represents the adsorption equilibrium coefficient, the low value of K_0 can be attributed to low adsorption. The photocatalytic performances of $[Co_2(4,4'\text{-bpy})](4,4'\text{-obb})_2$, $[Ni_2(4,4'\text{-bpy})_2](4,4'\text{-obb})_2\cdot H_2O$, and $[Zn_2(4,4'\text{-bpy})](4,4'\text{-obb})_2$ were also confirmed to be better than commercial TiO_2 (Degussa P-25) under the same conditions. The band gap values of these MOFs followed a sequence of $[Co_2(4,4'\text{-bpy})](4,4'\text{-obb})_2 < [Ni_2(4,4'\text{-bpy})_2](4,4'\text{-obb})_2\cdot H_2O < [Zn_2(4,4'\text{-bpy})](4,4'\text{-obb})_2$, but the kinetic rates and degradation efficiencies of these three MOF catalysts followed a reverse order with respect to their band gap values.

In order to further understand the photocatalytic degradation of the organic dyes in $[Co_2(4,4'\text{-bpy})](4,4'\text{-obb})_2$, $[Ni_2(4,4'\text{-bpy})_2](4,4'\text{-obb})_2\cdot H_2O$, and $[Zn_2(4,4'\text{-bpy})](4,4'\text{-obb})_2$,[63] a simple

Table 2 Performances of some MOFs constructed with d-block metals as photocatalysts for the degradation of organic pollutants in aqueous media

MOF[a]	E_g (eV)	Irrigation	Organic pollutants	Initial concentration (mg L^{-1})	Time (min)	Degradation efficiency (%)	Ref.
MOF-5	3.40	UV	Phenol	40.0	180	50	68
MOF-5	3.40	UV	DTBP	40.0	180	100	62
$(emim)_2[InK(btec)_{1.5}(H_2O)_2]$	3.15	UV	MB	5	180	90	96
$(emim)[In_3(\mu_3\text{-}OH)_2(btec)_2]\cdot 2H_2O$	3.8	UV	MB	5	840	100	97
$Zn_3(btc)_2$ (thin film)	—	UV-vis	$MB(H_2O_2)$	10	60	99	98
MIL-88A	2.05	Vis	$MB(H_2O_2)$	32	20	100[c]	99
$[Zn_4(O)(tdc)_3(4,4'\text{-bimb})_4]\cdot 5.25H_2O\cdot CH_3OH$	—	Vis	X3B	3.69	540	100[c]	100
NTU-9	1.74	Vis	$RhB(H_2O_2)$	47.9	80	100	101
NTU-9	1.74	Vis	$MB(H_2O_2)$	31.9	20	100	101
$[Cu^{II}(salimcy)](Cu^{I}I)_2\cdot DMF$	—	Vis	$MB(H_2O_2)$	12	22	96	102
$[Cu^{II}(salimcy)](Cu^{I}I)_2\cdot DMF$	—	Vis	$RhB(H_2O_2)$	12	50	95	102
$[Cu^{II}(salimcy)](Cu^{I}I)_2\cdot DMF$	—	Vis	$MO(H_2O_2)$	12	55	100	102
$Cu(Br\text{-}ip)(bitmb)(H_2O)$	—	Vis	$MY(H_2O_2)$	3.75	180	89	103
$(tpp)_2[Cd_3(4,4'\text{-obb})_4]$	—	Vis	MB	3	360	98.5	104
$Cu(hfipbb)(2,2'\text{-bpy})(H_2O)_2$	—	Vis	RhB	9.58	360	95	105
$Cu_2(hfipbb)_2(4,4'\text{-bpy})(H_2O)$	—	Vis	RhB	9.58	360	70	105
$(Me_4N)_6[Cu_{12}(OMe)_6(pz)_6(btc)_6]\cdot 18H_2O$	—	UV	RhB	9.58	320	61	106
$(Me_4N)_6[Cu_{12}(OH)_6(pz)_6(btc)_6]\cdot 21H_2O$	—	UV	RhB	9.58	320	51	106
$[Cd(4,4'\text{-bpy})(H_2O)_2(S_2O_3)]\cdot 2H_2O$	2.91	UV	MB	25	60	86[c]	107
$Cd_2(4,4'\text{-bpy})_3(S_2O_3)_2$	2.75	UV	MB	25	60	84[c]	107
$Cd_2(4,4'\text{-bpy})_{2.5}(S_2O_3)_2$	2.75	UV	MB	25	60	76[c]	107
$[Cd(4,4'\text{-bpy})(H_2O)_2(S_2O_3)]\cdot 2H_2O$	2.91	UV	RBL	100	90	90[c]	107
$Cd_2(4,4'\text{-bpy})_3(S_2O_3)_2$	2.75	UV	RBL	100	90	85[c]	107
$Cd_2(4,4'\text{-bpy})_{2.5}(S_2O_3)_2$	2.75	UV	RBL	100	90	85[c]	107
$[Cd(4,4'\text{-bpy})(H_2O)_2(S_2O_3)]\cdot 2H_2O$	2.91	UV	MV	100	90	99[c]	107
$Cd_2(4,4'\text{-bpy})_3(S_2O_3)_2$	2.75	UV	MV	100	90	99[c]	107
$Cd_2(4,4'\text{-bpy})_{2.5}(S_2O_3)_2$	2.75	UV	MV	100	90	99[c]	107
$[Cd(4,4'\text{-bpy})(H_2O)_2(S_2O_3)]\cdot 2H_2O$	2.91	UV	MR	100	90	95[c]	107
$Cd_2(4,4'\text{-bpy})_3(S_2O_3)_2$	2.75	UV	MR	100	90	95[c]	107
$Cd_2(4,4'\text{-bpy})_{2.5}(S_2O_3)_2$	2.75	UV	MR	100	90	95[c]	107
$[Cd(3,3'\text{-bpy})(H_2O)_2(S_2O_3)]\cdot 2H_2O$	2.91	UV	BBR	100	90	95[c]	107
$Cd_2(4,4'\text{-bpy})_3(S_2O_3)_2$	2.75	UV	BBR	100	90	97[c]	107
$Cd_2(4,4'\text{-bpy})_{2.5}(S_2O_3)_2$	2.75	UV	BBR	100	90	97[c]	107
$[Cd(4,4'\text{-bpy})(H_2O)_2(S_2O_3)]\cdot 2H_2O$	2.91	Sunlight	MB	25	90	70[c]	107
$Cd_2(4,4'\text{-bpy})_3(S_2O_3)_2$	2.75	Sunlight	MB	25	90	68[c]	107
$Cd_2(4,4'\text{-bpy})_{2.5}(S_2O_3)_2$	2.75	Sunlight	MB	25	90	60[c]	107
$[Cd(4,4'\text{-bpy})(H_2O)_2(S_2O_3)]\cdot 2H_2O$	2.91	Sunlight	RBL	100	90	95[c]	107
$Cd_2(4,4'\text{-bpy})_3(S_2O_3)_2$	2.75	Sunlight	RBL	100	90	78[c]	107
$Cd_2(4,4'\text{-bpy})_{2.5}(S_2O_3)_2$	2.75	Sunlight	RBL	100	90	75[c]	107
$[Cd(4,4'\text{-bpy})(H_2O)_2(S_2O_3)]\cdot 2H_2O$	2.91	Sunlight	MV	100	90	70[c]	107
$Cd_2(4,4'\text{-bpy})_3(S_2O_3)_2$	2.75	Sunlight	MV	100	90	65[c]	107
$Cd_2(4,4'\text{-bpy})_{2.5}(S_2O_3)_2$	2.75	Sunlight	MV	100	90	63[c]	107
$[Cd(4,4'\text{-bpy})(H_2O)_2(S_2O_3)]\cdot 2H_2O$	2.91	Sunlight	MR	100	90	75[c]	107
$Cd_2(4,4'\text{-bpy})_3(S_2O_3)_2$	2.75	Sunlight	MR	100	90	68[c]	107
$Cd_2(4,4'\text{-bpy})_{2.5}(S_2O_3)_2$	2.75	Sunlight	MR	100	90	66[c]	107
$[Cd(4,4'\text{-bpy})(H_2O)_2(S_2O_3)]\cdot 2H_2O$	2.91	Sunlight	BBR	100	90	90[c]	107
$Cd_2(4,4'\text{-bpy})_3(S_2O_3)_2$	2.75	Sunlight	BBR	100	90	85[c]	107
$Cd_2(4,4'\text{-bpy})_{2.5}(S_2O_3)_2$	2.75	Sunlight	BBR	100	90	84[c]	107
$Co_2(tkcomm)(llpd)_2$	1.98	UV	MB	16	90	81	108
$Mn_2(tkcomm)(llpd)_2$	3.09	UV	MB	16	90	88	108
$Zn_2(tkcomm)(llpd)_2$	3.26	UV	MB	16	90	78	108
$Cd_2(tkcomm)(llpd)_2$	3.31	UV	MB	16	90	87	108
$Zn(1,4\text{-bdc})(dpbpdca)\cdot$solvents	—	UV	RhB	5.0	810	85[c]	109
$Cu_4(dcpcpb)_2(\mu_3\text{-}OH)_2(CH_3OH)_2(H_2O)$	3.49	UV	MB	16	90	64	110
$Co_2(dcpcpb)(\mu_3\text{-}OH)(H_2O)_2$	2.96	UV	MB	16	90	73	110
$Cu_4(dcpcpb)_2(\mu_3\text{-}OH)_2(CH_3OH)_2(H_2O)$	3.49	UV	RhB	4.79	90	19	110
$Co_2(dcpcpb)(\mu_3\text{-}OH)(H_2O)_2$	2.96	UV	RhB	4.79	90	79	110
$Mn_2(ptp)_{4/3}(pbcpp)_2$	—	UV	MO	5.6	90	40	111
$[Cu_5(H_2tmbtmp)_2(btb)_2(OH)_2]\cdot 3H_2O$	—	UV	MB	10	120	59	112
$Cd(tdc)(bix)(H_2O)$	3.31	UV	MO	20	150	90	113
$Gd(H_2O)_3Co(2,3\text{-pdc})$	—	UV	RBBR	100	90	88[c]	114

Table 2 (*Contd.*)

MOF[a]	E_g (eV)	Irrigation	Organic pollutants	Initial concentration (mg L^{-1})	Time (min)	Degradation efficiency (%)	Ref.
$Pb_2(ttt)(ox)_{1/2}(H_2O)$	3.33	UV	MO	6.6	150	13	115
$Pb_3(ttt)_2(H_2O)_2$	3.32	UV	MO	6.6	150	13.7	115
$Cd(npdyda)(H_2O)_2$	4.4	UV	MO	4.9	60	60[c]	116
Pb(npdyda)(DMF)	4.3	UV	MO	4.9	60	60[c]	116
Cd(npdyda)(phen)	3.8	UV	MO	4.9	60	80[c]	116
$Cd_5(npdyda)_5(2,2'\text{-bpy})_2$	5.0	UV	MO	4.9	60	42[c]	116
$Zn(NH_2bdc)(bix)\cdot(DMF)_2$	—	Visible	X3B	3.69	540	98[c]	117
$[Cu_3(4\text{-bpah})_4(1,3,5\text{-btc})_2]\cdot 8H_2O$	—	UV	MB	10	240	50[c]	118
$[Cu_3(4\text{-bpah})_3(1,2\text{-bdc})_3(H_2O)_2]\cdot 4H_2O$	—	UV	MB	10	240	53[c]	118
$Cu(4\text{-bpah})(1,3\text{-bdc})(H_2O)$	—	UV	MB	10	240	54[c]	118
$Co(4\text{-bpah})(1,3\text{-bdc})(H_2O)$	—	UV	MB	10	240	25[c]	118
$Ni(4\text{-bpah})(1,3\text{-bdc})(H_2O)$	—	UV	MB	10	240	55[c]	118
$Zn(4\text{-bpah})(1,3\text{-bdc})(H_2O)$	—	UV	MB	10	240	55[c]	118
Cd(4-bpah)(1,3-bdc)	—	UV	MB	10	240	40[c]	118
$[Cd(3\text{-bpah})(1,3\text{-bdc})]\cdot H_2O$	—	UV	MB	10	240	65[c]	118
$[Cu_2(3\text{-bpah})(1,3\text{-bdc})_2]\cdot H_2O$	—	UV	MB	10	240	68[c]	118
$Ag_7(4,4'\text{-tmbpt})(Hcb\text{-}iso\text{-}p)_2(cb\text{-}iso\text{-}p)(H_2O)$	3.36	UV	MB	17.6	90	73	119
$[NaCd_3(4,4'\text{-tmbpt})(cb\text{-}iso\text{-}p)_2(OH)]\cdot H_2O$	3.44	UV	MB	17.6	90	65	119
$[Cd_3(3,4'\text{-tmbpt})_2(cb\text{-}iso\text{-}p)_2(H_2O)]\cdot 1.5H_2O$	3.50	UV	MB	17.6	90	54	119
$[Zn_4(dpcpbe)_2(\mu_3\text{-}OH)_2(H_2O)_{1.5}]\cdot 2H_2O$	3.49	UV	MB	3.2	90	32	120
$Zn_5Na(dpcpbe)_2(\mu_3\text{-}OH)_4(CH_3CH_2O)(H_2O)_2$	3.53	UV	MB	3.2	90	31	120
$[Cd_4(dpcpbe)_2(bime)_{0.5}(\mu_3\text{-}OH)_2\text{-}(H_2O)_{1.5}]\cdot 2H_2O$	3.52	UV	MB	3.2	90	29	120
$Zn_4(dpcpbe)_2(bet)_{0.5}(\mu_3\text{-}OH)_2(H_2O)$	3.46	UV	MB	3.2	90	32	120
$Cu_6(\mu_3\text{-}O)(\mu_3\text{-}OH)(pz)_6(btc)$	—	UV	RhB	9.58	105	98	121
$Cd_2(bpe)_3(H_2O)_4(S_2O_3)_2$	2.53	UV	MR	100	90	50[c]	122
$Cd_2(bpe)_3(H_2O)_4(S_2O_3)_2$	2.53	UV	RBL	100	90	55[c]	122
$Cd(bpe)S_2O_3$	2.53	UV	MR	100	90	60[c]	122
$Cd(bpe)S_2O_3$	2.53	UV	RBL	100	90	62[c]	122
$[Co_2(tkcomm)(tkiymm)]\cdot 4.25H_2O$	3.78	UV	MB	17.6	75	95	123
$[Co_2(tkcomm)(tkiymm)]\cdot 4.25H_2O$	3.78	Vis	MB	3.51	300	49.6	123
$[Co_2(tkcomm)(tkiymm)]\cdot 4.25H_2O$	3.78	UV	RhB	9.58	600	66	123
$[Co_2(tkcomm)(tkiymm)]\cdot 4.25H_2O$	3.78	UV	X3B	3.69	600	56.7	123
$[Ni(sdb)(bitmb)(H_2O)]\cdot H_2O$	2.12	UV	$MY(H_2O_2)$	3.75	180	43.7	124
$[Cd(sdb)(bitmb)\cdot(H_2O)]\cdot(THF)(H_2O)$	3.89	UV	$MY(H_2O_2)$	3.75	180	24.7	124
$[Zn_2(sdb)_2(bitmb)]\cdot(THF)_2$	4.08	UV	$MY(H_2O_2)$	3.75	180	51.9	124
$Co_2(sdb)_2(bitmb)$	2.11	UV	$MY(H_2O_2)$	3.75	180	82.3	124
$[Cu_3(3\text{-dpsea})(1,3,5\text{-btc})_2(H_2O)_5]\cdot 4H_2O$	—	UV	MB	17.6	120	56	125
$[Cu(3\text{-dpyh})_{0.5}(1,4\text{-ndc})]\cdot H_2O$	—	UV	MB	17.6	120	67	125
Cu(ptz)(I)[b]	1.65	Vis	$MB(H_2O_2)$	18.7	24	98	126
Cu(ptz)(I)[b]	1.65	Vis	$RhB(H_2O_2)$	18.7	35	100	126
Cu(ptz)(I)[b]	1.65	Vis	$MO(H_2O_2)$	18.7	45	95	126
Cu(ptz)(II)[b]	2.24	Vis	$MB(H_2O_2)$	18.7	24	85[c]	126
Cu(ptz)(II)[b]	2.24	Vis	$RhB(H_2O_2)$	18.7	35	70[c]	126
Cu(ptz)(II)[b]	2.24	Vis	$MO(H_2O_2)$	18.7	45	70[c]	126
MIL-53(Fe)	2.72	UV-vis	MB	140	40	11	27
MIL-53(Fe)	2.72	Vis	MB	140	40	30	27
MIL-53(Fe)	2.72	UV-vis	$MB(H_2O_2)$	140	20	99	27
MIL-53(Fe)	2.72	Vis	$MB(H_2O_2)$	140	20	20	27
MIL-53(Al)	3.87	UV-vis	MB	140	60	30	27
MIL-53(Cr)	3.20	UV-vis	MB	140	60	32	27
Cu/ZIF-67	1.95	Vis	MO	16.35	25	100	91
$[Co_2(4,4'\text{-bpy})](4,4'\text{-obb})_2$	3.11	UV	OG	100	100	90[c]	63
$[Co_2(4,4'\text{-bpy})](4,4'\text{-obb})_2$	3.11	UV	RhB	100	100	62[c]	63
$[Co_2(4,4'\text{-bpy})](4,4'\text{-obb})_2$	3.11	UV	RBBR	100	100	100[c]	63
$[Co_2(4,4'\text{-bpy})](4,4'\text{-obb})_2$	3.11	UV	MB	100	100	85[c]	63
$[Ni_2(4,4'\text{-bpy}](4,4'\text{-obb})_2\cdot 2H_2O$	3.89	UV	OG	100	100	85[c]	63
$[Ni_2(4,4'\text{-bpy}](4,4'\text{-obb})_2\cdot 2H_2O$	3.89	UV	RhB	100	100	47[c]	63
$[Ni_2(4,4'\text{-bpy}](4,4'\text{-obb})_2\cdot 2H_2O$	3.89	UV	RBBR	100	100	95[c]	63
$[Ni_2(4,4'\text{-bpy}](4,4'\text{-obb})_2\cdot 2H_2O$	3.89	UV	MB	100	100	80[c]	63
$[Zn_2(4,4'\text{-bpy})](4,4'\text{-obb})_2$	4.02	UV	OG	100	100	70[c]	63
$[Zn_2(4,4'\text{-bpy})](4,4'\text{-obb})_2$	4.02	UV	RhB	100	100	43[c]	63
$[Zn_2(4,4'\text{-bpy})](4,4'\text{-obb})_2$	4.02	UV	RBBR	100	100	80[c]	63

Table 2 (*Contd.*)

MOF[a]	E_g (eV)	Irrigation	Organic pollutants	Initial concentration (mg L^{-1})	Time (min)	Degradation efficiency (%)	Ref.
$[Zn_2(4,4'\text{-bpy})](4,4'\text{-obb})_2$	4.02	UV	MB	100	100	72[c]	63
Cu(dm-bim)	2.49	Vis	MB	18.7	20	96	90
Cu(dm-bim)	2.49	Vis	RhB	18.7	34	100	90
Cu(dm-bim)	2.49	Vis	MO	18.7	45	95	90
$[Zn_4O(2,6\text{-ndc})_3(DMF)_{1.5}(H_2O)_{0.5}]\cdot 4DMF\cdot 7.5H_2O$	2.85	UV-vis	MO	20	120	65[c]	93
$[Zn_4O(2,6\text{-ndc})_3(DMF)_{1.5}(H_2O)_{0.5}]\cdot 4DMF\cdot 7.5H_2O$	2.85	Vis	MO	20	120	45[c]	93
$[Mn_3(btc)_2(4,4'\text{-bimb})_2]\cdot 4H_2O$	4.04	UV	X3B	3.69	600	65[c]	94
$[Mn_3(btc)_2(bimb)_2]\cdot 4H_2O$	4.04	Vis	X3B	3.69	600	15[c]	94
$[Co_3(btc)_2(bimb)_2]\cdot 4H_2O$	3.72	UV	X3B	3.69	600	100	94
$[Co_3(btc)_2(bimb)_2]\cdot 4H_2O$	3.72	Vis	X3B	3.69	600	70[c]	94
$[Zn_4(2\text{-mim})_6WO_4]\cdot 1.5DMF$ (HZIF-1W)	2.2	Vis	$MO(H_2O_2)$	16.35	120	24.5	127
$[Zn_4(2\text{-mim})_6MoO_4]\cdot 2DMF$ (HZIF-1Mo)	1.32	Vis	$MO(H_2O_2)$	16.35	120	81.6	127
Fe_3O_4@MIL-100(Fe)	—	UV-vis	MB	40	100	35	89
Fe_3O_4@MIL-100(Fe)	—	UV-vis	$MB(H_2O_2)$	40	100	99	89
Fe_3O_4@MIL-100(Fe)	—	Vis	MB	40	20	20	89
Fe_3O_4@MIL-100(Fe)	—	Vis	$MB(H_2O_2)$	40	200	99.77	89
MIL-53(Fe)	2.7	Vis	RhB	10	50	62.1	88
MIL-53(Fe)		Vis	$RhB(H_2O_2)$	10	50	100	88
$(Me_3Sn)_4Fe(CN)_6$	—	UV	MB	17.6	30	92	92
$[Co_2(1,4\text{-bdc})(ncp)_2]\cdot 4H_2O$	—	Vis	OG	45.2	300	67.59	128
$[Co_2(1,4\text{-bdc})(ncp)_2]\cdot 4H_2O$	—	Vis	RhB	47.9	300	67.52	128
$[Co_2(1,4\text{-bdc})(ncp)_2]\cdot 4H_2O$	—	Vis	MB	35.1	300	62.75	128
$[Co_2(1,4\text{-bdc})(ncp)_2]\cdot 4H_2O$	—	Vis	MV	40.8	300	33.29	128
$[Ni_2(4,4'\text{-bimb})_3(H_2O)_6]\cdot(aobtc)\cdot(DMF)_2\cdot(H_2O)_2$		Vis	X3B	3.69	540	70[c]	129
$[Cd(3,3',4,4'\text{-bptcH}_2)(H_2O)]\cdot(bimb)$		Vis	X3B	3.69	540	50[c]	129
$[Cu(3\text{-dpye})(3\text{-npa})(H_2O)]\cdot 3H_2O$	—	UV	MB	10	240	70[c]	130
$Cu(3\text{-dpye})_{0.5}(5\text{-aip})(H_2O)$	—	UV	MB	10	240	70[c]	130
$[Cu(3\text{-dpye})(1,3\text{-bdc})]\cdot 3H_2O$	—	UV	MB	10	240	80[c]	130
$Cu_3(3\text{-dpye})(1,2\text{-bdc})_2(\mu_2\text{-OH})_2$	—	UV	MB	10	240	64[c]	130
$Cu_3(3\text{-dpyb})(1,2\text{-bdc})_2(\mu_2\text{-OH})_2$	—	UV	MB	10	240	66[c]	130
$[Cu(3\text{-dpyh})_{0.5}(1,2\text{-bdc})]\cdot H_2O$	—	UV	MB	10	240	83[c]	130
$Cu(3\text{-dpyh})_{0.5}(5\text{-aip})(H_2O)$	—	UV	MB	10	240	66[c]	130
$[Co(3\text{-dpyh})(5\text{-Hip})(H_2O)_3]\cdot H_2O$	—	UV	MB	10	240	52	131
$[Co(3\text{-dpyh})(5\text{-nip})]\cdot H_2O$	—	UV	MB	10	240	39	131
$[Co(3\text{-dpyh})(5\text{-mip})]\cdot H_2O$	—	UV	MB	10	240	34	131
$[Co(3\text{-dpyh})_{0.5}(5\text{-aip})(H_2O)]\cdot 2H_2O$	—	UV	MB	10	240	47	131
$Co(btec)_{0.5}(4,4'\text{-bimb})$	2.68	Vis	X3B	3.69	540	80[c]	95
$Ni(btec)_{0.5}(bimb)$	2.63	Vis	X3B	3.69	540	80[c]	95
$Cd(btec)_{0.5}(bimb)_{0.5}$	2.32	Vis	X3B	3.69	540	90[c]	95
$Cd(3\text{-NO}_2\text{-bdc})(bbi)$	—	Vis	X3B	3.69	540	60	132
$Co(3\text{-NO}_2\text{-bdc})(bbi)$	—	Vis	X3B	3.69	540	80	132
$Cu(3\text{-dpyh})(3\text{-nph})(H_2O)_2$	—	UV	MB	10	120.	73	133
$Ni(3\text{-dpyh})(3\text{-nph})(H_2O)_2$	—	UV	MB	10	120	73	133
$Co(3\text{-dpyh})(3\text{-nph})(H_2O)_2$	—	UV	MB	10	120	85	133
$[Cu_9(OH)_6(bte)_2(sip)_4(H_2O)_3]\cdot 6H_2O$	—	UV	$MO(H_2O_2)$	10	280	76.1	134
$Cd(nddda)(H_2O)_2$	4.4	UV	MO	2.15	60	60[c]	116
Pb(nddda)(DMF)	4.3	UV	MO	2.15	60	62[c]	116
Cd(nddda)(phen)	3.8	UV	MO	2.15	60	81[c]	116
$Cd_5(nddda)_5(2,2'\text{-bpy})_2$	5.0	UV	MO	2.15	60	45[c]	116
$Cu_2(btec)(btx)_{1.5}$		Vis	$MO(H_2O_2)$	10	95	96.1	135
$Co_2(bip)_2(H_2O)$	—	UV	MB	10	180	79	136
$[Co(bip)(phen)(H_2O)]\cdot H_2O$	—	UV	MB	10	180	42	136
$[Co_2(1,4\text{-biyb})_2(2\text{-cmsn})_2(H_2O)]\cdot H_2O$	—	UV	MB	10	180	64	137
$Cd(1,4\text{-biyb})(2\text{-cmsn})(H_2O)$	—	UV	MB	10	180	37	137
$[Zn(1,4\text{-biyb})(2\text{-cmsn})]\cdot 2H_2O$	—	UV	MB	10	180	54	137
$Cd(1,4\text{-biyb})(adtz)(H_2O)$	—	UV	MB	10	180	72	137
$[Zn(1,4\text{-biyb})(adtz)]\cdot H_2O$	—	UV	MB	10	180	62	137
$[Ag_2(pdbmb)_2(CF_3SO_3)_2]\cdot H_2O$	3.03	UV-vis	MB	1000	540	90	138
$Fe_2(bhbdh)$	—	Vis	$RhB(H_2O_2)$	0.2	15	90	139
$Fe_2(bhbdh)$	—	Vis	$MB(H_2O_2)$	0.13	15	90	139

Table 2 (*Contd.*)

MOF[a]	E_g (eV)	Irrigation	Organic pollutants	Initial concentration (mg L^{-1})	Time (min)	Degradation efficiency (%)	Ref.
$[Ag_4(4,4'\text{-bpy})_4(ap)_2]\cdot 11H_2O$	3.2	UV	MB	5	180	98.2	140
$[Ag_2(4,4'\text{-bpy})_2](npdc)]\cdot 2H_2O$	3.2	UV	MB	5	180	99.8	140
$[Ag_2(dpe)_{1.5}(sbdc)_{0.5}(sbdc)_{0.5}]\cdot 7H_2O$	3.3	UV	MB	5	180	99.9	140

[a] MOF-5 = $[Zn_4O(1,4\text{-bdc})_3]\cdot(DMF)_8(C_6H_5Cl)$, (1,4-bdc = 1,4-benzenedicarboxylate; DMF = dimethylformamide; C_6H_5Cl = chlorobenzene); emim = 1-ethyl-3-methylimidazolium bromide; btec = 1,2,4,5-benzenetetracarboxylate; btc = 1,3,5-benzenetricarboxylate; tdc = 2,5-thiophenedicarboxylate; 4,4′-bibm = 4,4′-bis(1-imidazolyl)biphenyl; NTU-9 = $Ti_2(dobdc)_3$ (H_4dobdc = 2,5-dihydroxyterephthalic acid); salimcy = *N*,*N*′-bis-[(imidazol-4-yl)methylene]cyclohexane-1,2-diamine; Br-ip = 5-bromoisophthalate; bitmb = 1,3-bis(imidazol-1-ylmethyl)-2,4,6-trimethylbenzene; H_2hfipbb = 4,4′-(hexafluoroisopropylidene)bis(benzoic acid); tpp = etraphenylphosphonium; 4,4′-obb = 4,4′-oxybis(benzoate); 2,2′-bpy = 2,2′-bipyridine; 4,4′-bpy = 4,4′-bipyridine; pz = pyrazolate; 3,3′-bpy = 2,2′-bipyridine; H_4tkcomm = tetrakis[4-(carboxyphenyl)-oxamethyl]methane acid; llpd = 4-tolyl-2,2′:6′,2″-terpyridine; dpbpdca = N^4,$N^{4'}$-di(pyridin-4-yl)biphenyl-4,4′-dicarboxamide; H_3dcpcpb = (3,5-dicarboxyl-phenyl)-(4-(2′-carboxyl-phenyl)-benzyl); ptp = 4′-(4-pyridyl)-4,2′:6′,4″-terpyridine; pbcpp = (4-phenyl)-2,6-bis(4-carboxyphenyl)pyridine; H_2tmbtmp = 2,4,6-trimethylbenzene-1,3,5-tris(methylenephosphonic acid); btb = 1,4-bis(1,2,4-triazol-1-yl)butane; bix = 1,4-bis(imidazol-1-ylmethyl)benzene; 2,3-pdc = pyridine-2,3-dicarboxylate; H_3ttt = 1,3,5-triazine-2,4,6-triyltrithio-triacetic acid; H_2ox = oxalic acid; H_2npdyda = naphthalene-1,5-diyldioxy-di-acetic acid; phen = phenanthroline; NH_2bdcH_2 = 2-amino-1,4-benzene dicarboxylic acid; 4-bpah = *N*,*N*′-bis(4-pyridinecarboxamide)-1,2-cyclohexane; 1,3,5-btc = 1,3,5-benzenetricarboxylate; 1,2-bdc = 1,2-benzenedicarboxylate; 1,3-bdc = 1,3-benzenedicarboxylate; 3-bpah = *N*,*N*′-bis(3-pyridinecarboxamide)-1,2-cyclohexane; 4,4′-tmbpt = 1-((1*H*-1,2,4-triazol-1-yl)methyl)-3,5-bis(4-pyridyl)-1,2,4-triazole; cb-iso-p = 5-(4-carboxybenzyloxy)isophthalate; 3,4′-tmbpt = 1-((1*H*-1,2,4-triazol-1-yl)methyl)-3-(4-pyridyl)-5-(3-pyridyl)-1,2,4-triazolet; H_3dpcpbe = (3,5-dicarboxyl-phenyl)-(4-(2′-carboxyl-phenyl)-benzyl)ether; bime = 1,2-bis(imidazol-1-yl)ethane; bet = 1,1′-(2′-oxybis(ethane-2,1-diyl))bis(1,2,4-triazol-1-yl); bpe = 1,2-di(4-pryridyl)ethylene; tkiymm = tetrakis(imidazol-1-ylmethyl)methane); sdb = 4,4′-sulfonyldibenzoate); 3-dpsea = *N*,*N*′-di(3-pyridyl)sebacicdiamide; 3-dpyh = *N*,*N*′-di(3-pyridinecarboxamide)-1,6-hexane; 1,4-ndc = 1,4-naphthalenedicarboxylate; ptz = 5-(3-pyridyl)tetrazole; Cu/ZIF-67 = copper doped Co-2-methylimidazole framework; dm-bim = 5,6-dimethylbenzimidazolate; 2,6-ndc = 2,6-naphthalenedicarboxylate; 4,4′-bimb = 4,4′-bis(1-imidazolyl)biphenyl; 2-mim = 2-imidazolate; Hncp = 2-(4-carboxyphenyl)imidazo(4,5-*f*)(1,10)-phenanthroline; H_4aobtc = azoxybenzene-3,3′,5,5′-tetracarboxylic acid; 3,3′,4,4′-bptcH_4 = 3,3′,4,4′-biphenyltetracarboxylate acid; 3-dpye = *N*,*N*′-bis(3-pyridinecarboxamide)-1,2-ethane; 3-dpyb = *N*,*N*′-bis(3-pyridinecarboxamide)-1,4-butane; 3-dpyh = *N*,*N*′-bis(3-pyridinecarboxamide)-1,6-hexane; 3-H_2npa = 3-nitrophthalic acid; 3-NO_2-bdcH_2 = 3-nitro-1,2-benzenedicarboxylic acid; bbi = 1,1′-(1,4-butanediyl)bis(imidazole); 5-H_2aip = 5-aminoisophthalic acid; 5-H_2nip = 5-nitroisophthalic acid, 5-H_2mip = 5-methylisophthalic acid; 5-H_2AIP = 5-aminoisophthalic acid); bte = 1,2-bis(1,2,4-triazol-1-yl)ethane; sip = 5-sulfoisophthalate; btx = 1,4-bis(1,2,4-triazol-1-ylmethyl)benzene; bip = 5-(benzyloxy)isophthalate; 3-dpyh = *N*,*N*′-bis (3-pyridinecarboxamide)-1, 6-hexane; 3-nph = 3-nitrophthalate; 1,4-biyb = 1,4-bis(imidazol-1-ylmethyl)benzene; 2-cmsnH_2 = 2-carboxymethylsulfanyl nicotinic acid; H_2adtz = 2,5-(*s*-acetic acid) dimercapto-1,3,4-thiadiazole; pdbmb = 6′,6″-(2-phenylpyrimidine-4,6-diyl)-bis(6-methyl-2,2′-bipyridine); bhbdh = bis[2-hydroxybenzaldehyde]hydrazone; dpe = 1,2-di(4-pyridyl)ethylene; H_2ap = 5-aminophthalic acid; H_2npdc = 2,6-naphthalenedicarboxylic acid; H_2sbdc = 4,4′-stilbenedicarboxylic acid. [b] Cu(ptz)(I) and Cu(ptz)(II) are isomers. [c] Values estimated from original figures of the references.

mechanism based upon highest occupied molecular orbital (HOMO) and lowest unoccupied molecular orbital (LUMO) was proposed. The HOMO and LUMO of the charge transfer state, in the absence of UV light, have two electrons in the HOMO, and no electrons in the LUMO. Once in the presence of UV light, one electron transfers from the HOMO to the LUMO.[149] Generally,

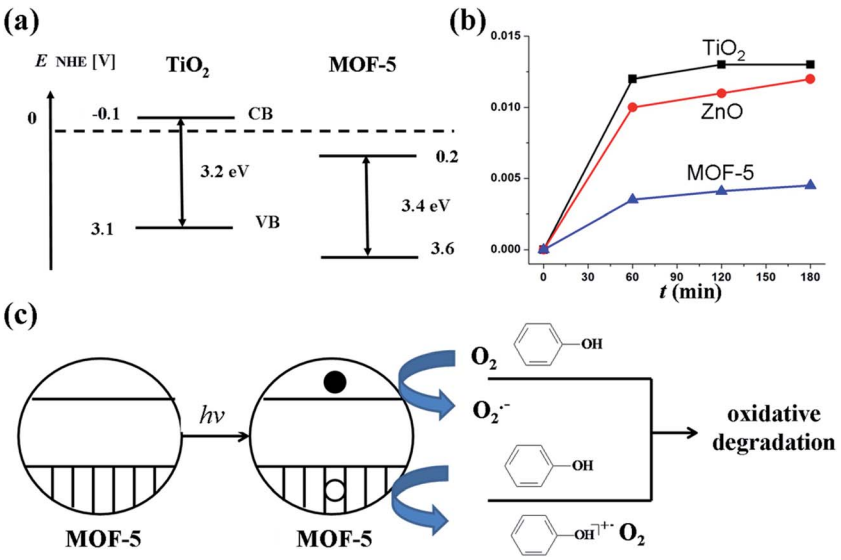

Fig. 1 (a) Calculated values of the band gap and position of the conduction and valence bands for MOF-5 in comparison with those of TiO_2. (b) Time conversion plots of phenol disappearance (the *y* axis represents "mol of phenol degraded per g per mol"). (c) A mechanistic proposal for the photodegradation of phenol using MOF-5 as the photocatalyst. Reprinted (adapted) with permission from ref. 68. Copyright (2007) Wiley-VCH.

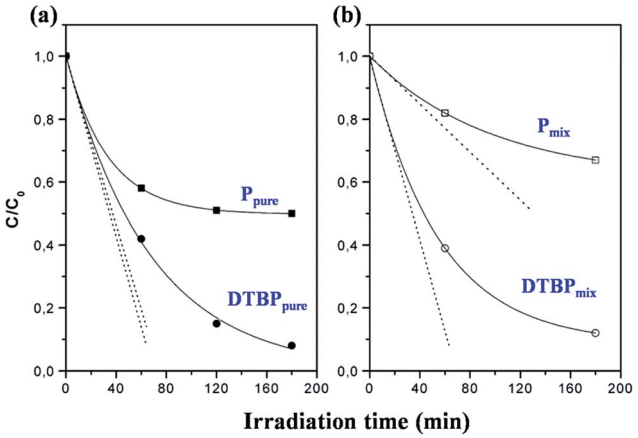

Fig. 2 Photodegradation curves of phenol (P) and 2,6-di-*tert*-butylphenol (DTBP), obtained using MOF-5 as a photocatalyst. (a) Curves correspond to photodegradation of 40 mg L^{-1} of the pure species; (b) curves correspond to competitive photodegradation (irradiation of a mixture of 20 mg L^{-1} of both molecules). Solid lines are the best fit to the experimental data obtained with a first-order exponential decay. Dotted straight lines show the initial degradation rates. Reprinted (adapted) with permission from ref. 62. Copyright (2007) American Chemical Society.

Table 3 Kinetic parameters for the degradation of different dyes using $[Co_2(4,4'\text{-bpy})](4,4'\text{-obb})_2$, $[Ni_2(4,4'\text{-bpy})_2](4,4'\text{-obb})_2\cdot H_2O$, and $[Zn_2(4,4'\text{-bpy})](4,4'\text{-obb})_2$ (ref. 63)

MOFs	Dyes	k_0 (min^{-1})	K_0 (mg L^{-1})
$[Co_2(4,4'\text{-bpy})](4,4'\text{-obb})_2$	OG	0.031	0.0022
$[Co_2(4,4'\text{-bpy})](4,4'\text{-obb})_2$	RHB	0.013	0.0035
$[Co_2(4,4'\text{-bpy})](4,4'\text{-obb})_2$	RBBR	0.033	0.0007
$[Co_2(4,4'\text{-bpy})](4,4'\text{-obb})_2$	MB	0.032	0.0064
$[Ni_2(4,4'\text{-bpy})_2](4,4'\text{-obb})_2\cdot H_2O$	OG	0.029	0.0049
$[Ni_2(4,4'\text{-bpy})_2](4,4'\text{-obb})_2\cdot H_2O$	RhB	0.008	0.0023
$[Ni_2(4,4'\text{-bpy})_2](4,4'\text{-obb})_2\cdot H_2O$	RBBR	0.029	0.0015
$[Ni_2(4,4'\text{-bpy})_2](4,4'\text{-obb})_2\cdot H_2O$	MB	0.027	0.0027
$[Zn_2(4,4'\text{-bpy})](4,4'\text{-obb})_2$	OG	0.020	0.0029
$[Zn_2(4,4'\text{-bpy})](4,4'\text{-obb})_2$	RhB	0.007	0.0020
$[Zn_2(4,4'\text{-bpy})](4,4'\text{-obb})_2$	RBBR	0.028	0.0069
$[Zn_2(4,4'\text{-bpy})](4,4'\text{-obb})_2$	MB	0.023	0.0029

the electron of the excited state in the LUMO can easily be lost, while the HOMO strongly demands one electron to return to its stable state. Generally, the excited M^{2+} center decays to its ground state quickly. However, if some molecules are located within a reasonable range and have an appropriate orientation, transitional active complexes could be formed. For example, for RhB in this case one α-hydrogen atom of the methylene group bonded to the electron-withdrawing nitrogen atom in RhB would give its electron to the metal species (MOFs herein), and simultaneously form H^+. This finally results in the cleavage of the C–N bond and stepwise *N*-deethylation of the RhB. Since the HOMO is then reoccupied, the excited electron must remain in the LUMO until it is captured by electronegative substances

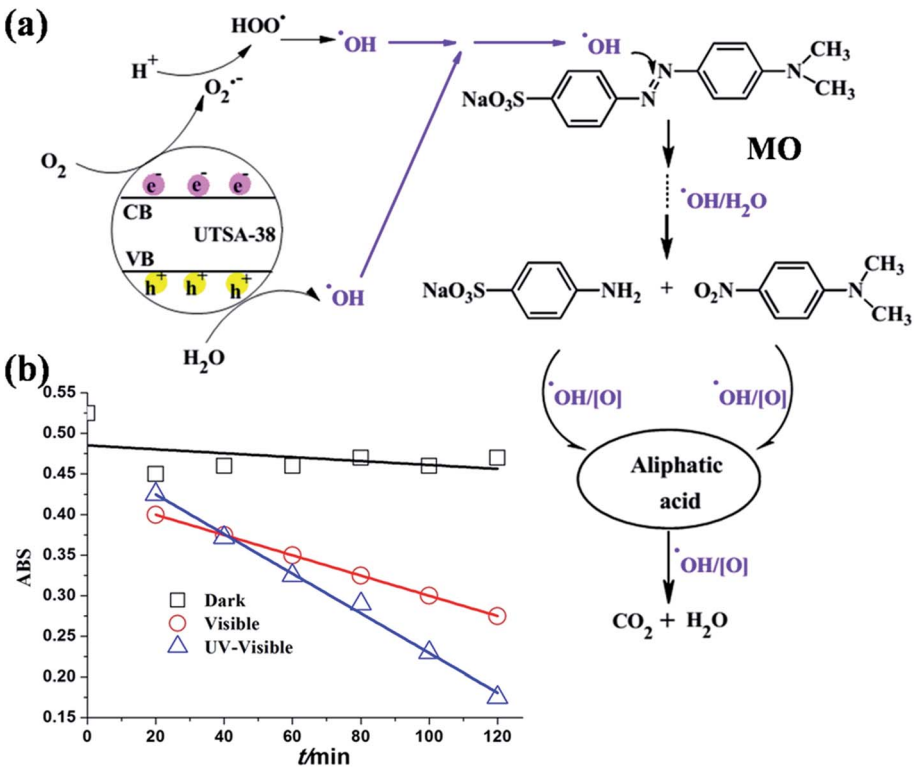

Fig. 3 (a) Main pathways proposed for methyl orange photodegraded by UTSA-38 under UV-visible or visible light irradiation. (b) Curves of absorbance of the methyl orange solution degraded by UTSA-38 as a function of irradiation time under UV-visible light, visible light and dark. Reprinted (adapted) with permission from ref. 93. Copyright (2011) The Royal Society of Chemistry.

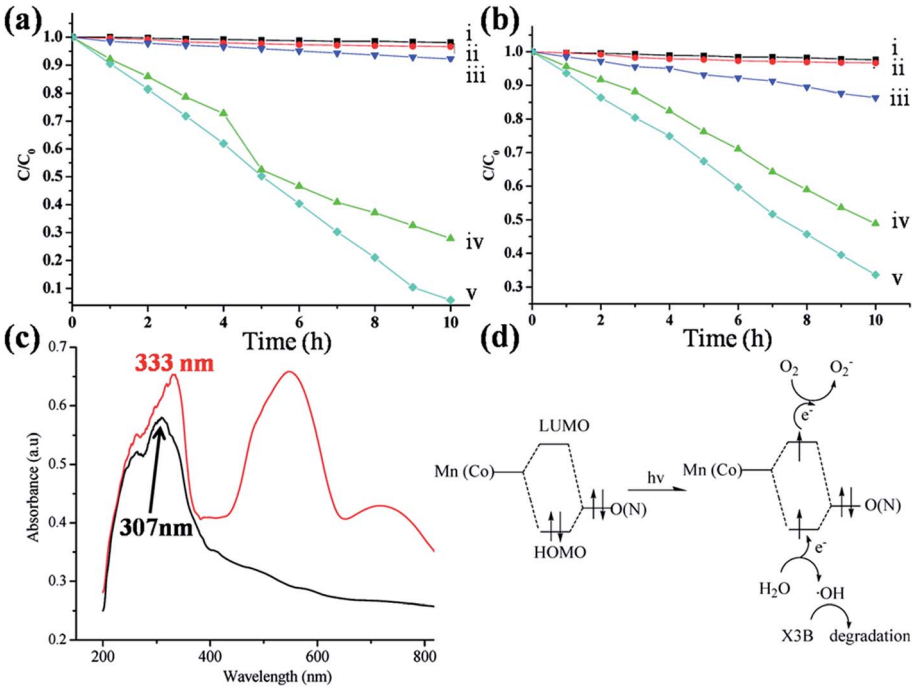

Fig. 4 (a) Experiments on the photodegradation of X3B: (i) X3B/$[Mn_3(btc)_2(bimb)_2]\cdot 4H_2O$/dark; (ii) X3B/UV light (without catalyst); (iii) X3B/$[Mn_3(btc)_2(bimb)_2]\cdot 4H_2O$/visible light; (iv) X3B/$[Mn_3(btc)_2(bimb)_2]\cdot 4H_2O$/*tert*-butyl alcohol/UV light; and (v) X3B/$[Mn_3(btc)_2(bimb)_2]\cdot 4H_2O$/UV light. (b) Experiments on the photodegradation of X3B: (i) X3B/$[Co_3(btc)_2(bimb)_2]\cdot 4H_2O$/dark; (ii) X3B/UV light (without catalyst); (iii) X3B/$[Co_3(btc)_2(bimb)_2]\cdot 4H_2O$/*tert*-butyl alcohol/UV light; (iv) X3B/$[Co_3(btc)_2(bimb)_2]\cdot 4H_2O$/visible light; and (v) X3B/$[Co_3(btc)_2(bimb)_2]\cdot 4H_2O$/UV light. (c) UV/vis diffuse-reflectance spectra of $[Mn_3(btc)_2(bimb)_2]\cdot 4H_2O$ (black line) and $[Co_3(btc)_2(bimb)_2]\cdot 4H_2O$ (red line) with $BaSO_4$ as background. (d) A simplified model of the photocatalytic reaction mechanism of X3B on $[Mn_3(btc)_2(bimb)_2]\cdot 4H_2O$ and $[Co_3(btc)_2(bimb)_2]\cdot 4H_2O$. Reprinted with permission from ref. 94. Copyright (2009) American Chemical Society.

such as molecular oxygen in solution, which would transform into the highly active peroxide anion and subsequently accomplish further oxidation and total degradation of RhB. A similar mechanism had been proposed recently for the degradation of organic dyes in the presence of metal carboxylates.[77,94,95,125]

The selective adsorption and photocatalytic degradation of different dyes with different MOFs have been explored by Natarajan and co-workers in $Cd_2(4,4'\text{-bpy})_3(S_2O_3)_2$, $Cd_2(4,4'\text{-bpy})_{2.5}(S_2O_3)_2$ and $[Cd(4,4'\text{-bpy})(H_2O)_2(S_2O_3)]\cdot 2H_2O$ (Table 1).[107] The mechanism of photocatalytic degradation towards anionic and cationic dyes was quite different herein. It was proposed that the hydroxyl radicals played an important role in breaking anthraquinonic anionic dyes like ARS,[150] and azoic anionic dyes such as OG and MO.[151] Meanwhile, cationic dyes like RBL were involved in surface-controlled *N*-de-ethylation reactions, resulting in the formation of intermediates that generally compete with the degradation of the original dye in solution.[152] They found that the sulfonated anionic dyes were significantly adsorbed by $Cd_2(4,4'\text{-bpy})_3(S_2O_3)_2$, $Cd_2(4,4'\text{-bpy})_{2.5}(S_2O_3)_2$, and $[Cd(4,4'\text{-bpy})(H_2O)_2(S_2O_3)]\cdot 2H_2O$ in the dark, but there was no apparent adsorption for non-sulfonated cationic dyes. Five non-sulfonated cationic dyes, MB, RBL, MV, MR, and BBR, were thus selected to carry out the photocatalytic degradation in the presence of the three MOFs, respectively, under UV light. The results revealed that these dyes were degraded, and the efficiencies are comparable to the Degussa P-25. In these MOFs, the ligand bpy was proposed to donate an electron to the Cd center, which helped to decompose the organic dye molecules. The mechanism involved in the photocatalytic degradation of these organic dyes in the presence of the three MOFs could be explained by considering the HOMO, filled d-orbital (d^{10} in Cd^{2+}), and the lowest LUMO, free s-orbital. In the presence of UV light, an electron would transfer from the HOMO to the LUMO. The electron in the LUMO could be readily lost from the excited state. Simultaneously, the HOMO would accept this electron to return to its stable state, and the excited Cd^{2+} center decays to the ground state quickly.[77] When organic molecules are presented in a reasonable concentration range with an appropriate orientation, then a transitional activated complex could be formed. The electron-withdrawing group attached to the carbon center of the dye would receive the electron. The hydrogen atom in organic dyes would give one electron and leave as an H^+ species. The electron would then be captured by the metal species, resulting in the cleavage of the C–N bond in a stepwise manner, to finish the total degradation of the organic dyes.[77]

The fact that the degradation efficiency of photocatalysts follows a reverse order with respect to their band gap values has also been proved. Two isostructural MOFs, $[Mn_3(btc)_2(bimb)_2]\cdot 4H_2O$ and $[Co_3(btc)_2(bimb)_2]\cdot 4H_2O$, were used to degrade an anionic organic dye X3B, by Wen and co-workers.[94]

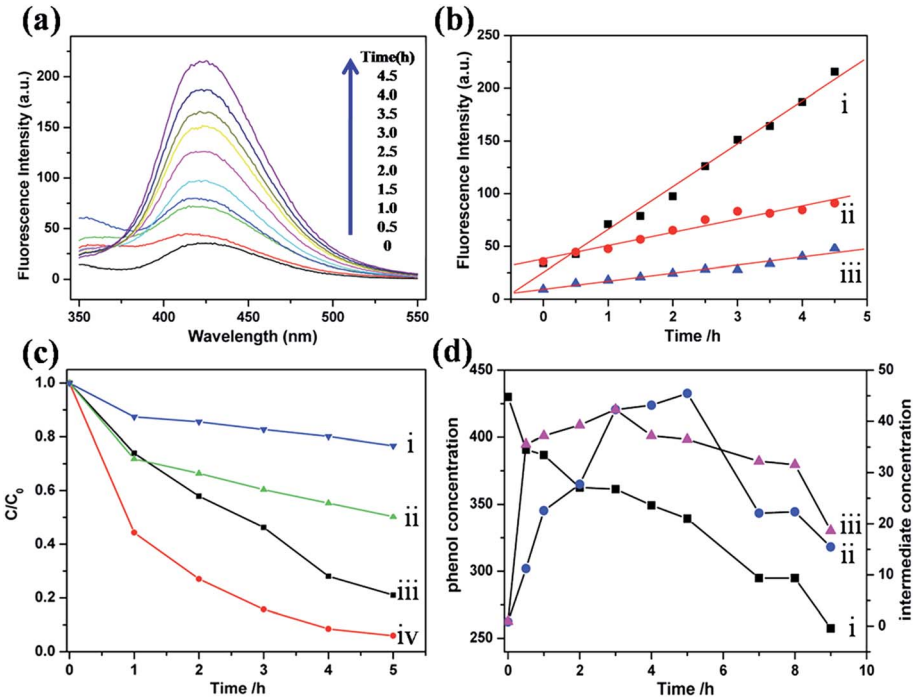

Fig. 5 (a) PL spectral changes observed during illumination of $Cd(btec)_{0.5}(bimb)_{0.5}$ in a 5×10^{-4} M basic solution of terephthalic acid (excitation at 315 nm). Each fluorescence spectrum was recorded every 30 min of visible illumination. (b) Comparison of the induced PL intensity at 425 nm for $Cd(btec)_{0.5}(bimb)_{0.5}$ (i), $Co(btec)_{0.5}(bimb)$ (ii) and $Ni(btec)_{0.5}(bimb)$ (iii). (c) Concentration changes of X3B as a function of irradiation time for $Cd(btec)_{0.5}(bimb)_{0.5}$ under different conditions: (i) $H_2O_2/Cd(btec)_{0.5}(bimb)_{0.5}$/dark, (ii) $Cd(btec)_{0.5}(bimb)_{0.5}$/visible light, (iii) H_2O_2/visible light, and (iv) $H_2O_2/Cd(btec)_{0.5}(bimb)_{0.5}$/visible light. (d) The concentration change of (i) phenol and its (ii) *ortho*- and (iii) *para*-intermediates in the presence of $Cd(btec)_{0.5}(bimb)_{0.5}$ under simulated solar light. Reprinted (adapted) with permission from ref. 95. Copyright (2011) American Chemical Society.

Compared with the control experiments (without photocatalyst), a distinctly shortened degradation time was observed, indicating that both MOF catalysts are active in the decomposition of X3B in the presence of both UV and visible light irradiation. It was found that the pseudo-first-order kinetics could fit well with the experimental data in both MOFs cases. For $[Mn_3(btc)_2(bimb)_2]\cdot 4H_2O$, the rate constant under UV light irradiation was found to be 1.1×10^{-1} h^{-1}, and that under visible light irradiation was 7.3×10^{-2} h^{-1}. While, for $[Co_3(btc)_2(bimb)_2]\cdot 4H_2O$, the rate constant under UV light and visible light irradiation was 2.6×10^{-1} and 1.3×10^{-1} h^{-1}, respectively. Although the two MOFs have the same topological structures, different central metal ions give distinct bandgap sizes (4.04 and 3.72 eV, respectively), which leads to discrepancies in their photocatalytic activity. As shown in Fig. 4c, the UV absorption bands of 307 nm for $[Mn_3(btc)_2(bimb)_2]\cdot 4H_2O$ and 333 nm for $[Co_3(btc)_2(bimb)_2]\cdot 4H_2O$ can be assigned to the ligand-to-metal charge transfer (LMCT). For the latter MOF, two additional peaks are observed at 547 and 721 nm, which probably originated from the d–d spin-allowed transition of the d^7 Co^{2+} ion. Meanwhile the absorption of the former MOF in the visible region is not as distinct as that of the latter, due to the d–d spin-forbidden transition of the d^5 Mn^{2+} ion. Clearly, the band gap energy of $[Mn_3(btc)_2(bimb)_2]\cdot 4H_2O$ is lower than that of $[Co_3(btc)_2(bimb)_2]\cdot 4H_2O$, leading to the degradation rate of X3B to follow a reverse order as illustrated in Fig. 4a and b. Therefore, the photocatalytic efficiency of $[Co_3(btc)_2(bimb)_2]\cdot 4H_2O$ under either UV or visible light was higher than that of $[Mn_3(btc)_2(bimb)_2]\cdot 4H_2O$. The former was able to degrade X3B almost completely in 10 h under UV irradiation. In a sense, the difference in the catalytic activity between $[Mn_3(btc)_2(bimb)_2]\cdot 4H_2O$ and $[Co_3(btc)_2(bimb)_2]\cdot 4H_2O$ can be attributed to their different UV/vis absorption properties, and further to different central metal atoms of the two MOFs.

In order to study the photocatalytic reaction mechanism in detail, they studied the photodegradation of X3B in the presence of *t*-butyl alcohol (TBA), a widely used $^{\bullet}OH$ scavenger.[94] It was found that the presence of TBA greatly depressed the degradation rate of X3B in $[Mn_3(btc)_2(bimb)_2]\cdot 4H_2O$ and $[Co_3(btc)_2(bimb)_2]\cdot 4H_2O$: the relevant rate constants decreased from 1.1×10^{-1} to 8.0×10^{-3} h^{-1} and from 2.6×10^{-1} to 1.4×10^{-2} h^{-1} under UV light. The $^{\bullet}OH$ quenching experiments suggested that the photodegradation of X3B in the two MOFs catalysts was predominately through the attack of $^{\bullet}OH$ radicals, rather than a direct hole oxidation. Based on these results, a simplified model of the photocatalytic reaction mechanism was proposed as depicted in Fig. 4d, in which the HOMO is mainly contributed to by the oxygen and (or) nitrogen 2p bonding orbitals (valence band) and the LUMO by empty Mn(Co) orbitals (conduction band). The charge transfer actually took place from oxygen and (or) nitrogen to Mn(Co) upon photoexcitation. In this case, the HOMO strongly demands one electron to return to

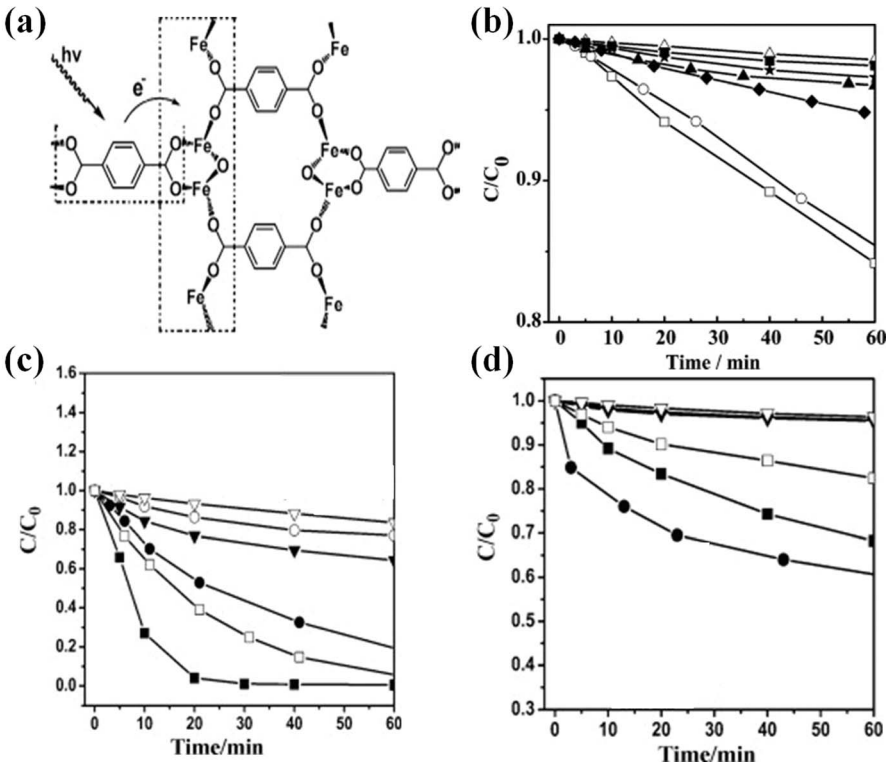

Fig. 6 (a) The chemical structure of MIL-53(Fe) and the electron transfer processes that occurs in MIL-53(Fe) when irradiated by light. (b) MB degradation profile under the irradiation of (■) without light, (△) visible light, (◆) UV-vis light, (▲) visible light in the presence of MIL-53(Fe) photocatalysts, and (□) UV-vis light in the presence of MIL-53(Fe) photocatalyst. (○) UV-vis light in the presence of TiO_2 photocatalysts, (★) visible light in the presence of TiO_2 photocatalyst. (c) and (d) The effect of different electron acceptor additives on MB photodegradation under the irradiation of (3) UV-vis light and (4) visible light, (■) in the presence of H_2O_2 and MIL-53(Fe), (□) in the presence of H_2O_2 and the absence of MIL-53(Fe), (●) in the presence of $(NH_4)_2S_2O_8$ and MIL-53(Fe), (○) in the presence of $(NH_4)_2S_2O_8$ and absence of MIL-53(Fe), (▼) in the presence of $KBrO_3$ and MIL-53(Fe), (▽) in the presence of $KBrO_3$ and the absence of MIL-53(Fe). Reprinted (adapted) with permission from ref. 27. Copyright (2011) Elsevier.

its stable state. Therefore, one electron was captured from the water molecule, which was oxygenated into the ˙OH active species. Meanwhile, the electrons (e^-) in the LUMO, combined with the oxygen adsorbed on the surfaces of the MOF to form $˙O_2^-$, further transformed to ˙OH. Finally, these formed ˙OH radicals cleaved X3B effectively to finish the photocatalytic process.[94]

Wen and co-workers also studied another series of MOFs, $Co(btec)_{0.5}(bimb)$, $Ni(btec)_{0.5}(bimb)$, and $Cd(btec)_{0.5}(bimb)_{0.5}$, which showed good photocatalytic properties for the degradation of X3B.[95] It was found that compared with

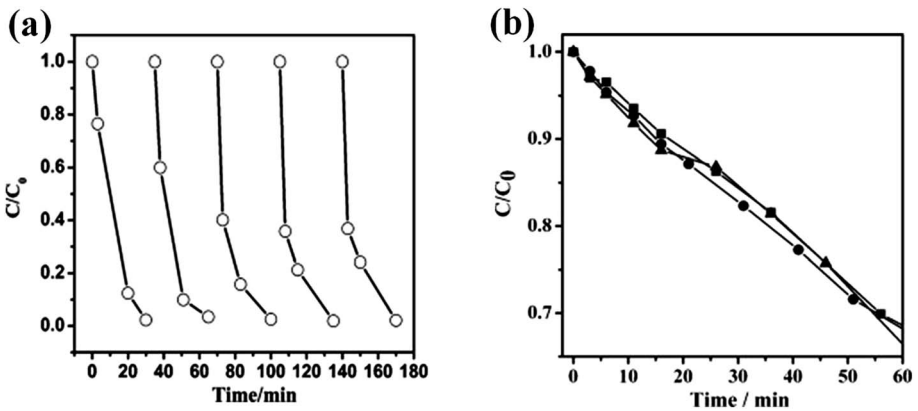

Fig. 7 (a) Changes in MB concentration during the five repeated processes over MIL-53(Fe) in the presence of H_2O_2 (10^{-5} mol L^{-1}). (b) MB degradation over MIL-53(Al) (▲), MIL-53(Fe) (●) and MIL-53(Cr) (■) photocatalysts under UV-vis light irradiation. Reprinted (adapted) with permission from ref. 27. Copyright (2011) Elsevier.

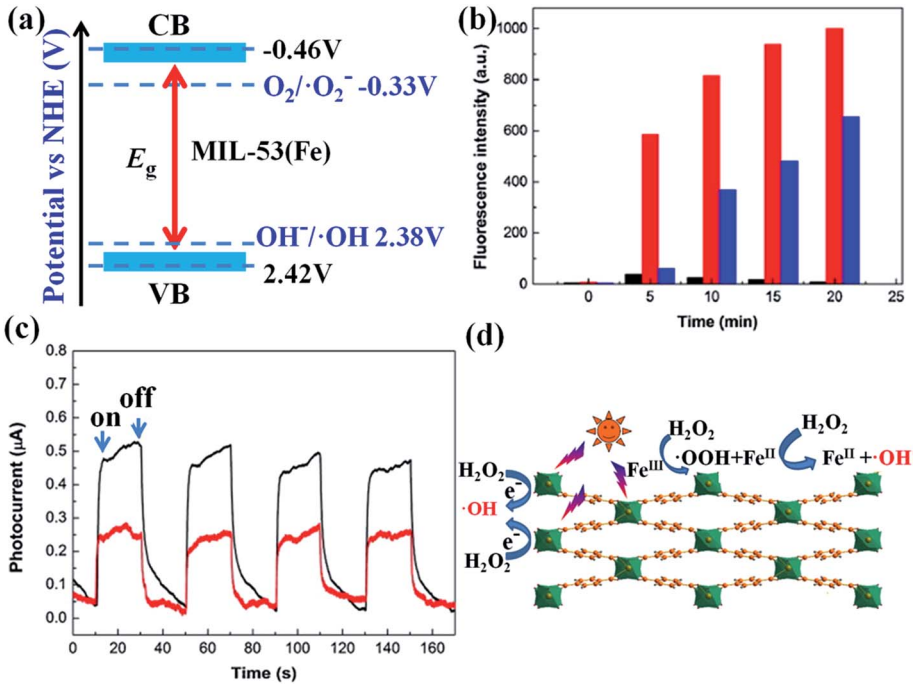

Fig. 8 (a) Estimated energy level diagram of the MIL-53(Fe). (b) Comparison of the PL intensities recorded every 5 min in catalytic systems of MIL-53/visible light (black column) and MIL-53(Fe)/H_2O_2 (red column) with MIL-53(Fe)/visible light/H_2O_2 (blue column) catalytic system. (c) Transient photocurrent responses of MIL-53(Fe) (black line) and MIL-53(Fe) with 70 mM H_2O_2 (red line) in 0.5 M Na_2SO_4 aqueous solutions under visible light irradiation. (d) Proposed mechanism for the activation of H_2O_2 by MIL-53(Fe) under visible light irradiation. Reprinted (adapted) with permission from ref. 88. Copyright (2014) Elsevier.

$[Mn_3(btc)_2(bimb)_2]\cdot 4H_2O$ and $[Co_3(btc)_2(bimb)_2]\cdot 4H_2O$,[94] the degradation rates under visible irradiation of these three MOFs on X3B were higher. This might be attributed to the more delocalized π electrons in the ligand 1,2,4,5-benzenetetracarboxylate, which could facilitate the LMCT transitions and decrease the electronic band gap of the MOFs, thereby enhancing the photocatalytic rate. Thus, it can be concluded that the semiconductor properties of the MOFs strongly depend on the resonance effects of their organic linkers.[153]

To investigate active species involved in the photocatalytic process on $Cd(btec)_{0.5}(bimb)_{0.5}$, the formation of hydroxyl radicals (˙OH) on the surface of this visible-illuminated MOF was detected by the photoluminescence (PL) technique, using terephthalic acid as a probe molecule.[154,155] With the increase in irradiation time, the PL spectra of a 5×10^{-4} M terephthalic acid solution in 2×10^{-3} M NaOH changed in the presence of $Cd(btec)_{0.5}(bimb)_{0.5}$. That is, a gradual increase in the PL intensity of photogenerated 2-hydroxyterephthalic acid (from terephthalic acid) at about 425 nm was observed with increasing irradiation time, as illustrated in Fig. 5a. However, no PL intensity increase was observed in the absence of $Cd(btec)_{0.5}(bimb)_{0.5}$, implying that the fluorescence was caused by the photocatalytic reaction of terephthalic acid with ˙OH formed at the MOF–water interface. It could also deduce that the number of ˙OH radicals formed at the catalyst surface is proportional to the light irradiation time, obeying the zero-order reaction rate kinetics.[156] The formation rate of ˙OH radicals could be expressed by the slope of these PL intensity *vs.* time lines, as shown in Fig. 5b. It was found that the formation rate of ˙OH radicals on $Cd(btec)_{0.5}(bimb)_{0.5}$ was much higher than that on $Co(btec)_{0.5}(bimb)$ and $Ni(btec)_{0.5}(bimb)$, indicating that the formation rate of ˙OH radicals was related to the photocatalytic activity of these MOFs. The associated photocatalytic degradation mechanism was thus similar to other reported MOFs.[129,157]

Generally, it is believed that the recombination of photogenerated hole–electron pairs limits the rate of photocatalytic degradation.[158] It has been found that H_2O_2 could increase the rate of hydroxyl radical formation in three ways: (i) it acted as an alternative electron acceptor to oxygen (eqn (1)), which inhibited the recombination of the photogenerated electrons and holes; (ii) the reduction of H_2O_2 at the conductance band produced a hydroxyl radical, or it accepted an electron from superoxide to give rise to the hydroxyl radical (eqn (2)); (iii) self-decomposition by illumination produced a hydroxyl radical (eqn (3)).

$$^{e}CB^{-} + H_2O_2 \rightarrow OH^{-} + {}^{\cdot}OH \quad (1)$$

$$^{\cdot}O_2^{-} + H_2O_2 \rightarrow OH^{-} + {}^{\cdot}OH + O_2 \quad (2)$$

$$H_2O_2 + h\nu \rightarrow 2{}^{\cdot}OH \quad (3)$$

The synergistic effect of H_2O_2 and MOF on the photodegradation of X3B was also investigated by Wen and co-workers.[121] The degradation of X3B in the presence of H_2O_2 (10 mL) and $Cd(btec)_{0.5}(bimb)_{0.5}$ (50 mg) under different

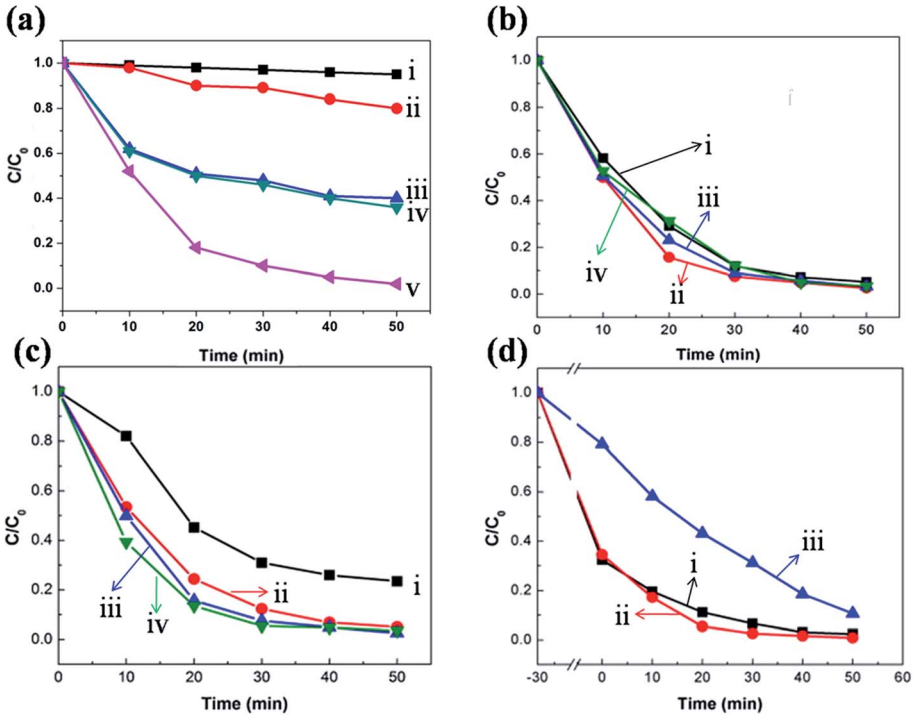

Fig. 9 (a) Degradation of RhB under different conditions: (i) visible light, (ii) visible light with H_2O_2, (iii) In the presence of MIL-53(Fe) and H_2O_2 in the dark, (iv) visible light in the presence of MIL-53(Fe), and (v) visible light in the presence of MIL-53(Fe) and H_2O_2. (b) Effect of initial pH on the degradation of RhB: (i) pH = 3, (ii) pH = 5, (iii) pH = 7, and (iv) pH = 9. Experimental conditions: RhB, 10 mg L^{-1}; H_2O_2, 20 mM and MIL-53(Fe), 0.4 g L^{-1}. (c) Effect of initial dye concentration on the degradation of RhB over MIL-53(Fe)/visible light/H_2O_2 system: (i) 5 mM, (ii) 10 mM, (iii) 20 mM, and (iv) 40 mM. Experimental conditions: H_2O_2, 20 mM; MIL-53(Fe), 0.4 g L^{-1}; and initial pH = 5. (d) Effect of H_2O_2 concentration on the degradation of RhB over MIL-53(Fe)/visible light/H_2O_2 system: (i) 5 mg L^{-1}, (ii) 10 mg L^{-1}, and (iii) 25 mg L^{-1}. Experimental conditions: RhB, 10 mg L^{-1}; MIL-53(Fe), 0.4 g L^{-1}; and initial pH = 5. Reprinted (adapted) with permission from ref. 88. Copyright (2014) Elsevier.

conditions is shown in Fig. 5c. It was found that the degradation of X3B was slow in the dark, with only 23.4% being degraded after 5 h. But, the visible-light irradiation greatly accelerated the photodegradation of X3B to achieve a 94.1% degradation after 5 h. It is much more interesting that the photocatalytic degradation rate constant of X3B on $Cd(btec)_{0.5}(bimb)_{0.5}$ was 0.56 h^{-1} in the presence of H_2O_2, being 1.8 times higher than that without H_2O_2 (0.31 h^{-1}) under other similar conditions.

Considering that the dyes can also be degraded through a photosensitized pathway, Wen and co-workers[95] selected a colorless molecule, phenol, acting as a model to test the photocatalytic activity of $Cd(btec)_{0.5}(bimb)_{0.5}$. As shown in Fig. 5d, it was found that the concentration of phenol decreased, while its *ortho*- and *para*-intermediates increased with increased light irradiation time (the conversion of the phenol was 40.13% and the selectivity for the intermediate catechol was 45.32% after 9 h irradiation). Control experiments (without catalyst or in the dark) showed that no obvious phenol degradation happened. These results demonstrated that $Cd(btec)_{0.5}(bimb)_{0.5}$ is quite an efficient visible light-responsible photocatalyst.[95]

In addition, Yuan and co-workers used MIL-53(Fe), constructed by –Fe–O–O–Fe–O–Fe– chains linked by terephthalate linkers (as illustrated in Fig. 6a) as a photocatalyst to decompose methylene blue (MB) dye.[27] Just like the TiO_2 semiconductor whose conduction band is constructed by empty Ti 3d orbitals, MIL-53(Fe) containing Fe(III) ions is also expected to be effective as a photocatalyst, based on the fact that the empty d orbitals in Fe(III) mix with the LUMOs of the organic linkers to

Table 4 Parameters for catalytic degradation rates of MB in the presence of $(Me_3Sn)_4Fe(CN)_6$ (ref. 92)

[MB] (M)	k (min^{-1}) × 10^2	R^a	$[H_2O_2]$ (M)	k (min^{-1}) × 10^2	R^a	$(Me_3Sn)_4Fe(CN)_6$ (mM)	k (min^{-1}) × 10^2	R^a	pH	k (min^{-1}) × 10^2	R^a
1×10^{-6}	35	0.983	10	15.7	0.988	0.025	28	0.997	4	24.8	0.995
5×10^{-6}	28	0.997	20	19.8	0.990	0.040	36.2	0.996	5	26.3	0.995
7×10^{-6}	21	0.995	30	28	0.997	0.05	48.6	0.989	5.5	27.2	0.998
1×10^{-5}	13.6	0.996	40	21.6	0.992	0.058	57	0.992	6	28	0.972
			0	13.2	0.983				7.5	18.6	0.992

[a] Correlation coefficient.

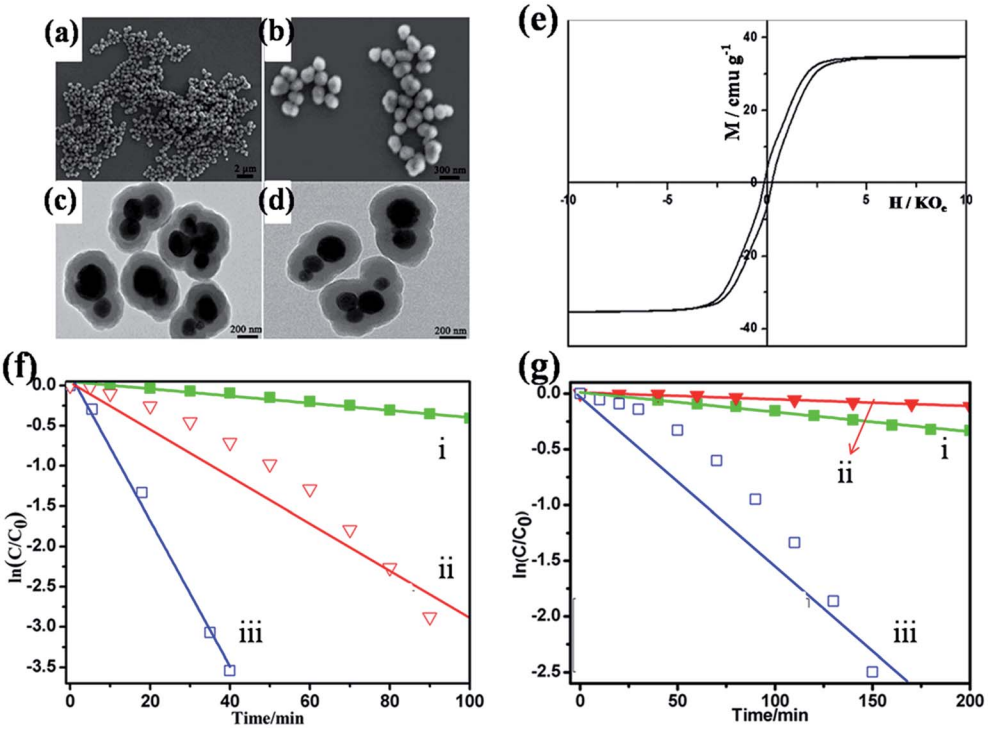

Fig. 10 (a and b) SEM and (c and d) TEM images of Fe_3O_4@MIL-100(Fe) core–shell microspheres obtained at 70 °C for 50 layers. (e) Room-temperature magnetization curves of samples of the Fe_3O_4@MIL-100(Fe) microspheres at 300 K. (f) First-order kinetics plot for the photodegradation of MB by Fe_3O_4@MIL-100(Fe) (i), TiO_2 and H_2O_2 (ii), and Fe_3O_4@MIL-100(Fe) and H_2O_2 (iii) under the irradiation of UV-vis light. (g) First-order kinetics plot for the photodegradation of MB by Fe_3O_4@MIL-100(Fe) (i), C_3N_4 and H_2O_2 (ii), and Fe_3O_4@MIL-100(Fe) and H_2O_2 (iii) under the irradiation of visible light. Reprinted (adapted) with permission from ref. 89. Copyright (2013) the Royal Society of Chemistry.

form the conduction band.[64] It was proposed that upon light irradiation, electron excitation could take place in the MOF, followed by electron transfer, as illustrated in Fig. 6a. The results showed that MIL-53(Fe) exhibited efficient photocatalytic properties for MB degradation under both UV-vis and visible light irradiation, even if the photodegradation rate was not so high (Fig. 6b). This relatively low degradation rate might be attributed to the recombination of photogenerated holes and electrons, which always leads to reduced holes for the degradation of organic dyes.[159,160] It was also found that the introduction of different inorganic oxidants (as electron acceptors), such as H_2O_2, $KBrO_3$, and $(NH_4)_2S_2O_8$, could greatly promote the photocatalytic properties of MIL-53(Fe), since these inorganic oxidants could suppress the electron-hole pair recombination according to eqn (4)–(6). As shown in Fig. 6b, all these inorganic oxidants accelerated the rate of MB decolorization both under UV-vis light and visible light irradiation. The enhanced impact follows the order $H_2O_2 > (NH_4)_2S_2O_8 > KBrO_3$ under UV-vis light irradiation, and $(NH_4)_2S_2O_8 > H_2O_2 > KBrO_3$ under visible light irradiation (Fig. 6c and d).

$$H_2O_2 + e^- \rightarrow {}^{\bullet}OH + OH^- \quad (4)$$

$$BrO_3^- + 2H^+ + e^- \rightarrow BrO_2^{\bullet} + H_2O \quad (5)$$

$$S_2O_8^{2-} + e^- \rightarrow SO_4^{2-} + SO_4^{-\bullet} \quad (6)$$

For the purpose of practical applications it is essential to evaluate the long-term stability of a photocatalyst. MIL-53(Fe) was checked five times as a photocatalyst to degrade MB. The results revealed no apparent loss of the catalytic activity for MB decolorization in MIL-53(Fe) during the five cycles (Fig. 7a). The structure and chemical states of MIL-53(Fe) before and after MB degradation reaction were identified by PXRD and XPS analysis, which revealed its excellent long-term stability in this case.

Both MIL-53(Al) and MIL-53(Cr), being isostructural to MIL-53(Fe), also displayed photocatalytic activities for MB decolorization, as illustrated in Fig. 7b. Study on this series of isostructural photocatalysts would provide valuable information on the effect of metal nodes of MOFs on their photocatalytic activities. It was found that after 60 min of UV-vis light irradiation, degrees of MB removal over MIL-53(Al) and MIL-53(Cr) were 30% and 32%, respectively, close to that over MIL-53(Fe). In photocatalysis, it is generally believed that photocatalytic activity increases with the increase in number of absorbed photons. The number of adsorbed protons presumably increases across different metal ions in the MIL-53 series because of the decreasing band gaps of 3.87, 3.20, and 2.72 eV for MIL-53(Al), MIL-53(Cr), and MIL-53(Fe), respectively. Then, the MIL-53(Fe) with the narrowest band gap among three MIL-53 photocatalysts was expected to exhibit the highest rate for MB degradation. However, it was found that these MOFs displayed similar rates for MB degradation. The reason is not clear

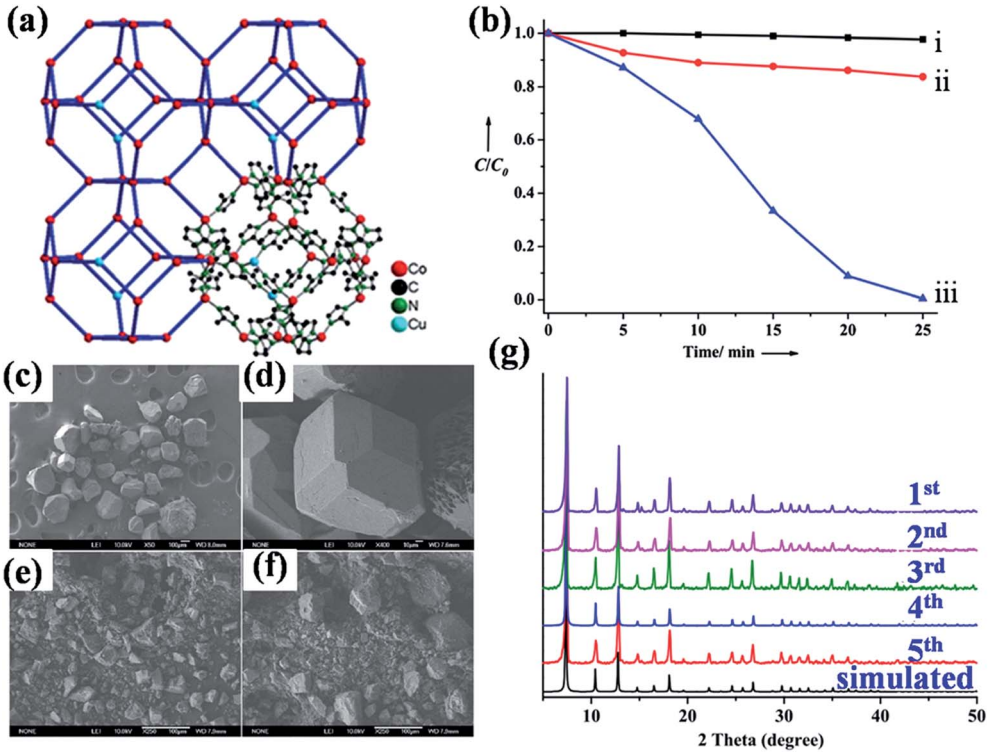

Fig. 11 (a) The SOD-type framework structure of Cu/ZIF-67. (b) Photodegradation of MO on ZIF-67 and Cu/ZIF-67 under visible-light illumination in the presence of H_2O_2 additive: MO–H_2O_2 solution (i); MO–H_2O_2 solution with ZIF-67 (ii); and MO–H_2O_2 solution with Cu/ZIF-67 (iii). (c) and (d) SEM images of crystals of Cu/ZIF-67; (e) SEM images of powder samples of Cu/ZIF-67 before photocatalytic experiments. (f) SEM images of powder samples of Cu/ZIF-67 after 5 photocatalytic experiments. (g) The PXRD pattern of Cu/ZIF-67 after photocatalytic experiments. Reprinted (adapted) with permission from ref. 91. Copyright (2012) the Royal Society of Chemistry.

yet. A similar result was found in MIL-88A photocatalysts for the decomposition of MB.[99]

In order to understand the mechanism of the synergistic effect in the MIL-53(Fe)/visible light/H_2O_2 system, Jiang and co-workers evaluated the band position of MIL-53(Fe), which is intimately close to the redox ability of the photoinduced charge carriers.[88] A typical Mott-Schottky plot of MIL-53(Fe) in the dark was measured at a frequency of 100 Hz, to give a flatband potential of −0.60 V *vs.* SCE (equivalent to −0.36 V *vs.* NHE). The conduction band (CB) of MIL-53(Fe) was thus estimated to be −0.46 V *vs.* NHE, which was more negative than the redox potential of $O_2/^{\bullet}O_2^{-}$ (−0.33 V *vs.* NHE) (Fig. 8a). This lower potential is conducive to the photogenerated electron transfer from the catalyst to adsorbed molecular oxygen. The valence band (VB) of MIL-53(Fe) was calculated to be 2.42 V *vs.* NHE. As shown in Fig. 8a, MIL-53(Fe) was apparently not effective for the oxidization of OH^- to $^{\bullet}OH$ radicals under visible light irradiation, because its VB value was very close to the redox potential of $^{\bullet}OH/OH^-$ (2.38 V *vs.* NHE). The redox potential of RhB is about 1.43 V *vs.* NHE,[161] lower than the VB level of MIL-53(Fe), implying that the direct hole oxidation process is energetically favorable. The formation of $^{\bullet}OH$ radicals in the catalytic system of MIL-53(Fe)/visible light/H_2O_2 was indeed detected by the photoluminescence (PL) method. For comparison, the MIL-53(Fe)/visible light and MIL-53(Fe)/H_2O_2 systems were also investigated under the same conditions (Fig. 8b). The stronger PL intensity in the MIL-53 (Fe)/visible light/H_2O_2 suggested that more $^{\bullet}OH$ radicals were generated, which could be attributed to the existence of synergistic effects from the combination of MIL-53(Fe) and H_2O_2.

To gain further insight into the synergistic effect in the MIL-53(Fe)/visible light/H_2O_2 system, the transient photocurrent response of MIL-53(Fe) with H_2O_2 in solution under visible light irradiation was measured. It was found that both systems were active in generating a photocurrent with a reproducible response towards on-off cycles, as shown in Fig. 8c. The photocurrent response of MIL-53(Fe) was greatly reduced with the introduction of H_2O_2, which indicated that H_2O_2 could react with photogenerated electrons to produce $^{\bullet}OH$ radicals. These results are closely consistent with the results from $^{\bullet}OH$-trapping PL spectra. The proposed mechanism for the activation of H_2O_2 by MIL-53(Fe) under visible light irradiation was illustrated in Fig. 8d.

In the photocatalytic degradation, a lot of factors affect the degradation efficiency, including pH, initial concentration of dye, scavenging agents, anions, catalyst dosage, reaction temperature, and so on.[162,163] In order to optimize the design of a process, it was important to identify which factors have the greatest influence. For this purpose, Jiang and co-workers explored the influences of pH, H_2O_2 dosage, and initial dye concentration on the degradation of RhB over MIL-53(Fe)/visible light/H_2O_2 system (Fig. 9a).[88] The results revealed that

Table 5 Performances of some MOFs constructed with f-block metals as photocatalysts for the degradation of organic pollutants in aqueous media

MOF[a]	E_g (eV)	Irrigation	Organic pollutants	Initial concentration (mg L^{-1})	Time (min)	Degradation efficiency (%)	Ref.
$[InRu(dcbpy)_3]\cdot((CH_3)_2NH_2)\cdot 6H_2O$	2.19	Vis	MO	10	120	80	182
$[Gd(5\text{-}NO_2\text{-bdc})(5\text{-}NO_2\text{-bdcH})(bpyo)_{0.5}]\cdot 2H_2O$	—	UV	X3B	3.69	600	70.0[b]	157
$Gd(H_2O)_3Co(2,3\text{-pdc})_3$	3.7	UV	RBBR	100	100	—	67
$Gd(H_2O)_3Co(2,3\text{-pdc})_3$	3.7	UV	OG	100	100	—	67
$[Ni_2(H_2O)_2(qa)_2(4,4'\text{-bpy})_2U_5O_{14}(H_2O)_2(OAc)_2]\cdot 2H_2O$	—	UV	MB	35.9	240	100[b]	76
$[Ni_2(H_2O)_2(qa)_2(4,4'\text{-bpy})_2U_5O_{14}(H_2O)_2(OAc)_2]\cdot 2H_2O$	—	Vis	MB	35.9	240	80[b]	76
$(UO_2)_8(1,4\text{-ndc})_{12}(4,4'\text{-bpyH}_2)_3(4,4'\text{-bpyH})_3$	—	UV	RhB	50	80	95[b]	75
$(UO_2)_8(1,4\text{-ndc})_{12}(4,4'\text{-bpyH}_2)_3(4,4'\text{-bpyH})_3$	—	Vis	RhB	50	600	100[b]	75
$(UO_2)_3O[Ag(2,2'\text{-bpy})_2]_2(1,4\text{-ndc})_3$	—	UV	RhB	50	80	100[b]	75
$(UO_2)_3O[Ag(2,2'\text{-bpy})_2]_2(1,4\text{-ndc})_3$	—	Vis	RhB	50	600	100[b]	75
$Ag(2,2'\text{-bpy})(UO_2)(1,4\text{-bdc})_{1.5}$	—	UV	RhB	47.9	35	100[b]	77
$Ag(2,2'\text{-bpy})(UO_2)(1,4\text{-bdc})_{1.5}$	—	Vis	RhB	47.9	240	90[b]	77
$Ag_2(phen)_2UO_2(btec)$	—	UV	RhB	47.9	120	99[b]	77
$(UO_2)_2(bta)(DMA)_2$	—	UV	RhB	10	130	100	209
$[(UO_2)_2(bta)(\mu_3\text{-}OH_2)]\cdot 2(HN(CH_3)_2)\cdot H_2O$	—	UV	RhB	10	130	50	209
$UO_2(1,4\text{-ndc})((CH_3)_2SO))_2$	—	UV-vis	RhB	479	70	100	210
$UO_2(1,4\text{-ndc})((CH_3)_2SO))_2$	—	Vis	RhB	479	180	100	210
$UO_2(1,4\text{-ndc})(CH_2OH)_2$	—	UV-vis	RhB	479	70	100	210
$UO_2(1,4\text{-ndc})(CH_2OH)_2$	—	Vis	RhB	479	180	98	210
$Gd(H_2O)_3Co(2,2\text{-pdc})_3$	—	UV	RBBR	100	90	90[b]	114
$[Sm(H_2O)_4(2,6\text{-pdc})]_3[Sm(H_2O)_3(2,6\text{-pdc})](SiMo_{12}O_{40})\cdot 3H_2O$	—	UV	RhB	9.58	240	85[b]	211
$[La(H_2O)_4(2,6\text{-pdc})]_4(PMo_{12}O_{40})F$	—	UV	RhB	9.58	240	85[b]	211
$[Yb(O)(Hbpcdb)_2(H_2bpcdb)_{0.5}(H_2O)_3](SiMo_{12}O_{40})\cdot 2.5CH_3CN\cdot 1.5H_2O$	—	UV	RhB	10	90	91.7	212
$[Ca(Hbpcdb)_2(bpcdb)_{0.5}(H_2O)_4](SiMo_{12}O_{40})\cdot 5CH_3CN\cdot H_2O$	—	UV	RhB	10	90	91.7	212

[a] dcbpy = 2,2′-bipyridine-4,4′-dicarboxylic acid; 5-NO_2-bdcH_2 = 5-nitro-1,3-benzenedicarboxylic acid; bpyo = 4,4′-bipyridine-*N*,*N*′-dioxide; 2,3-pdc = pyridine-2,3-dicarboxylic acid; H_2qa = quinolinic acid; 4,4′-bpy = 4,4′-bipyridine; 1,4-H_2ndc = 1,4-naphthalenedicarboxylic acid; 2,2′-bpy = 2,2′-bipyridine; 1,4-bdc = 1,4-benzenedicarboxylate; phen = phenanthroline; btec = 1,2,4,5-benzenetetracarboxylate; H_4bta = 1,2,4,5-benzenetetracarboxylic acid; 2,3-pdc = pyridine-2,3-dicarboxylic acid; 2,6-pdc = pyridine-2,6-dicarboxylic acid; bpcdb = 1,4-bis(pyridinil-4-carboxylato)-l,4-dimethylbenzene. [b] Values estimated from original figures of the references.

the MIL-53(Fe) catalyst could work effectively over a wide pH range from 3.0 to 9.0. However, the degradation rate of RhB decreased with the increase of pH from 5.0 to 9.0 (as shown in Fig. 9b), which could be attributed to the fact that H_2O_2 is not stable in alkaline medium (decomposes to form O_2 and H_2O[164]). As shown in Fig. 9c, the degradation efficiency of RhB was found to strongly depend on the initial dye concentration from 5 to 10 mg L^{-1}. As an explanation, the number of RhB molecules per volume unit in solution increased by increasing the initial dye concentration, which could enhance effective contact between oxidizing species and dye molecules, resulting in higher degradation efficiency. However, the efficiency was significantly decreased when the concentration of RhB increased from 10 to 25 mg L^{-1}. This is because the more RhB dye there was in solution, the less permeable the solution was to incident light, which resulted in the low efficiencies of light utilization and low rates of photochemical processes.[165] When H_2O_2 concentration increased from 5 to 20 mM, the degradation efficiency increased correspondingly from 77 to 98%, because of an increase in $^{\bullet}OH$ radicals with increasing concentration of H_2O_2.[166,167] However, on increasing H_2O_2 concentration from 20 to 40 mM, the degradation efficiency was not further enhanced (as illustrated in Fig. 9d), which could be explained by surplus H_2O_2 molecules acting as scavengers of $^{\bullet}OH$ radicals to generate perhydroxy radicals with lower potential (see eqn (7) and (8)).[168]

$$H_2O_2 + OH^{\bullet} \rightarrow H_2O + HOO^{\bullet} \quad (7)$$

$$HOO^{\bullet} + OH^{\bullet} \rightarrow H_2O + O_2 \quad (8)$$

Etaiw and El-bendary also studied the effect of dye initial concentration, catalyst amount, pH, and scavenging agent amount on MB degradation over the $(Me_3Sn)_4Fe(CN)_6$ photocatalyst.[92] The initial MB concentrations were set in the range 1.0×10^{-6} to 1.0×10^{-5} M in the presence of 0.1 M H_2O_2 and 0.025 mmol $(Me_3Sn)_4Fe(CN)_6$ as the photocatalyst at pH 5.5. Initially, a large degree of removal was observed, which was due to the fast decomposition of H_2O_2, producing more $^{\bullet}OH$ radicals. The lifetime of $^{\bullet}OH$ radicals is a few nanoseconds, so they only reacted where they are found.[169] As listed in Table 4, increasing the MB concentration led to a decrease in the degradation rate. However, even at a higher concentration (1.0×10^{-5} M), complete decolorization was observed after a longer time of 110 min. This could be explained by the generation of $^{\bullet}OH$ radicals on the surface of the catalyst being reduced at

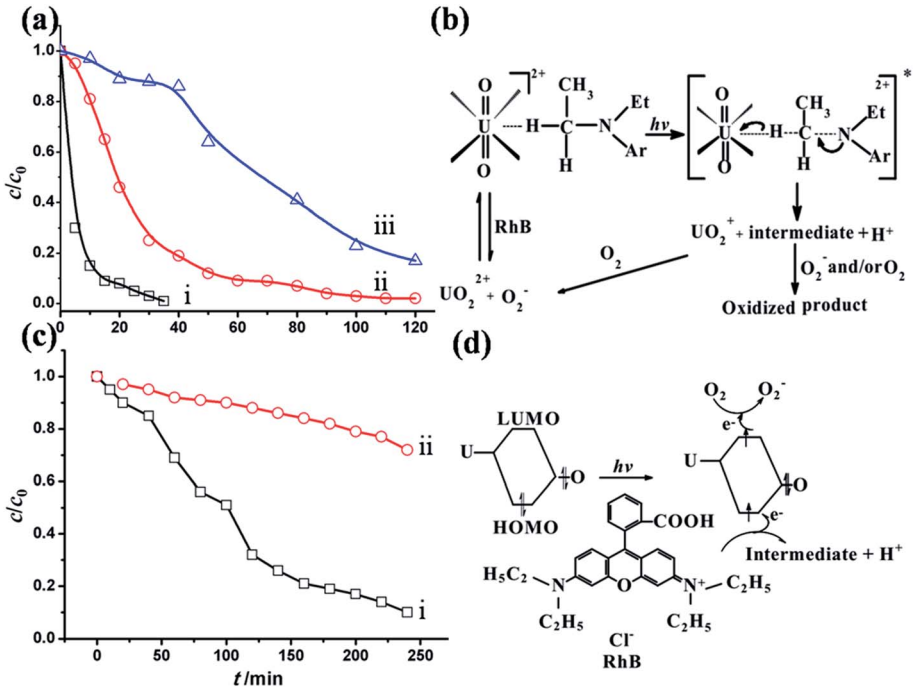

Fig. 12 (a) Concentration changes of RhB irradiated with UV light as a function of irradiation time t_{irr} in the presence of Ag(2,2′-bpy)(UO_2)(1,4-bdc)$_{1.5}$ (i), Ag_2(phen)$_2UO_2$(btec) (ii), and Degussa P-25 (iii). C_t and C_0 stand for the RhB concentrations after and before irradiation. (b) Photo-excitation of Ag(2,2′-bpy)(UO_2)(1,4-bdc)$_{1.5}$ or Ag_2(phen)$_2UO_2$(btec) and oxidation of the RhB substrate. (c) Concentration changes of RhB under irradiation with xenon-lamp light in the presence of Ag(2,2′-bpy)(UO_2)(1,4-bdc)$_{1.5}$ (i) and Degussa P-25 (ii). (d) Proposed photodegradation pathways of the RhB substrate in the presence of Ag(2,2′-bpy)(UO_2)(1,4-bdc)$_{1.5}$ or Ag_2(phen)$_2UO_2$(btec). Reprinted (adapted) with permission from ref. 77. Copyright (2012) Wiley-VCH.

Table 6 Kinetics parameters for the degradation of dyes using $M(H_2O)_3Co(pda)_3$ (M = Gd, Dy, and Y)[67]

MOF	Dye	k_0 (min^{-1})	K_0 (mg L^{-1})
$Gd(H_2O)_3Co(pda)_3$	RBBR	0.025	0.002
$Gd(H_2O)_3Co(pda)_3$	OG	0.018	0.003
$Dy(H_2O)_3Co(pda)_3$	RBBR	0.012	0.015
$Dy(H_2O)_3Co(pda)_3$	OG	0.009	0.005
$Y(H_2O)_3Co(pda)_3$	RBBR	0.032	0.018
$Y(H_2O)_3Co(pda)_3$	OG	0.007	0.003

higher concentrations, since the active sites were covered by dye molecules. Therefore, as the initial concentration of the dye increased, the catalyst surface needed for the degradation should also be increased. By increasing the amount of catalysts from 0.025 to 0.058 mmol, the rate of degradation thus increased. In this work, the effect of pH on the reaction rate was also studied at the constant concentration of the dye and H_2O_2 as well as a fixed amount of the catalyst at 25 °C. As illustrated in Table 4, in acid media, the deprotonation of H_2O_2 increased with increasing pH, which led to an increase in the decomposition rate of H_2O_2, therefore leading to facile formation of $^{\bullet}OH$ radicals. But in the alkaline medium, oxidizing species (hydroperoxy anion, HO_2^-) also formed (as listed in eqn (9) and (10)), which reacted with the non-dissociated molecules of H_2O_2, forming oxygen and water. Furthermore, the deactivation of $^{\bullet}OH$ was more obvious at a higher pH of the solution. The reaction of $^{\bullet}OH$ and HO_2^- was approximately 100 times faster than its reactions with H_2O_2. The effect of the initial H_2O_2 concentration (10–60 mmol) was investigated in the dye concentration of 5.0×10^{-6} M at pH 6.0. The results showed that the initial H_2O_2 concentration strongly affected the degradation rate of MB. At low H_2O_2 concentrations, the formation of the $^{\bullet}OH$ radicals was the kinetic determining step. It was found that an increase in the H_2O_2 concentration up to 30 mmol led to a dramatic rise in decomposition of the dyes. However, a further increase in the H_2O_2 concentration partly inhibited the oxidation rate,[88,168] implying the existence of an optimal dosage in H_2O_2. Higher concentration of H_2O_2 led to the production of more $^{\bullet}OH$ radicals, which preferentially reacted with excess H_2O_2, which competed with the destruction of the dye chromophores, being undesirable.[170]

$$^{\bullet}OH + MB \rightarrow \text{oxidation products} \quad (9)$$

$$^{\bullet}OH + H_2O_2 \rightarrow \text{oxidation products} \quad (10)$$

Ti-based MOFs, MIL-125 and its NH_2-functionalized isostructure (MIL-125-NH_2) were also used as photocatalysts to split water or reduce CO_2.[78,171–175] Zhang and co-workers reported that Ti(IV)-based MOF NTU-9 displayed a strong absorption in the visible region with a bandgap of 1.72 eV and exhibited good photocatalytic activity in the degradation of RhB and MB

Table 7 Performances of some MOFs constructed with d-block metals as photocatalysts for the degradation of organic pollutants in aqueous media

MOF[a]	E_g (eV)	Irrigation	Organic pollutants	Initial concentration (mg L^{-1})	Time (min)	Degradation efficiency (%)	Ref.
$\{[Sm(H_2O)_4(2,6\text{-pdc})]_3\}\{[Sm(H_2O)_3(2,6\text{-pdc})]\}(SiMo_{12}O_{40})\cdot 3H_2O$	—	UV	RhB	9.58	240	85[b]	134
$[La(H_2O)_4(2,6\text{-pdc})]_4\ (PMo_{12}O_{40})F$	—	UV	RhB	9.58	240	85[b]	134
$[Yb(O)(Hbpcdb)_2(H_2bpcdb)_{0.5}(H_2O)_3](SiMo_{12}O_{40})\cdot 2.5CH_3CN\cdot 1.5H_2O$	—	UV	RhB	10	90	91.7	135
$[Ca(Hbpcdb)_2(bpcdb)_{0.5}(H_2O)_4](SiMo_{12}O_{40})\cdot 5CH_3CN\cdot H_2O$	—	UV	RhB	10	90	91.7	135
$[Ag(4,4'\text{-bpy})]_4V_4O_{12}\cdot 2H_2O$	2.77	UV	MB	6.0	180	70	73
$[Ag(dpa)]_4V_4O_{12}\cdot 4H_2O$	2.95	UV	MB	6.0	180	65	73
$Ag_4(pzc)_2V_2O_6$	2.45	UV	MB	6.0	90	80	73
$Ag_4(pzc)_2V_2O_6$	2.45	Vis	MB	6.0	180	80	73
$[Ag(bbi)][(Ag(bbi))_4(Ag_3(V_4O_{12})_2)]\cdot 2H_2O$	—	UV	MB	10.0	90	70	241
$Cu_2^{I}(1,3\text{-btp})_2]\ [Cu_2^{I}(trans\text{-}1,3\text{-btp})_2Mo_6O_{18}(O_3AsPh)_2$	2.6	UV	MB	17.6	120	76	238
$Cu^{I}_4\ (1,5\text{-btp})_4Mo_6O_{18}(O_3AsPh)_2$	2.1	UV	MB	17.6	120	93	238
$Cu^{I}_4\ (1,6\text{-bth})_2Mo_6O_{18}(O_3AsPh)_2$	1.9	UV	MB	17.6	120	97	238
$[Cu_8(1,3\text{-btp})_8[Mo_{12}O_{46}(AsPh)_4]_2]\cdot 3H_2O$	1.72	Vis	MB	17.6	180	70	249
$Cu_6Na_2(Htrb)_4(Mo_6O_{19})(MoO_4)_6$	3.13	UV	MB	17.6	120	63	250
$[Zn_3(Htrb)(Mo_{10}O_{34})]\cdot 8H_2O$	2.87	UV	MB	17.6	120	61	250
$[Zn_2(Htrb)(\beta\text{-}Mo_8O_{26})(H_2O)_2]\cdot 6H_2O$	3.15	UV	MB	17.6	120	60	250
$[Co_2(Htrb)(\beta\text{-}Mo_8O_{26})(H_2O)_2]\cdot 6H_2O$	2.64	UV	MB	17.6	120	56	250
$[Co_2(Htrb)(\gamma\text{-}Mo_8O_{26})(H_2O)_6]\cdot 8H_2O$	2.91	UV	MB	17.6	120	58	250
$[Cu_2(2,4'\text{-tmbpt})_2(\beta\text{-}Mo_8O_{26})(H_2O)_2]\cdot 7H_2O$	2.88	UV	MB	17.6	120	60	245
$[Cu(2,4'\text{-tmbpt})(\gamma\text{-}Mo_8O_{26})_{0.5}(H_2O)]\cdot H_2O$	2.13	UV	MB	17.6	120	57	245
$Co(2,4'\text{-Htmbpt})_2(\gamma\text{-}Mo_8O_{26})(H_2O)_2$	2.45	UV	MB	17.6	120	52	245
$Zn(2,4'\text{-Htmbpt})_2(\gamma\text{-}Mo_8O_{26})(H_2O)_2$	2.94	UV	MB	17.6	120	83	245
$[Ni(2,4'\text{-tmbpt})(\alpha\text{-}Mo_8O_{26})_{0.5}(H_2O)]\cdot 2.5H_2O$	2.62	UV	MB	17.6	120	76	245
$Ag(2,4'\text{-Htmbpt})(\beta\text{-}Mo_8O_{26})_{0.5}$	2.75	UV	MB	17.6	120	59	245
$[Zn_4(htpmb)_2(\theta\text{-}Mo_8O_{26})(H_2O)_{6.5}]\cdot 0.5H_2O$	2.63	UV	MB	17.6	120	76	246
$[Zn_6(htpmb)_2(\gamma\text{-}Mo_8O_{26})_2(SO_4)(H_2O)_6]\cdot 6.5H_2O$	3.33	UV	MB	17.6	120	71	246
$[Cd_2(htpmb)(\gamma\text{-}Mo_8O_{26})(H_2O)_2]\cdot 4.5H_2O$	3.20	UV	MB	17.6	120	79	246
$[Cu(phen)_2]_4(W_{10}O_{32})$	—	Vis	RRN	11.2	60	19.9	251
$[Cu_6(PO_4)_2(H_2O)_4(phen)_6](P_2W_{18}O_{62})$	—	Vis	MO	15	120	98.35	252
$[Cu^{I}bbi]_4(SiW_{12}O_{40})\cdot H_2O$	—	UV	RhB	8.62	420	100	253
$[K_2(H_2O)_2Na_2(H_2O)_2Na_2(H_2O)_6](P_2W_{18}O_{62})(Me_{10}Q_5)_2\cdot 7H_2O$	—	Vis	MO	10	180	99.96	21
$[K_2(H_2O)_2Na_2(H_2O)_2Na_2(H_2O)_6](P_2W_{18}O_{62})(Me_{10}Q_5)_2\cdot 7H_2O$	—	Vis	RhB	10	120	91.32	21
$[CoCl_{0.5}(H_2O)_{0.5}(Hdppzc)_2](PW_{12}O_{40})_{0.5}\cdot 3.5H_2O$		Vis	RhB	10	80	90	254
$Cu^{I}_3(1,4\text{-biyb})_2(tpb)[PMo^{VI}_8V^{V}_4O_{40}(V^{IV}O)_2]\cdot 2H_2O$	—	UV	RhB	7.2	300	55	255
$CoH(bix)_4(PMo^{VI}_8V^{V}_4O_{40}(V^{IV}O)_2)$	—	UV	RhB	9.58	150	55	256
$[(H_2bix)_2(NaHP_2Mo_5O_{23})]\cdot 2H_2O$	—	UV	RhB	9.58	150	35	256
$H_2(bix)_4[Cd(H_2O)_4][Cd(HPO_4)_4(H_2PO_4)_4(MoO_2)_{12}(OH)_6]\cdot 10H_2O$	—	UV	RhB	9.58	150	47	256
$(H_2en)_3(Co_3P_4Mo_4O_{28})$	—	UV	RhB	9.58	150	43	256
$(H_2en)_2[Cu(pzca)_2(Mo_8O_{26})]\cdot 4H_2O$	—	UV	MB	17.6	300	73.5	257
$[Ni(bix)_2](VW_{12}O_{40})\cdot(H_2bix)\cdot H_2O$	—	UV	RhB	10	420	86.7	258
$[Co(bix)_2](VW_{12}O_{40})\cdot(H_2bix)\cdot 2H_2O$	—	UV	RhB	10	420	91.2	258
$[Ag_8(pbpb)_4(\alpha\text{-}Mo_8O_{26})(\beta\text{-}Mo_8O_{26})(H_2O)_3]\cdot H_2O$	2.50	UV	MB	3.2	90	75[c]	259
$Cu^{I}_4(btb)_2(m\text{-}OH)(PW_{12}O_{40})$	—	UV	MB	10	150	87	260
$[Cu^{II}_2(btb)_4(m\text{-}Cl)(PW_{12}O_{40})]\cdot 3H_2O$	—	UV	MB	10	150	85	260
$(C_5H_4NH)COOH]_3(PMo_{12}O_{40})$	—	UV	RhB	9.58	240	85[b]	211
$[Ag_7(bte)_4(H_2O)(HP_2W^{VI}_{16}W^{V}_2O_{62})]\cdot 2H_2O$	—	UV	MB	17.6	90	74.7	261
$[Ag_7(1,3\text{-btp})_5(HP_2W^{VI}_{16}W^{V}_2O_{62})]\cdot H_2O$	—	UV	MB	17.6	90	83.5	261
$[Ag_4(btb)_{3.5}(P_2W_{18}O_{62})](H_2btb)\cdot 2H_2O$	—	UV	MB	17.6	90	85.5	261
$[Cu_2(bpce)_3(SiMo_{12}O_{40})(H_2O)_6]\cdot 2H_2O$	—	UV	MB	10	240	82[b]	261
$[Cu_2(bpcb)_3(SiMo_{12}O_{40})(H_2O)_6]\cdot 9H_2O$	—	UV	MB	10	240	90[b]	262
$[Cu_2(bpcb)_3(SiW_{12}O_{40})(H_2O)_6]\cdot 6H_2O$	—	UV	MB	10	240	80[b]	262
$[Cu_2(bpch)_3(SiMo_{12}O_{40})(H_2O)_6]\cdot 4H_2O$	—	UV	MB	10	240	97[b]	262
$[Cu_2(bpch)_3(SiW_{12}O_{40})(H_2O)_6]\cdot 4H_2O$	—	UV	MB	10	240	80	262
$[Cu_3(2\text{-pytz})_2(4,4'\text{-bpy})_4(H_2O)_6](H_4SiW_{12}O_{40})_2\cdot 6H_2O$	—	UV	RhB	4.79	120	70	263
$[Cu_2(2\text{-pytz})(phen)\text{-}(OH)]_2(SiW_{12}O_{40})\cdot H_2O$	—	UV	RhB	4.79	120	61	263
$K_2[Ag_6(5\text{-pytz})_4](PW_{12}O_{40})$	—	UV	RhB	4.79	360	72	264
$[Ag_7(ptz)_4(NO_3)(H_2O)](H_4P_2W_{18}O_{62})\cdot 5H_2O$	—	UV	MB	0.64	180	86.1	264

Table 7 (*Contd.*)

MOF[a]	E_g (eV)	Irrigation	Organic pollutants	Initial concentration (mg L^{-1})	Time (min)	Degradation efficiency (%)	Ref.
$[Ag_6(ptz)_4(H_2O)_2](HPMo_{12}O_{40})\cdot 3H_2O$	—	UV	MB	0.64	180	42.7	265
$[Ag_7(ptz)_4](PW_{12}O_{40})\cdot 4H_2O$	—	UV	MB	0.64	180	93.7	233,265
$Co_6(\mu_3\text{-}OH)_3(H_2O)_9(bpyb)(PW_9O_{34})$	—	UV	MB	320	90	91.9	266
$[Cu(II)_2Cu(I)_3(OH)_4(H_2O)_2(tpt)_4](PW_{12}O_{40})$	—	Vis	$MO(H_2O_2)$	15	150	91	267
$[Cu(1,4\text{-}bimb)]_2(HPW_{12}O_{40})\cdot 3H_2O$	—	UV	RhB	10	180	72.6	268
$(1,4\text{-}H_2bimb)_2SiW_{12}O_{40}$	—	UV	RhB	10	180	66.8	268
$(1,4\text{-}H_2bimb)_3CoW_{12}O_{40}$	—	UV	RhB	10	180	58.9	268
$[Cu^{I}_8(bta)_4(Hbta)_8(SiMo_{12}O_{40})]\cdot 2H_2O$	—	UV	MB	320	140	91.5	269
$[Cu^{II}_6(OH)_4(bta)_4(SiW_{12}O_{40})(H_2O)_6]\cdot 6H_2O$	—	UV	MB	320	140	96.5	269
$[HMn^{II}(bix)_4](PMo^{VI}_8V^{V}_4O_{40}(V^{IV}O)_2)\cdot 2H_2O$	—	UV	RhB	9.58	210	60[b]	270
$[Zn(bix)_4](PMo^{VI}_9V^{V}_3O_{40}(V^{IV}O)_2)\cdot 2H_2O$	—	UV	RhB	9.58	210	88[b]	270
$[Cu(bix)_4](PMo^{VI}_9V^{V}_3O_{40}(V^{IV}O)_2)\cdot 4H_2O$	—	UV	RhB	9.58	210	88[b]	270
$[Cu^{I}(bix)]_2[Cu^{I}(bix)](bix)(PMo_{12}O_{40})\cdot 4H_2O$	—	UV	RhB	9.58	210	90[b]	270
$[Mn(salen)_2(H_2O)_2](AlMo_6(OH)_6O_{18})(arg)\cdot 16H_2O$	—	UV	RhB	9.58	300	100	271
$[Mn(salen)_2(H_2O)_2](CrMo_6(OH)_6O_{18})(arg)\cdot 11H_2O$	—	UV	RhB	9.58	300	99.6	271
$Cu^{II}(bbi)_{1.5}(H_2bbi)_2(P_2W_{18}O_{62})$	—	UV	RhB	8.6	360	71.6	272
$Cu^{II}_{2.5}(mimin)(Hmimin)(bbi)_3(P_2W_{18}O_{62})_3\cdot H_2O$	—	UV	RhB	8.6	360	61.2	272
$Cu^{II}(bbtz)(H_2bbi)(1,3\text{-}H_2btp)(P_2W_{18}O_{62})$	—	UV	RhB	8.6	360	86.2	272
$Ag_6Cl_2(mmt)_4(H_4SiMo_{12}O_{40})(H_2O)_2$	—	UV	MB	10	90	45[b]	273
$Ag_4(bmte)_2(H_2O)_2(SiMo_{12}O_{40})$	—	UV	MB	10	90	75[b]	273
$Ag_4(bmtr)_2(H_2O)_2(SiMo_{12}O_{40})$	—	UV	MB	10	90	80[b]	273
$Ag_4(bmtb)_3(SiMo_{12}O_{40})$	—	UV	MB	10	90	72[b]	273
$[Cu^{II}(1,2\text{-}bppmb)]_2H(BW_{12}O_{40})\cdot 4H_2O$	—	UV	RhB	20	40	91	274
$[Cu^{I}(1,2\text{-}bppmb)]_4(SiW_{12}O_{40})\cdot 5H_2O$	—	UV	RhB	20	40	91	274
$[Cu(1,4\text{-}bppmb)]_3H_2(BW_{12}O_{40})\cdot 5H_2O$	—	UV	RhB	20	40	91	274
$[Ag_3(3,3'\text{-}tmbpt)_2(\alpha\text{-}H_2Mo_8O_{26})_{0.5}(\beta\text{-}Mo_8O_{26})_{0.5}]\cdot 3.5H_2O$	2.94	UV	MB	16	90	80	275
$[Ag_2(3,3'\text{-}tmbpt)(\varepsilon\text{-}Mo_8O_{26})_{0.5}]\cdot 1.75H_2O$	2.96	UV	MB	16	90	91	275
$[Ag_2(3,4'\text{-}tmbpt)_2(\beta\text{-}Mo_8O_{26})_{0.5}]\cdot 0.5H_2O$	2.78	UV	MB	16	90	84	275
$Ag(3,4'\text{-}Htmbpt)(\beta\text{-}Mo_8O_{26})_{0.5}$	3.39	UV	MB	16	90	91	275
$[Zn(phen)_2(H_2O)]_2[VW_{12}O_{40}]\cdot 3H_2O$	—	UV	MB	10	90	90	276
$[Co_2(btb)_4(H_2O)][H_2P_2W_{18}O_{62}]\cdot 3H_2O$	—	UV	MB	10	120	91	277
$[Co_2(btb)_4(H_2O)][H_2As_2W_{18}O_{62}]\cdot 6H_2O$	—	UV	MB	10	120	84	277
$(NH_4)_2[Mn(salen)(H_2O)_2]_4[V_{10}O_{28}]\cdot 6H_2O$	—	UV	RhB	6.7	360	97.4	278
$K[La(H_2O)_4(2,6\text{-}pdc)]_4[BW_{12}O_{40}]\cdot 2H_2O$	3.11	UV	Thiophene	200	720	49	279
$K[Ce(H_2O)_4(2,6\text{-}pdc)]_4[BW_{12}O_{40}]\cdot 2H_2O$	3.11	UV	Thiophene	200	720	97	279
$K[Tb(H_2O)_3(2,6\text{-}pdc)]_4[BW_{12}O_{40}]\cdot 6H_2O$	3.11	UV	Thiophene	200	720	68	279
$K[Dy(H_2O)_3(2,6\text{-}pdc)]_4[BW_{12}O_{40}]\cdot 6H_2O$	3.11	UV	Thiophene	200	720	46	279
$K[Er(H_2O)_3(2,6\text{-}pdc)]_4[BW_{12}O_{40}]\cdot 6H_2O$	3.11	UV	Thiophene	200	720	42	279
$[Cu_2(2,2'\text{-}tmbpt)_2(SiW_{12}O_{40})]\cdot 9H_2O$	2.62	UV	MB	16	120	41	280
$[Cu2(2,3'\text{-}tmbpt)_2(SiW_{12}O_{40})]\cdot 6H_2O$	3.17	UV	MB	16	120	51	280
$[Cu_2(2,4'\text{-}tmbpt)_2(SiW_{12}O_{40})(H_2O)_2]\cdot 6.5H_2O$	3.00	UV	MB	16	120	58	280
$[Cu_2(4,4'\text{-}tmbpt)_2(SiW_{12}O_{40})(H_2O)_4]\cdot 13.5H_2O$	3.54	UV	MB	16	120	74	280
$[Cu(4,4'\text{-}Htmbpt)(4,4'\text{-}tmbpt)(PW_{12}O_{40})(H_2O)_2]\cdot 7H_2O$	2.71	UV	MB	16	120	81	280
$[Cu_2(2,2'\text{-}tmbpt)_2(SiW_{12}O_{40})]\cdot 9H_2O$	2.62	UV	RhB	19.2	120	51	280
$[Cu_2(2,3'\text{-}tmbpt)_2(SiW_{12}O_{40})]\cdot 6H_2O$	3.17	UV	RhB	19.2	120	—	280
$[Cu_2(2,4'\text{-}tmbpt)_2(SiW_{12}O_{40})(H_2O)_2]\cdot 6.5H_2O$	3.00	UV	RhB	19.2	120	55	280
$[Cu_2(4,4'\text{-}tmbpt)_2(SiW_{12}O_{40})(H_2O)_4]\cdot 13.5H_2O$	3.54	UV	RhB	19.2	120	56	280
$[Cu(4,4'\text{-}Htmbpt)(4,4'\text{-}tmbpt)(PW_{12}O_{40})(H_2O)_2]\cdot 7H_2O$	2.71	UV	RhB	19.2	120	74	280
$[Cu(dap)_2]_{5.5}(Y(\alpha\text{-}PW_{11}O_{39})_2)\cdot 4H_2O$	—	UV	RhB	9.58	840	79	281
$Na_6[Cu(gly)(H_2O)]_2[[Cu(H_2O)](H_2W_{12}O_{42})]\cdot 21H_2O$	—	UV	RhB	8.6	300	75	282
$Na[Na(H_2O)_6][Na(H_2O)_4]_3[[Cu(gly)_2]]_2(H_5(H_2W_{12}O_{42}))\cdot 8.5H_2O$	—	UV	RhB	8.6	300	60	282
$[Cu_4^{II}Cu_2^{I}(pzca)_6(HPCuMo_{11}O_{39})(H_2O)_6]\cdot 2H_2O$	—	UV	MB	10	210	50	283
$H[(bitdc)Ni(H_2O)_3]_2(IMo_6O_{24})\cdot 6H_2O$	—	UV	RhB	9.58	660	97.3	284
$[Cd(Htrz)_3]_2(SiW_{12}O_{40})\cdot 2H_2O$	3.16	UV	RhB	4.79	210	71	285
$Co(bpce)(H_2Mo_4O_{14})(H_2O)_2$	—	UV	MB	10	210	94.6	286
$Ni(bpce)(H_2Mo_4O_{14})(H_2O)_2$	—	UV	MB	10	210	90.5	286
$[Cu_3(btyb)_3(PMo_{12}O_{40})_2]\cdot 9H_2O$	2.70	UV	RhB	4.79	165	94.2	287
$[Cu_3(btyb)_3(PW_{12}O_{40})_2]\cdot 9H_2O$	3.13	UV	RhB	7.19	165	93.7	287
$[Mn(salen)(CH_3OH)_2]_3(PMo_{12}O_{40})$	—	UV	RhB	4.79	300	94.85	288
$[Mn(salen)(CH_3OH)_2]_3(PW_{12}O_{40})$	—	UV	RhB	4.79	300	77.08	288

Table 7 (*Contd.*)

MOF[a]	E_g (eV)	Irrigation	Organic pollutants	Initial concentration (mg L^{-1})	Time (min)	Degradation efficiency (%)	Ref.
$[Cu_2(SiW_{12}O_{40})(bpce)(phen)_2(H_2O)]\cdot 3H_2O$	—	UV	MB	10	240	84	289
$Cu_2(SiW_{12}O_{40})(bpcb)(phen)_2(H_2O)_4$	—	UV	MB	10	240	78	289
$[Cu_2(SiW_{12}O_{40})(bpch)(phen)_2(H_2O)_4]\cdot 6H_2O$	—	UV	MB	10	240	83	289
$(H_4teta)_4[Na[Mo^V{}_{12}(OH)_6(HPO_4)_7(PO_4)_7O_{24}]]\cdot 11H_2O$	—	UV	RhB	2	240	28.1	290
$(H_4teta)_4[Na[Mo^V{}_{12}(OH)_6(HPO_4)_7(PO_4)_7O_{24}]]\cdot 11H_2O$	—	Sunlight	RhB	2	240	21.2	290
$[Cu_6{}^I(ptz)_6](H_3PMo_{12}O_{40})\cdot 2H_2O$	—	UV	MB	10	180	99	291
$[Cu_6{}^I(ptz)_6](H_3PMo_{12}O_{40})\cdot 2H_2O$	—	UV	MB	10	180	67	291
$(en)(en)_4Zn_2Na[Na[Mo_6O_{16}(HPO_4)_3(PO_4)(OH)_3(H_2O)]_2]\cdot 3H_2O$	—	UV	RhB	100	240	82	292
$(SiMo_{12}O_{40})(H_2bipy)_2\cdot 2H_2O$	—	UV	MB	10	60	82	293
$(H_2bpp)_4[PW_{11}CuO_{39}](PW_{12}O_{40})$	—	UV	MB	10	90	60	294
$H_5(bpe)_3(SiW_{11}CoO_{39})\cdot 2H_2O$	—	UV	MB	10	90	93	294
$[(H_2toym)_4(Mo_8O_{26})_2]\cdot 15H_2O$	2.99	UV	MB	10	120	54.7	295
$[(H_2toym)_2(SiW_{12}O_{40})]\cdot 6H_2O$	2.65	UV	MB	10	120	80.4	295

[a] 4,4′-Bpy = 4,4′-bipyridine; dpa = 1,2-bis(4-pyridyl)-ethane; pzc = pyrazinecarboxylate; bbi = 1,1′-(1,4-butanediyl)bis(imidazole); 1,3-btp = 1,3-bis(1,2,4-triazol-1-yl)propane; *trans*-1,3-btp = *trans*-1,3-bis(1,2,4-triazol-1-yl)propane; 1,5-btp = 1,5-bis(1,2,4-triazol-1-yl)pentane; 1,6-bth = 1,6-bis(1,2,4-triazol-1-yl)hexane; Htrb = hexakis(1,2,4-triazol-ylmethy1)benzene; 2,4′-tmbpt = 1-((1*H*-1,2,4-triazol-1-yl)methyl)-3-(2-pyridyl)-5-(4-pyridyl)-1,2,4-triazole; htpmb = hexakis(3-(1,2,4-triazol-4-yl)phenoxy-methyl)benzene; phen = phenanthroline; Hdppzc = dipyrido[3,2-*a*:2′,3′-*c*]-phenazine-2-carboxylic acid; 1,4-biyb = 1,4-bis(imidazol-1-ylmethyl)benzene; tpb = 1,2,4,5-tetra(4-pyridyl)-benzene; bix = 1,4-bis(imidazol-1-ylmethyl)benzene; en = 1,2-ethylenediamine; Hpzca = 2-pyrazinecarboxylic acid; pbpb = 1,1′-(1,3-propanediyl)-bis[2-(4-pyridyl)benzimidazole; btb = 1,4-bis(1,2,4-triazol-1-yl)butane; bte = 1,2-bis(1,2,4-triazol-1-yl)ethane; bpce = *N*,*N*′-bis(3-pyridinecarboxamide)-1,2-ethane; bpcb = *N*,*N*′-bis(3-pyridinecarboxamide)-1,4-butane; bpch = *N*,*N*′-bis(3-pyridinecarboxamide)-1,6-hexane; 2-pytz = 2-(pyridyl)tetrazolate; 5-pytz = 5-(pyridyl) tetrazolate; ptz = 5-(3-pyridyl)tetrazole; bpyb = 4,4′-bis(1,2,4-triazol-1-ylmethyl)biphenyl; tpt = tris(4-pyridyl)triazine; 1,4-bimb = 1,4-bis(imidazol-1-ylmethyl)biphenyl; H_4bta = 1,2,4,5-benzenetetracarboxylic acid; Hbta = 1-*H*-1,2,3-benzotriazole; salen = *N*,*N*′-ethylene-bis(salicylideneiminate); mimin = methylimidazol; bbtz = 1,4-bis(triazol-1-ylmethyl)benzene; mmt = 1-methyl-5-mercapto-1,2,3,4-tetrazole; bmte = 1,2-bis(1-methyl-5-mercapto-1,2,3,4-tetrazole)ethane; bmtr = 1,3-bis(1-methyl-5-mercapto-1,2,3,4-tetrazole)propane; bmtb = 1,4-bis(1-methyl-5-mercapto-1,2,3,4-tetrazole)butane); 1,2-bppmb = 1,2-(bis(3-(2-pyridyl)pyrazole-1-ylmethyl)benzeneb; 1,4-bppmb = 1,4-(bis(3-(2-pyridyl) pyrazole-1-ylmethyl)benzeneb; 3,3′-tmbpt = 1-((1*H*-1,2,4-triazol-1-yl)methyl)-3,5-bis(3-pyridyl)-1,2,4-triazole; 3,4′-tmbpt = 1-((1*H*-1,2,4-triazol-1-yl) methyl)-3-(4-pyridyl)-5-(3-pyridyl)-1,2,4-triazole; 2,6-pdc = pyridine-2,6-dicarboxylate; 2,2′-tmbpt = 1-((1*H*-1,2,4-triazol-1-yl)methyl)-3,5-bis(2-pyridyl)-1,2,4-triazole; 2,3′-tmbpt = 1-((1*H*-1,2,4-triazol-1-yl)methyl)-3-(3-pyridyl)-5-(2-pyridyl)-1,2,4-triazole; 4,4′-tmbpt = 1-((1*H*-1,2,4-triazol-1-yl) methyl)-3,5-bis(4-pyridyl)-1,2,4-triazole; dap = 1,2-diaminopropane; gly = glycin; bitdc = *N*,*N*′-bis(isonicotinoyl)-*trans*-1,2-diaminocyclohexane; Htrz = 1-*H*-1,2,4-triazole; btyb = 4-bis(1,2,4-triazol-1-ylmethyl)-benzene; H_4teta = tetraprotonated triethylenetetramine; bpp = 1,3-di(4-pyridyl) propane); bpe = 1,2-di(4-pryridyl)ethylene; toym = 2,4,6-tris[1-(4-oxidroxypyridinium)-ylmethyl]-mesitylene. [b] Values estimated from original figures of the references.

in aqueous solution under visible light.[101] It was observed that the photocatalytic degradation of RhB (C_0 = 47.9 mg L^{-1}) and MB (C_0 = 31.9 mg L^{-1}) were finished after 80 and 20 min, respectively. NTU-9 also showed high photoactivity and good photostability. Ti(IV)-based MOFs thus act as promising candidates for the development of efficient visible light photocatalysts.

Inspired by the fact that some enzymes contain multiple metal-based catalytic units,[176] much effort has been made to synthesize catalyst materials containing bi-/multi-metallic centers. Li and co-workers prepared a bimetallic MOF, $[Cu^{II}(salimcy)](Cu^{I}I)_2\cdot DMF$, containing Cu(II)-salen-based units and Cu(I) iodide clusters, which was used to photocatalytically decompose organic dyes under visible light irradiation.[102] In order to investigate the role of Cu(II) and Cu(I) ions in the decomposition of organic dyes, they performed the degradation of MB in the presence of $[Cu^{II}(salimcy)](Cu^{I}I)_2\cdot DMF$ in the dark and under visible light irradiation. The results revealed that 65% and 95% of MB with an initial concentration of 12 mg L^{-1} were decomposed in the absence and presence of visible-light illumination, respectively. In the former case, the Cu(II) ions in $[Cu^{II}(salimcy)](Cu^{I}I)_2\cdot DMF$ were crucial in decomposing MB, as confirmed in other studies, in which Cu(II) ions were demonstrated to play a key catalytic role in oxidation reactions.[177] Meanwhile, under visible-light illumination, the degradation of MB was enhanced by the cooperative decomposition achieved by photoactive Cu(I) entities.[90] Similar situations have been observed in the decomposition of RhB and MO over this MOF.[102]

Similarly, Ru(II)–polypyridine complexes, as metallo-organic ligands, have also been explored in the application of a MOF-based multifunctional catalyst and other fields.[178–181] Luo and co-workers synthesized MOF $[InRu(dcbpy)_3]((CH_3)_2NH_2)\cdot 6H_2O$, which showed broad visible-light absorption and strong red luminescence emission based on the photoactive $Ru(dcbpy)_3{}^{2+}$ metalloligand.[182] The photocatalytic activity of this MOF was evaluated by the photodecomposition of methyl orange (MO), one of the most stable azo dyes. The results revealed that about 80% of MO molecules were decomposed in the presence of the MOF catalyst upon visible light irradiation for 120 min. The decomposition of MO might be attributed to the highly active hydroxyl radicals ($^{\bullet}OH$) that were generated during the redox cycles of the $[Ru(dcbpy)_3]^{4-}$ metalloligands. This MOF was also confirmed to be stable during photocatalysis.

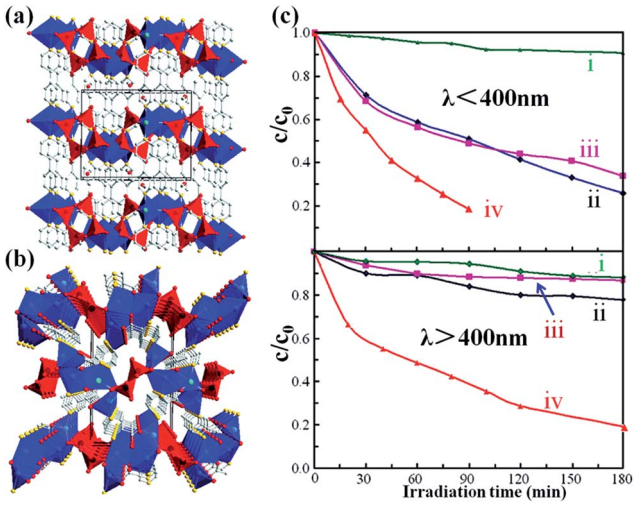

Fig. 13 (a) Structures of $[Ag(4,4'\text{-bpy})]_4V_4O_{12}\cdot 2H_2O$ viewed down the [001] direction of the unit cells (outlined). Blue polyhedra = Ag-centered coordination environments, red polyhedra = VO_4, red spheres = O, yellow spheres = N, white spheres = C, and light-blue spheres = Ag. (b) Polyhedral structural view of $Ag_4(pzc)_2V_2O_6$ down the [100] direction of the unit cell (outlined). Blue polyhedra = Ag-centered coordination environments, red polyhedra = VO_5, red spheres = O, yellow spheres = N, white spheres = C, and light-blue spheres = Ag. All H atoms are omitted for clarity. (c) Photocatalytic decomposition of MB solutions (6.0 mg L^{-1}, 50 mL) using 150 mg of the three silver vanadates, either under UV (upper) or under visible-light (lower) irradiation for $[Ag(4,4'\text{-bpy})]_4V_4O_{12}\cdot 2H_2O$ (ii), $[Ag(dpa)]_4V_4O_{12}\cdot 4H_2O$ (iii), $Ag_4(pzc)_2V_2O_6$ (iv). Photolysis of MB without the use of the photocatalysts (i). Reprinted (adapted) with permission from ref. 74. Copyright (2008) American Chemical Society.

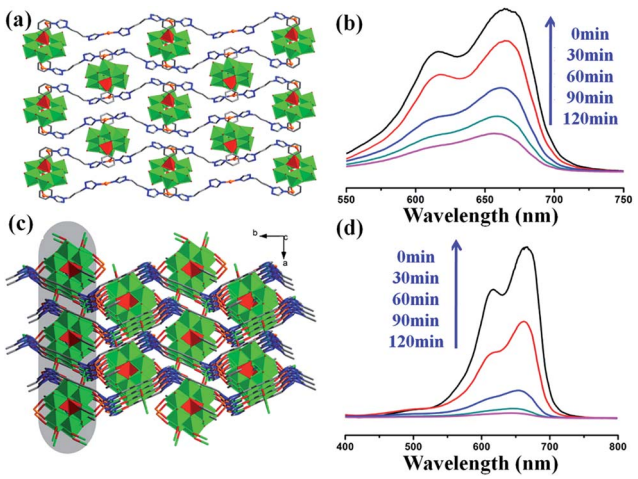

Fig. 14 (a) 2D highly undulated layer in $[Cu^I_2(1,3\text{-btp})_2][Cu^I_2(trans\text{-}1,3\text{-btp})_2Mo_6O_{18}(O_3AsPh)_2]$. (b) UV-vis absorption spectra of the MB solution during the decomposition reaction under UV light irradiation in the presence of $[Cu^I_2(1,3\text{-btp})_2][Cu^I_2(trans\text{-}1,3\text{-btp})_2Mo_6O_{18}(O_3AsPh)_2]$. (c) View of the 3D framework of $Cu^I_4(1,6\text{-bth})_2Mo_6O_{18}(O_3AsPh)_2$ formed by infinite chains and parallel layers. (d) UV-vis absorption spectra of the MB solution during the decomposition reaction under UV light irradiation in the presence of $Cu^I_4(1,6\text{-bth})_2Mo_6O_{18}(O_3AsPh)_2$. Reprinted (adapted) with permission from ref. 238. Copyright (2013) American Chemical Society.

On the other hand, one of the difficulties hindering the large-scale application of photocatalysts is their separation from reaction systems. Qiu and co-workers used magnetic Fe_3O_4 nanoparticles as the core to fabricate a Fe_3O_4@MIL-100(Fe) core–shell microsphere composite (Fig. 10a–d).[89] The magnetic properties of the material were investigated by vibrating sample magnetometry (VSM) (Fig. 10e), which showed a magnetic hysteresis loop, suggesting its strong magnetic response to a varying magnetic field. The magnetic separation of the composite was confirmed to be feasible by using an external magnetic field. The optical properties of the material were investigated by UV-vis diffuse reflectance spectroscopy. The result revealed that the main optical absorption band was around 485 nm, with strong visible light absorption ability. The photocatalytic degradation of MB dye in aqueous solution using Fe_3O_4@MIL-100(Fe) core–shell microspheres as the photocatalyst was investigated under UV-vis light and visible light irradiation, respectively. The results showed that this photocatalyst had remarkable photocatalytic activity for MB decolorization both under UV-vis and visible light irradiation, in comparison with typical photocatalysts, such as TiO_2 and C_3N_4 (Fig. 10f and g). It was found that without H_2O_2 the photodegradation efficiency of MB is very low, with about 35% degradation of MB being observed after 40 min of UV-vis light irradiation. When using H_2O_2, the photocatalytic efficiency of this catalyst was obviously improved, up to 99% MB degradation under similar conditions. This is due to the fact that H_2O_2 as the electron acceptor could suppress the electron–hole pair recombination, thus enhancing the photodegradation efficiency.

For comparison, the reaction kinetics of the MB degradation catalyzed by various photocatalysts was also studied. The experimental data was fitted by a first-order model as expressed by $-\ln(C/C_0) = kt$. As shown in Fig. 10f, Fe_3O_4@MIL-100(Fe) exhibited a higher rate constant of 0.1042 min^{-1} for the MB photodegradation under UV-vis irradiation, nearly three times larger than that of TiO_2 (0.0371 min^{-1}) under the same reaction conditions. Under visible light, the rate constant (0.01977 min^{-1}) when using Fe_3O_4@MIL-100(Fe) was 33 times more than that in C_3N_4 (6.074×10^{-4} min^{-1}, close to that in the literature[183]). The recycling reactions were carried out for the photodegradation of MB over Fe_3O_4@MIL-100(Fe) under visible light irradiation.[89] In five consecutive cycles, the MB photodegradation rate constant values were 0.0164, 0.0162, 0.0157, 0.0151, and 0.0146 min^{-1}, respectively, indicating that the Fe_3O_4@MIL-100(Fe) has good catalytic stability. The integrality of its structure was also identified by PXRD and UV-vis absorption spectra. A possible mechanism for the photocatalytic degradation of MB over Fe_3O_4@MIL-100(Fe) was also proposed, as illustrated in Fig. 12d. Just like the TiO_2 semiconductor whose CB is constructed by empty Ti 3d orbitals, MIL-100(Fe) containing transition metals were also expected to be semiconductors, since the empty d orbitals of metal ions mixed with the LUMOs of the organic linkers to form the CB. In the presence of light irradiation, the electron (e^-) can be excited from VB of MIL-100(Fe) to enter into its CB and produce holes (h^+) in the VB. The photoinduced electrons transfer to H_2O_2/

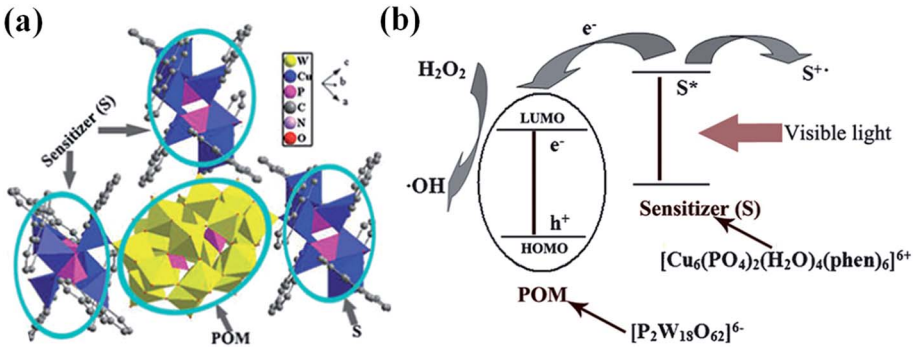

Fig. 15 (a) Relationships between the hexacopper phosphate cluster as the sensitizer and the Wells–Dawson polyoxoanions as the POM unit in CuPW. (b) Proposed photodegradation mechanism on CuPM. Reprinted (adapted) with permission from ref. 252. Copyright (2010) The Royal Society of Chemistry.

H_2O, giving rise to more ˙OH, which hindered the recombination of electrons and holes efficiently. The photogenerated holes with strong oxidation ability could directly oxidize adsorbed organic molecules, and the resulting ˙OH could also decompose MB molecules that were adsorbed on the surface of Fe_3O_4@MIL-100(Fe) particles. Anyway, Fe_3O_4@MIL-100(Fe) exhibited both excellent photodegradation performances and good magnetic characteristics, making it a good and feasible photocatalyst for the decolorization of organic pollutants in wastewater.

Zeolitic imidazolate frameworks (ZIFs), usually constructed from tetrahedrally coordinated divalent cations (Zn^{2+} or Co^{2+}) linked by imidazolate ligands, are a subclass of MOFs with high thermal and chemical stability, as well as tunable zeotype topologies.[184–186] Zhang and co-workers investigated ZIF-67 (ref. 187) (with a SOD structural topology as shown in Fig. 11a) and its Cu ion doped composite Cu/ZIF-67 for the photocatalytic degradation of methyl orange under visible-light illumination (MO).[91] It was found that the photocatalytic activity of Cu/ZIF-67 was gradually enhanced with time increasing from 0 to 25 min, as shown in Fig. 11b. After 25 min, the MO in the solution almost disappeared. Moreover, Cu/ZIF-67 was stable in repeated applications with a nearly constant photocatalytic degradation rate, which was confirmed by SEM images and PXRD as shown in Fig. 11c–g. In contrast, ZIF-67 couldn't achieve such a photocatalytic degradation. These results indicated the importance of Cu-doping in tuning the photocatalytic activity of ZIF-67, although both materials possess the same topological structures and similar band gaps (E_g = 1.98 and 1.95 eV for ZIF-67 and Cu/ZIF-67, respectively). Furthermore, electron paramagnetic resonance (EPR) tests indicated that no Cu^{2+} signal was observed in the spectra. Based on the obviously enhanced photocatalytic properties of MO, the presence of Cu^{+} ions in the structure of Cu/ZIF-67 was suggested.[188,189] Some reported examples also demonstrated that Cu^{2+} ions can be reduced into Cu^{+} ions under solvothermal conditions in the presence of heterocyclic ligands.[190] These Cu^{+} ions with potential tetrahedral coordination geometry might also replace some tetrahedral Co^{2+} sites in the host framework of ZIF-67, although the structural details are still unclear. In this work, a doping strategy was thus successfully applied to tune the photocatalytic properties of a ZIF material.

Following that, the same group reported the photocatalytic degradation of methyl orange in two new ZIFs, $[Zn_4(2\text{-mim})_6WO_4]\cdot 1.5(DMF)$ (HZIF-1W) and $[Zn_4(2\text{-mim})_6MoO_4]\cdot 2(DMF)$ (HZIF-1Mo) constructed from two kinds of tetrahedral building blocks, which combined structural features of both zeolites and ZIFs.[127] It is interesting that the TO_4 (T = W or Mo) units used in these HZIFs are not traditional SiO_4 or AlO_4 units as in aluminosilicate zeolites, but catalytically active MoO_4 or WO_4. To compare the photocatalytic activities, commercial TiO_2 and ZIF-8 were also employed for the degradation of methyl orange under the same conditions. The bandgap sizes of HZIF-1Mo, HZIF-1W, TiO_2 and ZIF-8 are 1.32, 2.2, 3.2 (ref. 159) and 4.9 eV,[127] respectively. It was observed that the degradation ratio of methyl orange was 5.9% (comparable to the control experiment without a catalyst), 19.8, 24.5, and 81.6% with ZIF-8, TiO_2, HZIF-1W, and HZIF-1Mo as photocatalysts, respectively, after 120 min under visible light irradiation. And, without the MoO_4^{2-} or WO_4^{2-} anions in the synthesis of HZIF-1Mo and HZIF-1W, the obtained ZIF-8 did not show any catalytic activity under similar conditions. The commercial TiO_2 showed lower activity than that of HZIF-1W and HZIF-1Mo, which can be attributed to the fact that TiO_2 has a weak absorption response towards visible light due to its wide band gap.

Because graphene can improve the photocatalytic activities of semiconductors by promoting the electron transfer and charge separation processes,[191–196] Li and co-workers explored the photocatalytic degradation of dye in the MOF–graphene composite.[197] They prepared MIL-53(Fe)–rGO (rGO = reduced graphene oxide) hybrids, FeMG-1, FeMG-2 and FeMG-3, with rGO content of *ca.* 1.3, 2.5, and 3.2 wt%, respectively, *via* a one-step solvothermal reaction. The photocatalytic activities of MIL-53(Fe), FeMG-1, FeMG-2, and FeMG-3 in the degradation of MB under UV light were investigated. The results revealed that FeMG-2 possessed the highest catalytic efficiency, in which 95% MB (C_0 = 30 mg L^{-1}) was decomposed, while 82% degradation of MB was achieved in the presence of MIL-53(Fe) under the same conditions. It implied that a suitable increase in rGO content could improve the photocatalytic efficiency of this type

of composite, but a further increase in rGO content might result in decreasing the degradation rate. A possible photocatalytic mechanism was proposed, where in the presence of light irradiation, MIL-53(Fe) absorbed light and was excited, and then the photo-induced electrons were transferred from the conduction band of MIL-53(Fe) to the rGO sheet. This process could efficiently separate the electrons and suppress electron–hole recombination. The electrons were then trapped by molecular oxygen to generate the superoxide radical ($^{\bullet}O_2^{-}$). Simultaneously, the holes (h^+) reacted with the hydroxyl ion (OH^-) or water molecules to form the hydroxyl radical ($^{\bullet}OH$). $^{\bullet}OH$ and $^{\bullet}O_2^{-}$ thus have strong oxidative ability to degrade MB molecules to form CO_2, H_2O, or other products. However, an excessive rGO could decrease photocatalytic activity because: (i) more rGO has stronger absorption towards light, so that less light was harvested by MIL-53(Fe), resulting in the production of fewer electrons, (ii) excessive rGO may promote recombination of electrons and holes.[198] Due to specific electrical and surface properties, excellent conductivity, and high surface area of graphene, it is quite interesting to study MOF-rGO hybrids for photocatalysis.[195,196,199–203]

On the other hand, the deposition of MOFs on substrates to fabricate MOF thin films has attracted much attention due to their potential applications in catalysis, sensors, and gas separation.[204–208] Li and co-workers fabricated the $Zn_3(btc)_2$ film by *in situ* microwave-assisted solvothermal synthesis.[98] The photocatalytic activity of this MOF film was evaluated by the photodegradation of MB dye under UV-vis and visible light irradiation. It was found that 99% of MB dye molecules (initial concentration 10 mg L^{-1}) could be degraded within 20 min in the presence of 0.5 mL H_2O_2 under UV-vis irradiation, while only 77% and 70% of MB were degraded using TiO_2 and H_2O_2 under the same conditions, respectively. It was also demonstrated that this film has good stability.

3. Organic pollutant degradation in f-block metal based MOFs

Compared with transition metal ions, lanthanide ions usually exhibited high coordination number and diverse connectivity, which could facilitate the formation of various and unpredicted structures of MOFs. Lanthanide MOFs are in an intermediate situation between the type of MOFs with photoluminescence localized on the organic linker and those behaving as semiconductors.[61] Lanthanide based MOFs are very promising because the organic linker could act as an antenna producing efficient photosensitization, as listed in Table 5.

$[Gd(5\text{-}NO_2\text{-bdc})(5\text{-}NO_2\text{-bdcH})](bpyo)_{0.5}\cdot 2H_2O$ was a rare example of a MOF with a 4f metal ion that exhibited a good photocatalytic activity for dye degradation under UV light.[157] It was confirmed this MOF was active in the decomposition of X3B under UV light irradiation with a rate constant of 0.1022 h^{-1}, while under visible light the rate was 0.0138 h^{-1}. Obviously, the photodegradation rate of X3B under visible light is much slower than that under UV light, implying that the photosensitization degradation reaction could be ignored under UV light.[213–215] It is interesting that TBA could depress the photodegradation rate of X3B in this MOF catalyst, indicating that the photocatalysis was predominately controlled through the attack of $^{\bullet}OH$ radicals, rather than a direct hole oxidation. The corresponding photocatalytic reaction mechanism was depicted in Fig. 12d. The HOMO was mainly contributed by 2p bonding orbitals of oxygen and the LUMO from empty Gd orbitals; charge transfer took place from oxygen to Gd upon photoexcitation. The HOMO demanded one electron to return to its stable state. Thus, one electron was captured from the water molecule, which was oxygenated into $^{\bullet}OH$. Then the $^{\bullet}OH$ radicals cleaved X3B effectively to finish the photocatalytic process.

Previous studies have shown that aqueous solutions of uranyl ions were photocatalytically active in the oxidation of organic substrates in the presence of air, but it was difficult to separate the uranyl ions from the reaction system, which rendered this catalyst system's practical application.[76,216–218] Therefore, it is interesting to synthesize water-insoluble uranyl-containing solid materials for photocatalytic applications. In this context, Chen and co-workers reported two uranyl-based MOFs, $Ag(2,2'\text{-bpy})(UO_2)(1,4\text{-bdc})_{1.5}$ and $Ag_2(phen)_2UO_2(btec)$, both of which were water-insoluble and active (than nanosized TiO_2 (P-25)) in the photocatalytic degradation of rhodamine B (RhB).[77] Fig. 12a and c showed the rate of RhB degradation in the aqueous solution in the presence of the two MOFs, respectively. After photocatalysis, both MOFs showed PXRD patterns nearly identical to those of the parent MOFs, indicating their stability towards photocatalysis. More importantly, $Ag(2,2'\text{-bpy})(UO_2)(1,4\text{-bdc})_{1.5}$ showed a remarkable photodegradation activity for RhB when a xenon lamp (wavelength longer than 400 nm) was used as the irradiation source (Fig. 12a and c). For comparison, the visible-light photocatalytic performance of P-25 was also tested, which showed only slight photocatalytic activity under xenon-light irradiation. In contrast, $Ag_2(phen)_2UO_2(btec)$ did not show any photocatalytic activity, even when irradiated under the xenon lamp for 240 min. The discrepancy in photocatalytic activities of the two MOFs can be attributed to their structural differences. The diffuse-reflectance UV/vis spectra revealed that $Ag(2,2'\text{-bpy})(UO_2)(1,4\text{-bdc})_{1.5}$ and $Ag_2(phen)_2UO_2(btec)$ had similar absorption features, consisting of absorption components in the UV and vis regions. The UV component was attributed to the charge-transfer electronic transition of the uranyl group, and the vis component responsible for the colors of the two MOFs arose from ligand-to-metal charge transfer (LMCT). In spite of similarities in UV/vis absorption behaviors, it could be noted that the charge-transfer transition of $Ag(2,2'\text{-bpy})(UO_2)(1,4\text{-bdc})_{1.5}$ occurred in the visible region, while that of $Ag_2(phen)_2UO_2(btec)$ lay in the near-UV region. The UV/vis absorptions of the two MOFs are clearly related to their structures. First, the uranium atoms are seven-coordinated in $Ag(2,2'\text{-bpy})(UO_2)(1,4\text{-bdc})_{1.5}$ and eight-coordinated in $Ag_2(phen)_2UO_2(btec)$. Fewer ligands around the uranium center in the former means less steric hindrance, which allows the access of more dye substrates to the U center. Secondly, the silver-centered moieties in $Ag(2,2'\text{-bpy})(UO_2)(1,4\text{-bdc})_{1.5}$ were packed almost parallel to the uranyl–organic layers, while in $Ag_2(phen)_2UO_2(btec)$, they occupied the interlayer

spaces. The larger interlayer region in the former makes it easier for the dye molecules accessing the active U centers, whereas the latter has a smaller interlayer region and fully coordinated U centers, which are unfavorable for access of the dye molecules. For the irradiation under visible light, the difference in photocatalytic activities mainly arose from the difference in visible-light excitations. The dependence of the photocatalytic activity on the structural features has also been demonstrated in other uranyl-containing MOFs $[Ni_2(H_2O)_2(qa)_2(4,4'\text{-bpy})_2U_5O_{14}(H_2O)_2(OAc)_2]\cdot 2H_2O$[71] and $(ZnO)_2(UO_2)_3(na)_4(OAc)_2$ (Hna = nicotinic acid).[218]

Furthermore, Chen and co-workers analyzed the total organic carbon (TOC) when the color of the solution completely disappeared in the catalysis of $Ag(2,2'\text{-bpy})(UO_2)(1,4\text{-bdc})_{1.5}$ and $Ag_2(phen)_2UO_2(btec)$ under UV irradiation.[77] The results revealed a TOC decrease of 34% and 40%, respectively, which showed that RhB was mineralized to a considerable extent in the presence of the two MOFs. The NO_3^- ions were detected in the degraded solution, suggesting the conversion of nitrogen in RhB into NO_3^-. The percentages of RhB converted into NO_3^- ions were about 30% and 34% after 40 min under UV and visible irradiation, respectively, in the presence of $Ag(2,2'\text{-bpy})(UO_2)(1,4\text{-bdc})_{1.5}$, and about 25% after 120 min under UV irradiation in $Ag_2(phen)_2UO_2(btec)$. Additionally, the formation of formic and acetic acids in the final products of the photocatalytic systems was also confirmed in these catalysis systems.

The intermediate species generated in the degradation of RhB photocatalyzed by $Ag(2,2'\text{-bpy})(UO_2)(1,4\text{-bdc})_{1.5}$ or $Ag_2(phen)_2UO_2(btec)$ were identified by positive-ion (M + H) mass spectra. It was found that the species with a m/z of 443.2 (RhB) transferred to those of 415.2 (*N*,*N*′,*N*″-triethylrhodamine), 387.1 (*N*,*N*′-diethylrhodamine), and 359.0 (*N*-ethylrhodamine), corresponding to stepwise loss of C_2H_5 moieties.[219,220] Decarboxylated species were also observed, confirmed by a mass spectrum signal at $m/z = 260.2$.[220] At the end of the photocatalytic reaction, an apparent decrease was noted in the signal intensity of $m/z = 443.2$, which indicated that RhB had effectively been photodegraded into other products with lower molecular weight.

Although photocatalysis in the two MOFs was carried out in heterogeneous systems, it was believed that the uranyl center photocatalytically behaved in a way similar to that in solution. The uranyl center in the two MOFs could be excited by photons, and then one electron in the HOMO jumped to the LUMO. Because the energies of the 5f, 6d, 7p, and 7s orbitals of uranium are comparable, it is quite difficult to determine the electron configuration and orbital combination in uranium compounds. The involved photocatalytic reaction mechanism was proposed in Fig. 12d. Despite the disputable electron configuration and orbital combination, it is clear that the double bonds between uranium and oxygen were involved in the photoexcitation. Because the HOMO is mainly contributed to by oxygen 2p bonding orbitals and the LUMO by empty uranium orbitals, charge transfer actually takes place from oxygen to uranium on photoexcitation to give uranium in +5 and oxygen in the −1 oxidation state, respectively. Presumably, the excited $^*UO_2^{2+}$ decays easily to its ground state. However, if some molecules are located within a reasonable range and have an appropriate orientation, for example RhB in this case, transitional active complexes could thus be formed. Thus, one α-hydrogen atom of the methylene group bonded to the nitrogen atom in RhB would give an electron and leave as a H^+ hole,[221] which is abstracted by uranyl species to result in the cleavage of the C–N bond and stepwise *N*-deethylation of RhB (Fig. 12b.) Since the HOMO is then reoccupied, the excited electron will remain in the LUMO until it is captured by electronegative substances such as molecular oxygen in solution, which would transform into a highly active peroxide anion and subsequently accomplish the further oxidation and total degradation of RhB.[222]

The role of oxygen in this photocatalysis mechanism was also studied by monitoring the photocatalytic activities. When the argon gas was bubbled into the system for 30 min before and during the irradiation, the photocatalytic reaction rate decreased rapidly in $Ag(2,2'\text{-bpy})(UO_2)(1,4\text{-bdc})_{1.5}$ and quickly dropped to zero in $Ag_2(phen)_2UO_2(btec)$. This result revealed that the presence of oxygen was essential for the photocatalytic reaction; otherwise, the U^V could not be oxidized back to U^{VI} for a new cycle. The peroxide anion formed from the molecular oxygen was an important intermediate for the further degradation of RhB. Furthermore, spin-trap ESR also demonstrated that no hydroxyl radicals are involved in these systems.

In addition, Jie and co-workers reported two other uranyl-based MOFs $(UO_2)_8(ndc)_{12}(4,4'\text{-bpyH}_2)_3(4,4'\text{-bpyH})_3$, and $(UO_2)_3O[Ag(2,2'\text{-bpy})_2]_2(ndc)_3$ with efficient photocatalytic activity towards RhB.[75] Typical UV/vis spectra of uranyl compounds usually consist of absorptions in both the UV region, arising from charge transfer electronic transition within the U=O bonds[223,224] and the visible region, resulting from ligand to metal charge transfer (LMCT) between the O (or N) atoms of the coordinating ligands and an empty orbital of the U(VI) ion.[225,226] The former is usually proven to be responsible for photocatalytic activities, in which RhB was degraded almost completely within 80 min under UV irradiation. While under visible light, it was demonstrated that the two MOFs had photocatalytic activities, but complete degradation of RhB can be achieved after 10 h under irradiation. Because the two MOFs have similar uranium contents of 33.6% and 30.9%, respectively, and similar structures, the similarity in their photocatalytic performances suggests that the uranyl units are responsible for their catalytic properties, whereas the Ag moieties are of less importance. However, the possibility to tune the catalytic properties of uranyl-containing materials by assembling other metal ions or nonmetal species is not excluded.[227] In this study, the impact of oxygen on the photocatalytic degradation reaction was also addressed. It was found that under visible irradiation, the RhB degraded at a constant rate in the first 3 h in the presence of various oxygen contents, but after that the rate increase lagged behind the rise in oxygen concentration.

Mixed-metal MOFs, particularly for d–f systems, are proposed to be much more effective in the photocatalytic degradation of dyes; the synthesis of these MOFs is however difficult. Up to now, only a few examples were

documented.[76,228,229] Natarajan and co-workers synthesized three 3d–4f MOFs, $M(H_2O)_3Co(pda)_3$ (M = Gd, Dy, and Y), consisting of a network of $MO_6(H_2O)_3$ and Co_3N_3 polyhedral units, with a band gap of 3.7 eV.[67] Compared to commercial TiO_2 (Degussa P-25), all these MOFs showed good photocatalytic activity for the decomposition of RBBR and OG. In order to quantify these reactions, the kinetics were determined by the Langmuir–Hinshelwood (L–H) method, $r_0 = k_0C_0/(1 + K_0C_0)$. The values of k_0 and K_0 in the degradation of the two dyes in these MOFs are shown in Table 6. For the degradation of RBBR the rate coefficient k_0 varied in the order $Y(H_2O)_3Co(pda)_3$ > $Dy(H_2O)_3Co(pda)_3$ > $Gd(H_2O)_3Co(pda)_3$, but for OG the order was $Gd(H_2O)_3Co(pda)_3$ > $Dy(H_2O)_3Co(pda)_3$ > $Y(H_2O)_3Co(pda)_3$. It is clear that in spite of having comparable band gaps, the degradation rates of the two dyes are different and depend on the MOFs. Furthermore, the degradation of another two azo dyes (methyl red and methyl orange) was investigated by using these MOFs. The degradation rates followed the order $Gd(H_2O)_3Co(pda)_3$ > $Dy(H_2O)_3Co(pda)_3$ > $Y(H_2O)_3Co(pda)_3$, the same as that of OG, confirming the high selectivity of $Gd(H_2O)_3Co(pda)_3$ for the azo dyes. These results also indicated that these three MOFs are not only photocatalytically active but also selective towards specific organic functional groups. The differences in the activities might be due to the differences in the efficiency of the electron transfers from the organic dyes to the carboxylate radicals of MOFs.

According to previous studies,[160,230,231] the low-spin Co^{3+} complexes usually possess ligand-field (LF), intraligand (IL) and charge-transfer (CT) excited states. Among them, the IL and CT states are active when nitrogen containing aromatic ligands are involved in bonding with Co^{3+}. In $M(H_2O)_3Co(pda)_3$, a similar situation existed in Co^{3+} species. The room temperature diffuse reflectance UV-vis spectra for these MOFs showed three peaks. The absorption band at 304 nm can be assigned to LMCT; another two peaks at 381 and 516 nm can be assigned to the d–d transition of the Co^{3+} ions. It is clear that the lanthanide ions in these MOFs do not participate effectively in the electron transfer because their f orbitals are well shielded from other ions. The photocatalytic effect of these MOFs should thus originate from Co^{3+} ions, even if it is difficult to ascertain precisely their electronic energy levels. Of the three types of electronic transfer states observed in these MOFs, the LMCT effect in the UV region is thus responsible for the observed photocatalytic activity. A similar mechanism had also been proposed in other 3d–5f mixed-metal systems for the degradation of organic dyes.[77]

4. Organic pollutant degradation in polyoxometalate (POM) based MOFs

Polyoxometalates (POMs), as metal-oxide clusters of early transition metals Mo, W, V, and so on have been widely investigated in various fields.[232–237] One of the attractive properties of POMs was photocatalytic activity,[238–240] which could photocatalytically break down the organic pollutants into non-polluting small molecules.[74,119,241,242] However, there are two main drawbacks slowing down the development of POMs acting as catalysts. (i) High solubility makes them difficult to recover and recycle;[243] (ii) most POMs showed low visible light photocatalytic activity because of a high energy gap between the well-defined HOMO and LUMO. It was found that only less than 5% of the solar light could usually be utilized, which restricts their application in photocatalysis.[244] In recent years, the introduction of POMs into MOFs has been emerging as one of the most promising strategies for optimizing the performance of POMs in catalysis.[234,235] Some MOFs constructed with POMs and organic ligands indeed showed good photocatalytic activities in the degradation of organic dyes,[238,245–248] as shown in Table 7.

Maggard and co-workers reported three silver-vanadate based MOFs, $[Ag(4,4'\text{-bpy})]_4V_4O_{12}\cdot 2H_2O$, $[Ag(dpa)]_4V_4O_{12}\cdot 4H_2O$, and $Ag_4(pzc)_2V_2O_6$, which were photocatalytically active in the decomposition of MB under UV/visible light.[74] As shown in Fig. 13a and c, $[Ag(4,4'\text{-bpy})]_4V_4O_{12}\cdot 2H_2O$ and $[Ag(dpa)]_4V_4O_{12}\cdot 4H_2O$ are constructed from neutral 2D $[Ag_4V_4O_{12}]_n$ layers pillared through the 4,4′-bpy ligands through coordinating to the Ag sites in each layer; but $Ag_4(pzc)_2V_2O_6$ is composed of a 3D $[Ag_2(ptz)^+]_n$ network containing $[VO_3^-]_n$ chains. As reported previously,[296–298] heterometallic oxides containing both d^0 and d^{10} transition metals usually showed a small optical bandgap with the absorption of visible-light, which could be used to drive the photocatalytic reaction. The three MOFs contained either 2D or 3D. "Ag_xVO_3" entities should have photocatalytic reactivity. The UV-vis diffuse reflectance revealed the optical bandgap values of 2.77, 2.95, and 2.45 eV in $[Ag(4,4'\text{-bpy})]_4V_4O_{12}\cdot 2H_2O$, $[Ag(dpa)]_4V_4O_{12}\cdot 4H_2O$, and $Ag_4(pzc)_2V_2O_6$, respectively. Photocatalytic studies demonstrated that these MOFs could efficiently decompose MB, at rates of 1.01, 0.64 and 2.65 mg L^{-1} H^{-1}, respectively. It is interesting that the photocatalytic activities of $[Ag(4,4'\text{-bpy})]_4V_4O_{12}\cdot 2H_2O$ and $[Ag(dpa)]_4V_4O_{12}\cdot 4H_2O$ are limited in the UV light region owing to their large bandgaps, while $Ag_4(pzc)_2V_2O_6$ is active under both UV and visible-light irradiation because of its smaller bandgap (Fig. 13c). It was found that $Ag_4(pzc)_2V_2O_6$ could achieve a 80% removal of MB after 180 min under visible-light irradiation, at a rate of 1.20 mg L^{-1} H^{-1}. It is worth noting that the photocatalytic rate of $Ag_4(pzc)_2V_2O_6$ under either UV or visible light is higher than $[Ag(4,4'\text{-bpy})]_4V_4O_{12}\cdot 2H_2O$ and $[Ag(dpa)]_4V_4O_{12}\cdot 4H_2O$. These results suggested that the cooperative effect from these complicated vanadate and Ag-oxide/organic chains aided in the transport of excited holes–electrons to the surface to initiate the photocatalytic degradation of MB.

Similarly, Ma and co-workers reported four MOFs $[Cu^I_2(1,3\text{-btp})_2][Cu^I_2(\textit{trans}\text{-}1,3\text{-btp})_2Mo_6O_{18}(O_3AsPh)_2]$ (**1**), $Cu^I_4(1,4\text{-btp})_4Mo_6O_{18}(O_3AsPh)_2$ (**2**), $Cu^I_4(1,5\text{-btp})_4Mo_6O_{18}(O_3AsPh)_2$ (**3**), and $Cu^I_4(1,6\text{-bth})_2Mo_6O_{18}(O_3AsPh)_2$ (**4**) constructed from $[Mo_6O_{18}(O_3AsPh)_2]^{4-}$ units and copper–organic fragments, with band gaps (E_g) of 2.6, 2.7, 2.1 and 1.9 eV, respectively.[238] The photocatalytic degradation experiments of MB revealed that the activities of **1**, **3**, and **4** increased from 35% (without catalysts) to 76%, 93%, and 97%, respectively, while **2** did not show any activity in degradation. Notably, although **1–3** have overall 3D structures, the extended As_2Mo_6-containing entities in **1** are different from those in **2** and **3**. The former contained the only

2D $[Mo_6O_{18}(O_3AsPh)_2]^{4-}$ (as As_2Mo_6) layer. However, in **3** and **4**, the $As_2Mo_6^-$ containing structures showed the 3D polycatenated framework and the 3D tetranodal (3,4,6)-connected framework, respectively. Obviously, in **3** and **4**, the photocatalytically active As_2Mo_6 polyoxoanions were distributed over the whole 3D framework, as shown in Fig. 14a and c. The photocatalytic results of **1**, **3**, and **4** indicated that the more extended 3D As_2Mo_6-containing frameworks of the latter two had an advantage over the 2D As_2Mo_6-containing layer of the former during the photocatalytic decomposition reaction with MB. In other words, the more extended $As_2Mo_6^-$ containing frameworks of **3** and **4** favored the transport of excited holes–electrons to the surfaces to initiate the photocatalytic decomposition reaction with MB,[238] as illustrated in Fig. 14b and d. After the photocatalytic reactions, the PXRD patterns were used in order to evaluate the photostabilities of the MOFs **1**, **3**, and **4**. The PXRD patterns were nearly identical to those of the original MOFs, implying that these three MOFs could be used as stable photocatalysts for the photodegradation of MB. Similar results could be found in other works reported by Ma and co-workers.[245–247,249]

$[Cu_6(PO_4)_2(H_2O)_4(phen)_6](P_2W_{18}O_{62})$ (CuPW) constructed from Wells–Dawson polyoxometalates and hexacopper phosphates is another POM-based MOF, showing efficient photocatalytic activity in the degradation of MO, reported by Cao and co-workers.[252] The visible light diffuse reflectance spectrum of CuPW showed a broad band centered at 690 nm, implying that the charge transfer existed between $[Cu_6(PO_4)_2(H_2O)_4(phen)_6]^{6+}$ and $(P_2W_{18}O_{62})^{6-}$. It was proposed that in this MOF, $[Cu_6(PO_4)_2(H_2O)_4(phen)_6]^{6+}$ units can act as a sensitizer (S), being induced by visible light, then the electrons can transmit into the LUMO of $(P_2W_{18}O_{62})^{6-}$ from them and deposit in its LUMO. The POM core is just like an electron reservoir, which could undergo electron-reduction processes without deforming the whole framework, as illustrated in Fig. 15a and b. In addition, in this system the adsorbed H_2O_2 could easily trap an electron in the LUMO of the POM anion to yield the oxidizing species $^{\bullet}OH$ radicals, which degrade dye molecules.

It is also interesting to combine POM with lanthanide ions due to their unusual coordination characteristics and exceptional optical and magnetic properties arising from 4f electrons.[299–301] It was found that the introduction of Ln(III)-ligand entities could enhance the photocatalytic activity of POMs, being similar to the case that lanthanide ions have the ability to enhance the photocatalytic activity of TiO_2.[302–304] Chen and co-workers reported three α-Keggin heteropolymolybdate based MOFs, $[2,6\text{-pdc}]_3(PMo_{12}O_{40})$, $[Sm(H_2O)_4(2,6\text{-pdc})]_3[Sm(H_2O)_3(2,6\text{-pdc})]\text{-}(SiMo_{12}O_{40})\cdot 3H_2O$, and $[La(H_2O)_4(2,6\text{-pdc})]_4(PMo_{12}O_{40})F$, which are active in the photocatalytic degradation of RhB.[211] The results revealed that the decomposition efficiencies of RhB over the latter two MOFs were higher than the former one. This result showed that the photocatalytic ability of a POM-based MOF can be enhanced by adding lanthanide ions into its structure, being comparable to those in TiO_2 based systems. It is proposed that in the latter two MOFs, lanthanide ions could be used as an electron trapper under UV irradiation, thereby decreasing the recombination rate of photo-generated electron–hole pairs, and increasing the quantum yield of the photocatalytic process.[305] In contrast, Wang and co-workers showed that the lanthanide ions could effectively prohibit the photodegradation of RhB in MOFs $[La(2,5\text{-Hpdc})(2,5\text{-pdc})(H_2O)_6La(2,5\text{-}H_2pdc)_{0.5}(\alpha\text{-}PW_{11}O_{39}H)La(H_2O)_4]_2\cdot 8H_2O$, $[Ce(2,5\text{-Hpdc})(2,5\text{-pdc})(H_2O)_6\ Ce(2,5\text{-}H_2pdc)_{0.5}(\alpha\text{-}PW_{11}O_{39}H)Ce(H_2O)_4]_2\cdot 12H_2O$, and $[Pr(2,5\text{-Hpdc})(2,5\text{-pdc})(H_2O)_6Pr(2,5\text{-}H_2pdc)_{0.5}\text{-}(\alpha\text{-}PW_{11}O_{39}H)Pr(H_2O)_4]_2\cdot 8H_2O$.[306] It was explained as: (i) these MOFs can absorb the UV irradiation; and (ii) the hydrogen bonding and weak π–π stacking interactions between RhB and these MOFs can enhance the chemical stability of RhB, finally resulting in its slow photodegradation.[307]

5. Conclusion and outlooks

MOFs are a class of new inorganic–organic materials constructed from well-defined molecular building blocks of metal-containing nodes and organic linkers. The ability to design a framework structure and incorporate molecular functional components into MOFs has opened the door for their various potential applications. Emerging research has demonstrated MOFs to be a new class of photocatalyst for potential applications in the environmental field, such as in organic pollutant degradation. Compared with conventional semiconductor photocatalytic systems, the photoactive MOF systems have some advantages in degrading organic pollutants: (i) versatile synthetic strategies, including solvothermal, vapor diffusion, emulsion-assistant precipitation, ultrasonication, and even post-synthesis modification, allow a high degree of crystalline quality and morphologies of MOFs photocatalysts; (ii) the well-defined crystalline structures of MOFs are beneficial in the characterization and study of the structure–property relationship of these solid photocatalysts; (iii) the modular nature of the MOFs synthesis allows the rational design and fine tuning of these catalysts at the molecular level, making the electronic structure of the MOFs catalysts to be easily tailored; (iv) the structural features of tunable active sites (*i.e.*, metal-oxoclusters and organic linkers) in MOFs lead to more efficient solar harnessing; (v) the intrinsic porosity and high surface area of MOFs can facilitate the diffusion of the pollutant and product molecules through their open channels, where active catalytic sites are located, thereby reaching a high efficiency of the catalytic reaction; (vi) different from typical TiO_2-based catalysts, the visible light photocatalytic activity can be easily introduced *via* the linker substitutions of organic chromophores in MOF structures, such as with an amino group;[61,174,308–310] (vii) the combination of the photocatalytic properties of TiO_2 with the strong adsorbing properties of some MOFs (like ZIF-8) can generate composite materials with enhanced catalytic efficiency and better visible light response.[311] Further development of these new photocatalysts will require a better understanding of the photochemical mechanisms in MOF materials and the crucial structural parameters controlling their photocatalytic activity. It should be pointed out that some MOFs were labeled as semiconductors based on their optical transition properties and electrochemical and photochemical activities.[61,312,313] However, recently Gascon and co-workers pointed out that such

semiconducting behavior only occurs in a very limited subset of MOFs.[72] In the photocatalysis, MOFs should be treated as molecular catalysts rather than as typical semiconductors.[72,314] To understand the photocatalysis mechanisms of MOFs, they suggested that HOMO–LUMO gap terminology should be utilized to describe the discrete character of the light-induced transitions in the MOFs.[72] In all, we believe that the MOFs are promising for use in wastewater treatment,[315] and to this end they could serve as an ideal choice for light harvesting to achieve the photocatalytic degradation of organic pollutants.[311]

Up to now, it is difficult to perform a high-throughput synthesis in kilogram quantities in a matter of hours at ambient pressure, which is an impediment in the achievement of practical applications of MOFs. The commonly used solvothermal methods, involving the use of autoclaves and slow-diffusion processes, take days or weeks to complete a MOF synthesis reaction, making the industrial preparation of these materials difficult.[1,316] On the other hand, the relatively poor stability is an additional disadvantage of most MOFs. Particularly, many MOFs are known to be unstable in the presence of water,[317] which limits their practical applications in solar energy utilization. Some MOFs based on "hard" metal ions (like Zr^{4+}, Ti^{4+}, and Fe^{3+}) linked by organic carboxylate ligands (*e.g.* UiOs, MIL-140, −125, −101), or soft metal ions (like Zn^{2+}) with imidazolate linkers (*e.g.* ZIFs) have however shown high stability in aqueous solutions. The development of these stable MOFs is thus promising and urgently required for their practical applications, such as photocatalytic pollutant degradation in wastewater treatment. In addition, most MOFs also suffer from weak mechanical properties, bad processability, and low electric conductivity, all of which hinder the integration of MOFs into functional solar devices.[262] Therefore, to get cheap, stable, and efficient MOFs served as photocatalysts for practical applications is still a challenge.

Availability of the cheap starting materials and the feasibility of obtaining products with high yield and high purity should be considered when designing new MOFs. Simultaneously, synthetic methods should be developed to obtain low-cost MOFs. Particularly, the choice of ligands and metal salts is significant in designing novel MOFs for photocatalysis, which determines the efficiency of their applications. Finally, we hope these new materials with high working capacity in photocatalysis can serve as alternatives to replace commercially-available metal oxides and sulfide catalysts. In the future, MOFs might be one of the most powerful photocatalysts for the green environment.

Acknowledgements

We thank the financial support from the Natural Science Foundation of China (no. 21271015, 21322601), the Program for New Century Excellent Talents in University (no. NCET-13-0647), the Beijing Municipal Natural Science Foundation (no. 2132013), the Beijing Natural Science Foundation & Scientific Research Key Program of Beijing Municipal Commission of Education (KZ201410016018), the Training Program Foundation for the Beijing Municipal Excellent Talents(2013D005017000004), the Importation & Development of High-Caliber Talents Project of Beijing Municipal Institutions (CIT&CD201404076), the China Postdoctoral Science of Foundation (2013M540831), and Academic Innovation Team of BUCEA.

References

1 A. A. Adeyemo, I. O. Adeoye and O. S. Bello, *Toxicol. Environ. Chem.*, 2012, **94**, 1846–1863.
2 G. Liu, X. Li, J. Zhao, H. Hidaka and N. Serpone, *Environ. Sci. Technol.*, 2000, **34**, 3982–3990.
3 G. L. Baughman and E. J. Weber, *Environ. Sci. Technol.*, 1994, **28**, 267–276.
4 J. Levec and A. Pintar, *Catal. Today*, 2007, **124**, 172–184.
5 I. Ali, M. Asim and T. A. Khan, *J. Environ. Manage.*, 2012, **113**, 170–183.
6 W.-T. Tsai, H.-C. Hsu, T.-Y. Su, K.-Y. Lin, C.-M. Lin and T.-H. Dai, *J. Hazard. Mater.*, 2007, **147**, 1056–1062.
7 C. Wang, J. Zhang, P. Wang, H. Wang and H. Yan, *Desalin. Water Treat.*, 2014, DOI: 10.1080/19443994.2013.873881.
8 S. Allen and B. Koumanova, *J. Univ. Chem. Technol. Metall.*, 2005, **40**, 175–192.
9 D. Wang, T. Silbaugh, R. Pfeffer and Y. Lin, *Powder Technol.*, 2010, **203**, 298–309.
10 D. Lin, Q. Zhao, L. Hu and B. Xing, *Chemosphere*, 2014, **103**, 188–196.
11 P. Padmanabhan, K. Sreekumar, T. Thiyagarajan, R. Satpute, K. Bhanumurthy, P. Sengupta, G. Dey and K. Warrier, *Vacuum*, 2006, **80**, 1252–1255.
12 U. I. Gaya and A. H. Abdullah, *J. Photochem. Photobiol., C*, 2008, **9**, 1–12.
13 M. N. Chong, B. Jin, C. W. Chow and C. Saint, *Water Res.*, 2010, **44**, 2997–3027.
14 H. Yang and H. Cheng, *Sep. Purif. Technol.*, 2007, **56**, 392–396.
15 J. Lu, T. Zhang, J. Ma and Z. Chen, *J. Hazard. Mater.*, 2009, **162**, 140–145.
16 H. Coleman, C. Marquis, J. Scott, S.-S. Chin and R. Amal, *Chem. Eng. J.*, 2005, **113**, 55–63.
17 D. H. Bremner, R. Molina, F. Martínez, J. A. Melero and Y. Segura, *Appl. Catal., B*, 2009, **90**, 380–388.
18 M. I. Litter, *Appl. Catal., B*, 1999, **23**, 89–114.
19 G. Li, Z. Wang, M. Yu, Z. Quan and J. Lin, *J. Solid State Chem.*, 2006, **179**, 2698–2706.
20 G. Li, M. Yu, Z. Wang, J. Lin, R. Wang and J. Fang, *J. Nanosci. Nanotechnol.*, 2006, **6**, 1416–1422.
21 J. Lü, J.-X. Lin, X.-L. Zhao and R. Cao, *Chem. Commun.*, 2012, **48**, 669–671.
22 M. R. Hoffmann, S. T. Martin, W. Choi and D. W. Bahnemann, *Chem. Rev.*, 1995, **95**, 69–96.
23 T. L. Thompson and J. T. Yates, *Chem. Rev.*, 2006, **106**, 4428–4453.
24 A. Mills and S. Le Hunte, *J. Photochem. Photobiol., A*, 1997, **108**, 1–35.
25 K. Ayoub, E. D. van Hullebusch, M. Cassir and A. Bermond, *J. Hazard. Mater.*, 2010, **178**, 10–28.

26 U. Akpan and B. Hameed, *J. Hazard. Mater.*, 2009, **170**, 520–529.
27 J. J. Du, Y. P. Yuan, J. X. Sun, F. M. Peng, X. Jiang, L. G. Qiu, A. J. Xie, Y. H. Shen and J. F. Zhu, *J. Hazard. Mater.*, 2011, **190**, 945–951.
28 K. Nakata and A. Fujishima, *J. Photochem. Photobiol., C*, 2012, **13**, 169–189.
29 A. Janczyk, E. Krakowska, G. Stochel and W. Macyk, *J. Am. Chem. Soc.*, 2006, **128**, 15574–15575.
30 A. Y. Nosaka, E. Kojima, T. Fujiwara, H. Yagi, H. Akutsu and Y. Nosaka, *J. Phys. Chem. B*, 2003, **107**, 12042–12044.
31 A. Fujishima, X. Zhang and D. A. Tryk, *Int. J. Hydrogen Energy*, 2007, **32**, 2664–2672.
32 R. Wang, K. Hashimoto, A. Fujishima, M. Chikuni, E. Kojima, A. Kitamura, M. Shimohigoshi and T. Watanabe, *Nature*, 1997, **388**, 431–432.
33 C. Wang, H.-Y. Li, G.-L. Guo and P. Wang, *Transition Met. Chem.*, 2013, **38**, 275–282.
34 C. Wang, G.-L. Guo and P. Wang, *Transition Met. Chem.*, 2013, **38**, 455–462.
35 C. Wang, G. Guo and P. Wang, *J. Mol. Struct.*, 2012, **1032**, 93–99.
36 C. Wang, Z. Wang, F. Gu and G. Guo, *J. Mol. Struct.*, 2011, **1004**, 39–44.
37 C. Wang, P. Wang and G. Guo, *Transition Met. Chem.*, 2010, **35**, 721–729.
38 C. Wang, Z. Wang, F. Gu and G. Guo, *J. Mol. Struct.*, 2010, **979**, 92–100.
39 J. Lee, O. K. Farha, J. Roberts, K. A. Scheidt, S. T. Nguyen and J. T. Hupp, *Chem. Soc. Rev.*, 2009, **38**, 1450–1459.
40 C.-Y. Sun, S.-X. Liu, D.-D. Liang, K.-Z. Shao, Y.-H. Ren and Z.-M. Su, *J. Am. Chem. Soc.*, 2009, **131**, 1883–1888.
41 R. J. Kuppler, D. J. Timmons, Q.-R. Fang, J.-R. Li, T. A. Makal, M. D. Young, D. Yuan, D. Zhao, W. Zhuang and H.-C. Zhou, *Coord. Chem. Rev.*, 2009, **253**, 3042–3066.
42 X.-S. Wang, S. Ma, D. Sun, S. Parkin and H.-C. Zhou, *J. Am. Chem. Soc.*, 2006, **128**, 16474–16475.
43 J.-R. Li, J. Yu, W. Lu, L.-B. Sun, J. Sculley, P. B. Balbuena and H.-C. Zhou, *Nat. Commun.*, 2013, **4**, 1538.
44 J.-R. Li, J. Sculley and H.-C. Zhou, *Chem. Rev.*, 2011, **112**, 869–932.
45 J.-R. Li and H.-C. Zhou, *Nat. Chem.*, 2010, **2**, 893–898.
46 J.-R. Li, D. J. Timmons and H.-C. Zhou, *J. Am. Chem. Soc.*, 2009, **131**, 6368–6369.
47 J.-R. Li, R. J. Kuppler and H.-C. Zhou, *Chem. Soc. Rev.*, 2009, **38**, 1477–1504.
48 L. Pan, D. H. Olson, L. R. Ciemnolonski, R. Heddy and J. Li, *Angew. Chem.*, 2006, **118**, 632–635.
49 N. L. Rosi, J. Eckert, M. Eddaoudi, D. T. Vodak, J. Kim, M. O'Keeffe and O. M. Yaghi, *Science*, 2003, **300**, 1127–1129.
50 J. L. Rowsell and O. M. Yaghi, *Angew. Chem., Int. Ed.*, 2005, **44**, 4670–4679.
51 D. J. Collins and H.-C. Zhou, *J. Mater. Chem.*, 2007, **17**, 3154–3160.
52 S. Ma and H.-C. Zhou, *Chem. Commun.*, 2010, **46**, 44–53.
53 K. Sumida, D. L. Rogow, J. A. Mason, T. M. McDonald, E. D. Bloch, Z. R. Herm, T.-H. Bae and J. R. Long, *Chem. Rev.*, 2011, **112**, 724–781.
54 J.-R. Li, Y. Ma, M. C. McCarthy, J. Sculley, J. Yu, H.-K. Jeong, P. B. Balbuena and H.-C. Zhou, *Coord. Chem. Rev.*, 2011, **255**, 1791–1823.
55 A. R. Millward and O. M. Yaghi, *J. Am. Chem. Soc.*, 2005, **127**, 17998–17999.
56 J. M. Simmons, H. Wu, W. Zhou and T. Yildirim, *Energy Environ. Sci.*, 2011, **4**, 2177–2185.
57 C. Wang, P. Wang and L. Feng, *Transition Met. Chem.*, 2012, **37**, 225–234.
58 L.-B. Sun, J.-R. Li, W. Lu, Z.-Y. Gu, Z. Luo and H.-C. Zhou, *J. Am. Chem. Soc.*, 2012, **134**, 15923–15928.
59 Y. Xie, H. Yang, Z. U. Wang, Y. Liu, H.-C. Zhou and J.-R. Li, *Chem. Commun.*, 2014, **50**, 563–565.
60 H.-C. Zhou, J. R. Long and O. M. Yaghi, *Chem. Rev.*, 2012, **112**, 673–674.
61 C. G. Silva, A. Corma and H. García, *J. Mater. Chem.*, 2010, **20**, 3141–3156.
62 F. X. Llabrés i Xamena, A. Corma and H. Garcia, *J. Phys. Chem. C*, 2007, **111**, 80–85.
63 P. Mahata, G. Madras and S. Natarajan, *J. Phys. Chem. B*, 2006, **110**, 13759–13768.
64 J. Gascon, M. D. Hernández-Alonso, A. R. Almeida, G. P. van Klink, F. Kapteijn and G. Mul, *ChemSusChem*, 2008, **1**, 981–983.
65 S. Bordiga, C. Lamberti, G. Ricchiardi, L. Regli, F. Bonino, A. Damin, K.-P. Lillerud, M. Bjorgen and A. Zecchina, *Chem. Commun.*, 2004, 2300–2301.
66 T. Tachikawa, J. R. Choi, M. Fujitsuka and T. Majima, *J. Phys. Chem. C*, 2008, **112**, 14090–14101.
67 P. Mahata, G. Madras and S. Natarajan, *Catal. Lett.*, 2007, **115**, 27–32.
68 M. Alvaro, E. Carbonell, B. Ferrer, F. X. Llabrés i Xamena and H. Garcia, *Chem. - Eur. J.*, 2007, **13**, 5106–5112.
69 Y. Horiuchi, T. Toyao, M. Takeuchi, M. Matsuoka and M. Anpo, *Phys. Chem. Chem. Phys.*, 2013, **15**, 13243–13253.
70 T. Zhang and W. Lin, *Chem. Soc. Rev.*, 2014, DOI: 10.1039/c4cs00103f.
71 S. Li and Q. Xu, *Energy Environ. Sci.*, 2013, **6**, 1656–1683.
72 M. A. Nasalevich, M. van der Veen, F. Kapteijn and J. Gascon, *CrystEngComm*, 2014, **16**, 4919–4926.
73 T. Zhang and W. Lin, *Struct. Bonding*, 2014, **157**, 89–104.
74 H. Lin and P. A. Maggard, *Inorg. Chem.*, 2008, **47**, 8044–8052.
75 Z.-L. Liao, G.-D. Li, M.-H. Bi and J.-S. Chen, *Inorg. Chem.*, 2008, **47**, 4844–4853.
76 Z.-T. Yu, Z.-L. Liao, Y.-S. Jiang, G.-H. Li, G.-D. Li and J.-S. Chen, *Chem. Commun.*, 2004, 1814–1815.
77 Z. T. Yu, Z. L. Liao, Y. S. Jiang, G. H. Li and J. S. Chen, *Chem. - Eur. J.*, 2005, **11**, 2642–2650.
78 T. Toyao, M. Saito, Y. Horiuchi, K. Mochizuki, M. Iwata, H. Higashimura and M. Matsuoka, *Catal. Sci. Technol.*, 2013, **3**, 2092–2097.
79 M. Kurmoo, *Chem. Soc. Rev.*, 2009, **38**, 1353–1379.

80 P. Valvekens, F. Vermoortele and D. De Vos, *Catal. Sci. Technol.*, 2013, **3**, 1435–1445.
81 L. Ma and W. Lin, in *Functional Metal–Organic Frameworks: Gas Storage, Separation and Catalysis*, Springer, 2010, pp. 175–205.
82 P. Horcajada, T. Chalati, C. Serre, B. Gillet, C. Sebrie, T. Baati, J. F. Eubank, D. Heurtaux, P. Clayette and C. Kreuz, *Nat. Mater.*, 2009, **9**, 172–178.
83 P. Horcajada, C. Serre, M. Vallet-Regí, M. Sebban, F. Taulelle and G. Férey, *Angew. Chem.*, 2006, **118**, 6120–6124.
84 H.-L. Jiang, B. Liu, T. Akita, M. Haruta, H. Sakurai and Q. Xu, *J. Am. Chem. Soc.*, 2009, **131**, 11302–11303.
85 S. L. James, *Chem. Soc. Rev.*, 2003, **32**, 276–288.
86 U. Mueller, M. Schubert, F. Teich, H. Puetter, K. Schierle-Arndt and J. Pastre, *J. Mater. Chem.*, 2006, **16**, 626–636.
87 S.-Y. Song, X.-Z. Song, S.-N. Zhao, C. Qin, S.-Q. Su, M. Zhu, Z.-M. Hao and H.-J. Zhang, *Dalton Trans.*, 2012, **41**, 10412–10421.
88 L. Ai, C. Zhang, L. Li and J. Jiang, *Appl. Catal., B*, 2014, **148–149**, 191–200.
89 C.-F. Zhang, L.-G. Qiu, F. Ke, Y.-J. Zhu, Y.-P. Yuan, G.-S. Xu and X. Jiang, *J. Mater. Chem. A*, 2013, **1**, 14329–14334.
90 T. Wen and J. Zhang, *Chem. Commun.*, 2013, **49**, 5660–5662.
91 H. Yang, X.-W. He, F. Wang, Y. Kang and J. Zhang, *J. Mater. Chem.*, 2012, **22**, 21849–21851.
92 S. E.-d. H. Etaiw and M. M. El-bendary, *Appl. Catal., B*, 2012, **126**, 326–333.
93 M. C. Das, H. Xu, Z. Wang, G. Srinivas, W. Zhou, Y.-F. Yue, V. N. Nesterov, G. Qian and B. Chen, *Chem. Commun.*, 2011, **47**, 11715–11717.
94 L.-L. Wen, F. Wang, J. Feng, K.-L. Lv, C.-G. Wang and D.-F. Li, *Cryst. Growth Des.*, 2009, **9**, 3581–3589.
95 L. Wen, J. Zhao, K. Lv, Y. Wu, K. Deng, X. Leng and D. Li, *Cryst. Growth Des.*, 2012, **12**, 1603–1612.
96 W.-J. Ji, Q.-G. Zhai, S.-N. Li, Y.-C. Jiang and M.-C. Hu, *Inorg. Chem. Commun.*, 2012, **24**, 209–211.
97 W.-J. Ji, Q.-G. Zhai, S.-N. Li, Y.-C. Jiang and M.-C. Hu, *Inorg. Chem. Commun.*, 2013, **28**, 16–19.
98 Z.-Q. Li, M. Zhang, B. Liu, C.-Y. Guo and M. Zhou, *Inorg. Chem. Commun.*, 2013, **36**, 241–244.
99 W.-T. Xu, L. Ma, F. Ke, F.-M. Peng, G.-S. Xu, Y.-H. Shen, J.-F. Zhu, L.-G. Qiu and Y.-P. Yuan, *Dalton Trans.*, 2014, **43**, 3792–3798.
100 L. Zhou, C. Wang, X. Zheng, Z. Tian, L. Wen, H. Qu and D. Li, *Dalton Trans.*, 2013, **42**, 16375–16386.
101 J. Gao, J. Miao, P.-Z. Li, Y. Zhao and B. Liu, *Chem. Commun.*, 2014, **50**, 3786–3788.
102 Y.-L. Hou, R. W.-Y. Sun, X.-P. Zhou, J.-H. Wang and D. Li, *Chem. Commun.*, 2014, **50**, 2295–2297.
103 K. K. Bisht, Y. Rachuri, B. Parmar and E. Suresh, *RSC Adv.*, 2014, **4**, 7352–7360.
104 S.-M. Chen, Y.-F. Chen, R. Lin, X.-P. Lei and J. Zhang, *CrystEngComm*, 2013, **15**, 10423–10426.
105 Y.-P. Wu, D.-S. Li, Y.-P. Duan, L. Bai and J. Zhao, *Inorg. Chem. Commun.*, 2013, **36**, 137–140.
106 X.-P. Zheng, Y. Lu, H. Zhang, Z.-M. Zhang and E.-B. Wang, *Inorg. Chem. Commun.*, 2013, **33**, 29–32.
107 A. K. Paul, G. Madras and S. Natarajan, *Phys. Chem. Chem. Phys.*, 2009, **11**, 11285–11296.
108 J. Guo, J.-F. Ma, J.-J. Li, J. Yang and S.-X. Xing, *Cryst. Growth Des.*, 2012, **12**, 6074–6082.
109 F. Luo, Z.-Z. Yuan, X.-F. Feng, S. R. Batten, J.-Q. Li, M.-B. Luo, S.-J. Liu, W.-Y. Xu, G.-M. Sun and Y.-M. Song, *Cryst. Growth Des.*, 2012, **12**, 3392–3396.
110 P. Du, Y. Yang, Y.-Y. Liu, Y.-C. He, H.-M. Zhang and J.-F. Ma, *Polyhedron*, 2014, **70**, 180–187.
111 Y.-Q. Chen, S.-J. Liu, Y.-W. Li, G.-R. Li, K.-H. He, Y.-K. Qu, T.-L. Hu and X.-H. Bu, *Cryst. Growth Des.*, 2012, **12**, 5426–5431.
112 S. Zhou, Z.-G. Kong, Q.-W. Wang and C.-B. Li, *Inorg. Chem. Commun.*, 2012, **25**, 1–4.
113 C. Y. Zhang, W. X. Ma, M. Y. Wang, X. J. Yang and X. Y. Xu, *Spectrochim. Acta, Part A*, 2014, **118**, 657–662.
114 P. Mahata, G. Sankar, G. Madras and S. Natarajan, *Chem. Commun.*, 2005, 5787–5789.
115 Y. Gong, P.-G. Jiang, Y.-X. Wang, T. Wu and J.-H. Lin, *Dalton Trans.*, 2013, **42**, 7196–7203.
116 Y. Gong, T. Wu and J. Lin, *CrystEngComm*, 2012, **14**, 3727–3736.
117 L. Wen, L. Zhou, B. Zhang, X. Meng, H. Qu and D. Li, *J. Mater. Chem.*, 2012, **22**, 22603–22609.
118 X. Wang, J. Luan, H. Lin, C. Xu, G. Liu, J. Zhang and A. Tian, *CrystEngComm*, 2013, **15**, 9995–10006.
119 W.-Q. Kan, B. Liu, J. Yang, Y.-Y. Liu and J.-F. Ma, *Cryst. Growth Des.*, 2012, **12**, 2288–2298.
120 P. Du, Y. Yang, J. Yang, B.-K. Liu and J.-F. Ma, *Dalton Trans.*, 2013, **42**, 1567–1580.
121 H. Zhang, Y. Lu, Z.-m. Zhang and E.-b. Wang, *Inorg. Chem. Commun.*, 2012, **17**, 9–12.
122 A. K. Paul, R. Karthik and S. Natarajan, *Cryst. Growth Des.*, 2011, **11**, 5741–5749.
123 J. Guo, J. Yang, Y.-Y. Liu and J.-F. Ma, *CrystEngComm*, 2012, **14**, 6609–6617.
124 K. K. Bisht, Y. Rachuri, B. Parmar and E. Suresh, *J. Solid State Chem.*, 2014, **213**, 43–51.
125 X. Wang, J. Luan, F. Sui, H. Lin, G. Liu and C. Xu, *Cryst. Growth Des.*, 2013, **13**, 3561–3576.
126 T. Wen, D.-X. Zhang and J. Zhang, *Inorg. Chem.*, 2012, **52**, 12–14.
127 F. Wang, Z. S. Liu, H. Yang, Y. X. Tan and J. Zhang, *Angew. Chem., Int. Ed.*, 2011, **50**, 450–453.
128 H.-Y. Sun, C.-B. Liu, Y. Cong, M.-H. Yu, H.-Y. Bai and G.-B. Che, *Inorg. Chem. Commun.*, 2013, **35**, 130–134.
129 F. Wang, X. Ke, J. Zhao, K. Deng, X. Leng, Z. Tian, L. Wen and D. Li, *Dalton Trans.*, 2011, **40**, 11856–11865.
130 X. Wang, J. Luan, H. Lin, Q. Lu, C. Xu and G. Liu, *Dalton Trans.*, 2013, **42**, 8375–8386.
131 X.-L. Wang, J. Luan, H.-Y. Lin, G.-C. Liu and M. Le, *Polyhedron*, 2014, **71**, 111–118.
132 H. Qu, L. Qiu, X.-K. Leng, M.-M. Wang, S.-M. Lan, L.-L. Wen and D.-F. Li, *Inorg. Chem. Commun.*, 2011, **14**, 1347–1351.

133 X.-L. Wang, J. Luan, H.-Y. Lin, C. Xu and G.-C. Liu, *Inorg. Chim. Acta*, 2013, **408**, 139–144.
134 X. Zhu, S. Zhao, Y.-F. Peng, B.-L. Li and B. Wu, *CrystEngComm*, 2013, **15**, 9154–9160.
135 G.-H. Cui, C.-H. He, C.-H. Jiao, J.-C. Geng and V. A. Blatov, *CrystEngComm*, 2012, **14**, 4210–4216.
136 X. Li, J. Li, M.-K. Li and Z. Fei, *J. Mol. Struct.*, 2014, **1059**, 294–298.
137 X.-L. Wang, Y. Qu, G.-C. Liu, J. Luan, H.-Y. Lin and X.-M. Kan, *Inorg. Chim. Acta*, 2014, **412**, 104–113.
138 M. Wałęsa-Chorab, V. Patroniak, M. Kubicki, G. Kądziołka, J. Przepiórski and B. Michalkiewicz, *J. Catal.*, 2012, **291**, 1–8.
139 J.-W. Ran, S.-W. Liu, P. Wu and J. Pei, *Chin. Chem. Lett.*, 2013, **24**, 373–375.
140 C. Wang, H. Jing and P. Wang, *J. Mol. Struct.*, 2014, **1074**, 92–99.
141 H. Li, M. Eddaoudi, M. O'Keeffe and O. M. Yaghi, *Nature*, 1999, **402**, 276–279.
142 F. X. Llabrés i Xamena, P. Calza, C. Lamberti, C. Prestipino, A. Damin, S. Bordiga, E. Pelizzetti and A. Zecchina, *J. Am. Chem. Soc.*, 2003, **125**, 2264–2271.
143 P. Calza, C. Pazé, E. Pelizzetti and A. Zecchina, *Chem. Commun.*, 2001, 2130–2131.
144 C. Galindo, P. Jacques and A. Kalt, *J. Photochem. Photobiol., A*, 2000, **130**, 35–47.
145 J. M. Joseph, H. Destaillats, H.-M. Hung and M. R. Hoffmann, *J. Phys. Chem. A*, 2000, **104**, 301–307.
146 J. Saien and S. Khezrianjoo, *J. Hazard. Mater.*, 2008, **157**, 269–276.
147 K. Vasanth Kumar and A. Selvaganapathi, *Dyes Pigm.*, 2007, **75**, 246–249.
148 B. Krishnakumar and M. Swaminathan, *Spectrochim. Acta, Part A*, 2011, **81**, 739–744.
149 S. Bhattacharya and S. S. Mandal, *Chem. Commun.*, 1996, 1515–1516.
150 M. Saquib and M. Muneer, *Dyes Pigm.*, 2002, **53**, 237–249.
151 M. Stylidi, D. I. Kondarides and X. E. Verykios, *Appl. Catal., B*, 2003, **40**, 271–286.
152 T. Watanabe, T. Takizawa and K. Honda, *J. Phys. Chem.*, 1977, **81**, 1845–1851.
153 B. Civalleri, F. Napoli, Y. Noël, C. Roetti and R. Dovesi, *CrystEngComm*, 2006, **8**, 364–371.
154 Q. Xiao, Z. Si, J. Zhang, C. Xiao and X. Tan, *J. Hazard. Mater.*, 2008, **150**, 62–67.
155 J. Yu, W. Wang, B. Cheng and B.-L. Su, *J. Phys. Chem. C*, 2009, **113**, 6743–6750.
156 X. Yu, J. Yu, B. Cheng and M. Jaroniec, *J. Phys. Chem. C*, 2009, **113**, 17527–17535.
157 D.-E. Wang, K.-J. Deng, K.-L. Lv, C.-G. Wang, L.-L. Wen and D.-F. Li, *CrystEngComm*, 2009, **11**, 1442–1450.
158 Z. Sun, Y. Chen, Q. Ke, Y. Yang and J. Yuan, *J. Photochem. Photobiol., A*, 2002, **149**, 169–174.
159 Y. Liu and R. O. Claus, *J. Am. Chem. Soc.*, 1997, **119**, 5273–5274.
160 J. K. Barton and A. L. Raphael, *J. Am. Chem. Soc.*, 1984, **106**, 2466–2468.
161 S. Yan, Z. Li and Z. Zou, *Langmuir*, 2010, **26**, 3894–3901.
162 A. Syoufian and K. Nakashima, *J. Colloid Interface Sci.*, 2008, **317**, 507–512.
163 H.-Y. Shu, M.-C. Chang and H.-J. Fan, *J. Hazard. Mater.*, 2004, **113**, 201–208.
164 S. Zhang, X. Zhao, H. Niu, Y. Shi, Y. Cai and G. Jiang, *J. Hazard. Mater.*, 2009, **167**, 560–566.
165 Q. Jiang, A.-M. Spehar, M. Håkansson, J. Suomi, T. Ala-Kleme and S. Kulmala, *Electrochim. Acta*, 2006, **51**, 2706–2714.
166 R. Idel-aouad, M. Valiente, A. Yaacoubi, B. Tanouti and M. López-Mesas, *J. Hazard. Mater.*, 2011, **186**, 745–750.
167 M. Xia, M. Long, Y. Yang, C. Chen, W. Cai and B. Zhou, *Appl. Catal., B*, 2011, **110**, 118–125.
168 Q. Chen, P. Wu, Y. Li, N. Zhu and Z. Dang, *J. Hazard. Mater.*, 2009, **168**, 901–908.
169 C. Galindo, P. Jacques and A. Kalt, *J. Photochem. Photobiol., A*, 2001, **141**, 47–56.
170 C. Galindo and A. Kalt, *Dyes Pigm.*, 1999, **40**, 27–35.
171 M. Dan-Hardi, C. Serre, T. O. Frot, L. Rozes, G. Maurin, C. M. Sanchez and G. R. Férey, *J. Am. Chem. Soc.*, 2009, **131**, 10857–10859.
172 Y. Horiuchi, T. Toyao, M. Saito, K. Mochizuki, M. Iwata, H. Higashimura, M. Anpo and M. Matsuoka, *J. Phys. Chem. C*, 2012, **116**, 20848–20853.
173 C. H. Hendon, D. Tiana, M. Fontecave, C. Sanchez, L. D'arras, C. Sassoye, L. Rozes, C. Mellot-Draznieks and A. Walsh, *J. Am. Chem. Soc.*, 2013, **135**, 10942–10945.
174 Y. Fu, D. Sun, Y. Chen, R. Huang, Z. Ding, X. Fu and Z. Li, *Angew. Chem.*, 2012, **124**, 3420–3423.
175 M. A. Nasalevich, M. G. Goesten, T. J. Savenije, F. Kapteijn and J. Gascon, *Chem. Commun.*, 2013, **49**, 10575–10577.
176 L. Que and W. B. Tolman, *Nature*, 2008, **455**, 333–340.
177 S. Afzal, W. A. Daoud and S. J. Langford, *ACS Appl. Mater. Interfaces*, 2013, **5**, 4753–4759.
178 Y. Numata, S. P. Singh, A. Islam, M. Iwamura, A. Imai, K. Nozaki and L. Han, *Adv. Funct. Mater.*, 2013, **23**, 1817–1823.
179 M. Hussain, A. El-Shafei, A. Islam and L. Han, *Phys. Chem. Chem. Phys.*, 2013, **15**, 8401–8408.
180 Z. Lu, M. Shen and T. P. Yoon, *J. Am. Chem. Soc.*, 2011, **133**, 1162–1164.
181 C.-J. Wallentin, J. D. Nguyen, P. Finkbeiner and C. R. J. Stephenson, *J. Am. Chem. Soc.*, 2012, **134**, 8875–8884.
182 S. Zhang, L. Han, L. Li, J. Cheng, D. Yuan and J. Luo, *Cryst. Growth Des.*, 2013, **13**, 5466–5472.
183 Y. Wang, R. Shi, J. Lin and Y. Zhu, *Energy Environ. Sci.*, 2011, **4**, 2922–2929.
184 X. C. Huang, Y. Y. Lin, J. P. Zhang and X. M. Chen, *Angew. Chem.*, 2006, **118**, 1587–1589.
185 Y.-Q. Tian, Y.-M. Zhao, Z.-X. Chen, G.-N. Zhang, L.-H. Weng and D.-Y. Zhao, *Chem. - Eur. J.*, 2007, **13**, 4146–4154.
186 A. Phan, C. J. Doonan, F. J. Uribe-Romo, C. B. Knobler, M. O'keeffe and O. M. Yaghi, *Acc. Chem. Res.*, 2010, **43**, 58–67.
187 R. Banerjee, A. Phan, B. Wang, C. Knobler, H. Furukawa, M. O'Keeffe and O. M. Yaghi, *Science*, 2008, **319**, 939–943.

188 L. Zheng, Y. Xu, Y. Song, C. Wu, M. Zhang and Y. Xie, *Inorg. Chem.*, 2009, **48**, 4003–4009.
189 S. L. Castro, S. G. Bailey, R. P. Raffaelle, K. K. Banger and A. F. Hepp, *Chem. Mater.*, 2003, **15**, 3142–3147.
190 X.-C. Huang, J.-P. Zhang and X.-M. Chen, *J. Am. Chem. Soc.*, 2004, **126**, 13218–13219.
191 G. Liao, S. Chen, X. Quan, H. Yu and H. Zhao, *J. Mater. Chem.*, 2012, **22**, 2721–2726.
192 V. Štengl, D. Popelková and P. Vláčil, *J. Phys. Chem. C*, 2011, **115**, 25209–25218.
193 Y. Fu and X. Wang, *Ind. Eng. Chem. Res.*, 2011, **50**, 7210–7218.
194 Y. Fu, P. Xiong, H. Chen, X. Sun and X. Wang, *Ind. Eng. Chem. Res.*, 2011, **51**, 725–731.
195 C. Petit and T. J. Bandosz, *Adv. Mater.*, 2009, **21**, 4753–4757.
196 C. Petit and T. J. Bandosz, *Adv. Funct. Mater.*, 2011, **21**, 2108–2117.
197 Y. Zhang, G. Li, H. Lu, Q. Lv and Z. Sun, *RSC Adv.*, 2014, **4**, 7594–7600.
198 H. Ma, J. Shen, M. Shi, X. Lu, Z. Li, Y. Long, N. Li and M. Ye, *Appl. Catal., B*, 2012, **121**, 198–205.
199 Z.-H. Huang, G. Liu and F. Kang, *ACS Appl. Mater. Interfaces*, 2012, **4**, 4942–4947.
200 R. Kumar, K. Jayaramulu, T. K. Maji and C. Rao, *Chem. Commun.*, 2013, **49**, 4947–4949.
201 Y. Zhao, M. Seredych, Q. Zhong and T. J. Bandosz, *RSC Adv.*, 2013, **3**, 9932–9941.
202 M. Jahan, Q. Bao, J.-X. Yang and K. P. Loh, *J. Am. Chem. Soc.*, 2010, **132**, 14487–14495.
203 C. Petit, B. Levasseur, B. Mendoza and T. J. Bandosz, *Microporous Mesoporous Mater.*, 2012, **154**, 107–112.
204 R. Jin, Z. Bian, J. Li, M. Ding and L. Gao, *Dalton Trans.*, 2013, **42**, 3936–3940.
205 L. E. Kreno, J. T. Hupp and R. P. Van Duyne, *Anal. Chem.*, 2010, **82**, 8042–8046.
206 S. R. Venna and M. A. Carreon, *J. Am. Chem. Soc.*, 2009, **132**, 76–78.
207 D. Zacher, O. Shekhah, C. Woll and R. A. Fischer, *Chem. Soc. Rev.*, 2009, **38**, 1418–1429.
208 O. Shekhah, J. Liu, R. A. Fischer and C. Woll, *Chem. Soc. Rev.*, 2011, **40**, 1081–1106.
209 Y.-N. Hou, Y.-H. Xing, F.-Y. Bai, Q.-L. Guan, X. Wang, R. Zhang and Z. Shi, *Spectrochim. Acta, Part A*, 2014, **123**, 267–272.
210 Y. Xia, K.-X. Wang and J.-S. Chen, *Inorg. Chem. Commun.*, 2010, **13**, 1542–1547.
211 X.-y. Chen, Y.-p. Chen, Z.-m. Xia, H.-b. Hu, Y.-q. Sun and W.-y. Huang, *Dalton Trans.*, 2012, **41**, 10035–10042.
212 X.-L. Hao, Y.-Y. Ma, Y.-H. Wang, W.-Z. Zhou and Y.-G. Li, *Inorg. Chem. Commun.*, 2014, **41**, 19–24.
213 Y. Xu and C. H. Langford, *Langmuir*, 2001, **17**, 897–902.
214 Z. Xiong, Y. Xu, L. Zhu and J. Zhao, *Environ. Sci. Technol.*, 2005, **39**, 651–657.
215 M. Hu, Y. Xu and J. Zhao, *Langmuir*, 2004, **20**, 6302–6307.
216 A. C. Bean, S. M. Peper and T. E. Albrecht-Schmitt, *Chem. Mater.*, 2001, **13**, 1266–1272.
217 Z.-T. Yu, G.-H. Li, Y.-S. Jiang, J.-J. Xu and J.-S. Chen, *Dalton Trans.*, 2003, 4219–4220.
218 W. Chen, H.-M. Yuan, J.-Y. Wang, Z.-Y. Liu, J.-J. Xu, M. Yang and J.-S. Chen, *J. Am. Chem. Soc.*, 2003, **125**, 9266–9267.
219 S. Horikoshi, A. Saitou, H. Hidaka and N. Serpone, *Environ. Sci. Technol.*, 2003, **37**, 5813–5822.
220 Y. Guo, C. Hu, C. Jiang, Y. Yang, S. Jiang, X. Li and E. Wang, *J. Catal.*, 2003, **217**, 141–151.
221 W. D. Jones, *Acc. Chem. Res.*, 2003, **36**, 140–146.
222 D. A. Nivens, Y. Zhang and S. M. Angel, *J. Photochem. Photobiol., A*, 2002, **152**, 167–173.
223 V. A. Volkovich, T. R. Griffiths, D. J. Fray and R. C. Thied, *Phys. Chem. Chem. Phys.*, 2001, **3**, 5182–5191.
224 P. M. Almond and T. E. Albrecht-Schmitt, *Inorg. Chem.*, 2002, **41**, 1177–1183.
225 R. S. Addleman, M. Carrott, C. M. Wai, T. E. Carleson and B. Wenclawiak, *Anal. Chem.*, 2001, **73**, 1112–1119.
226 J. Huang, X. Wang and A. J. Jacobson, *J. Mater. Chem.*, 2003, **13**, 191–196.
227 M. J. Sarsfield and M. Helliwell, *J. Am. Chem. Soc.*, 2004, **126**, 1036–1037.
228 Q.-Y. Chen, Q.-H. Luo, Z.-L. Wang and J.-T. Chen, *Chem. Commun.*, 2000, 1033–1034.
229 B. Zhao, P. Cheng, Y. Dai, C. Cheng, D. Z. Liao, S. P. Yan, Z. H. Jiang and G. L. Wang, *Angew. Chem., Int. Ed.*, 2003, **42**, 934–936.
230 M. B. Fleisher, K. C. Waterman, N. J. Turro and J. K. Barton, *Inorg. Chem.*, 1986, **25**, 3549–3551.
231 S. Moghaddas, P. Hendry, R. J. Geue, C. Qin, A. M. Bygott, A. M. Sargeson and N. E. Dixon, *J. Chem. Soc., Dalton Trans.*, 2000, 2085–2089.
232 J.-L. Wang, C. Wang and W. Lin, *ACS Catal.*, 2012, **2**, 2630–2640.
233 J.-Q. Sha, J.-W. Sun, C. Wang, G.-M. Li, P.-F. Yan, M.-T. Li and M.-Y. Liu, *CrystEngComm*, 2012, **14**, 5053–5064.
234 Y. Liu, X. Lin, G. Liu, J. Ying and A. Tian, *J. Inorg. Organomet. Polym. Mater.*, 2012, **22**, 946–951.
235 C.-H. Li, K.-L. Huang, Y.-N. Chi, X. Liu, Z.-G. Han, L. Shen and C.-W. Hu, *Inorg. Chem.*, 2009, **48**, 2010–2017.
236 X. Zhao, D. Liang, S. Liu, C. Sun, R. Cao, C. Gao, Y. Ren and Z. Su, *Inorg. Chem.*, 2008, **47**, 7133–7138.
237 Y.-Q. Lan, S.-L. Li, X.-L. Wang, K.-Z. Shao, D.-Y. Du, H.-Y. Zang and Z.-M. Su, *Inorg. Chem.*, 2008, **47**, 8179–8187.
238 B. Liu, J. Yang, G. C. Yang and J. F. Ma, *Inorg. Chem.*, 2013, **52**, 84–94.
239 Y. Guo, Y. Wang, C. Hu, Y. Wang, E. Wang, Y. Zhou and S. Feng, *Chem. Mater.*, 2000, **12**, 3501–3508.
240 B. Nohra, H. El Moll, L. M. Rodriguez Albelo, P. Mialane, J. Marrot, C. Mellot-Draznieks, M. O'Keeffe, R. Ngo Biboum, J. Lemaire and B. Keita, *J. Am. Chem. Soc.*, 2011, **133**, 13363–13374.
241 Y. Hu, F. Luo and F. Dong, *Chem. Commun.*, 2011, **47**, 761–763.
242 A. Mylonas and E. Papaconstantinou, *J. Photochem. Photobiol., A*, 1996, **94**, 77–82.
243 L. Ni, J. Ni, Y. Lv, P. Yang and Y. Cao, *Chem. Commun.*, 2009, 2171–2173.

244 Y.-Q. Lan, S.-L. Li, X.-L. Wang, K.-Z. Shao, D.-Y. Du, H.-Y. Zang and Z.-M. Su, *Inorg. Chem.*, 2008, **47**, 8179–8187.
245 W.-Q. Kan, J. Yang, Y.-Y. Liu and J.-F. Ma, *Dalton Trans.*, 2012, **41**, 11062–11073.
246 W. Wang, J. Yang, W.-Q. Kan and J.-F. Ma, *CrystEngComm*, 2013, **15**, 5844–5852.
247 Z. Zhang, J. Yang, Y.-Y. Liu and J.-F. Ma, *CrystEngComm*, 2013, **15**, 3843–3853.
248 Y. G. Chen, K. Liu, F. X. Meng and Y. Sun, *Synth. React. Inorg. Met.-Org. Chem.*, 2007, **37**, 179–184.
249 B. Liu, Z.-T. Yu, J. Yang, W. Hua, Y.-Y. Liu and J.-F. Ma, *Inorg. Chem.*, 2011, **50**, 8967–8972.
250 Z. Zhang, J. Yang, Y.-Y. Liu and J.-F. Ma, *CrystEngComm*, 2013, **15**, 3843.
251 Y.-G. Chen, K. Liu, F.-X. Meng and Y. Sun, *Synth. React. Inorg. Met.-Org. Chem.*, 2007, **37**, 179–184.
252 H. Yang, T. Liu, M. Cao, H. Li, S. Gao and R. Cao, *Chem. Commun.*, 2010, **46**, 2429–2431.
253 X. Gan, X. Hu, Z. Shi and Y. Yin, *J. Coord. Chem.*, 2013, **66**, 2930–2939.
254 D. Shi, A. Ren, C. Liu, H. Bai, G. Che, H. Sun and R. Cong, *Chin. J. Inorg. Chem.*, 2013, **29**, 2649–2654.
255 J.-X. Meng, Y.-G. Li, H. Fu, X.-L. Wang and E.-B. Wang, *CrystEngComm*, 2011, **13**, 649–655.
256 J.-X. Meng, Y. Lu, Y.-G. Li, H. Fu and E.-B. Wang, *CrystEngComm*, 2011, **13**, 2479–2486.
257 C. Wang, Z. Xie, K. E. deKrafft and W. Lin, *J. Am. Chem. Soc.*, 2011, **133**, 13445–13454.
258 Q. Lan, J. Zhang, Z.-M. Zhang, Y. Lu and E.-B. Wang, *Dalton Trans.*, 2013, **42**, 16602–16607.
259 H.-Y. Liu, L. Bo, J. Yang, Y.-Y. Liu, J.-F. Ma and H. Wu, *Dalton Trans.*, 2011, **40**, 9782–9788.
260 A. Tian, X. Lin, X. Liu, J. Ying and X. Wang, *RSC Adv.*, 2013, **3**, 17188–17194.
261 X. Wang, D. Zhao, A. Tian and J. Ying, *Dalton Trans.*, 2014, **43**, 5211–5220.
262 J.-L. Wang, C. Wang and W. Lin, *ACS Catal.*, 2012, **2**, 2630–2640.
263 J.-Q. Sha, J.-W. Sun, M.-T. Li, C. Wang, G.-M. Li, P.-F. Yan and L.-J. Sun, *Dalton Trans.*, 2013, **42**, 1667–1677.
264 J. Sun, M. Li, J. Sha, P. Yan, C. Wang, S. Li and Y. Pan, *CrystEngComm*, 2013, **15**, 10584–10589.
265 X. Wang, N. Li, A. Tian, J. Ying, G. Liu, H. Lin, J. Zhang and Y. Yang, *Dalton Trans.*, 2013, **42**, 14856–14865.
266 X. Wang, X. Liu, A. Tian, J. Ying, H. Lin, G. Liu and Q. Gao, *Dalton Trans.*, 2012, **41**, 9587–9589.
267 Z. Fu, Y. Zeng, X. Liu, D. Song, S. Liao and J. Dai, *Chem. Commun.*, 2012, **48**, 6154–6156.
268 H.-J. Pang, H.-Y. Ma, J. Peng, C.-J. Zhang, P.-P. Zhang and Z.-M. Su, *CrystEngComm*, 2011, **13**, 7079–7085.
269 X. Wang, Y. Wang, G. Liu, A. Tian, J. Zhang and H. Lin, *Dalton Trans.*, 2011, **40**, 9299–9305.
270 Y. Ding, J.-X. Meng, W.-L. Chen and E.-B. Wang, *CrystEngComm*, 2011, **13**, 2687–2692.
271 Q. Wu, W.-L. Chen, D. Liu, C. Liang, Y.-G. Li, S.-W. Lin and E. Wang, *Dalton Trans.*, 2011, **40**, 56–61.
272 H. Fu, Y. Li, Y. Lu, W. Chen, Q. Wu, J. Meng, X. Wang, Z. Zhang and E. Wang, *Cryst. Growth Des.*, 2011, **11**, 458–465.
273 X.-L. Wang, Q. Gao, A.-X. Tian and G.-C. Liu, *Cryst. Growth Des.*, 2012, **12**, 2346–2354.
274 X. Wang, M.-M. Zhang, X.-L. Hao, Y.-H. Wang, Y. Wei, F.-S. Liang, L.-J. Xu and Y.-G. Li, *Cryst. Growth Des.*, 2013, **13**, 3454–3462.
275 W.-Q. Kan, B. Liu, J. Yang, Y.-Y. Liu and J.-F. Ma, *Cryst. Growth Des.*, 2012, **12**, 2288–2298.
276 Y. Yu, H. Pang, H. Ma, Y. Song and K. Wang, *J. Cluster Sci.*, 2013, **24**, 17–29.
277 X.-L. Wang, D. Zhao and A.-X. Tian, *J. Cluster Sci.*, 2013, **24**, 259–271.
278 S. Lin, Q. Wu, H. Tan and E. Wang, *J. Coord. Chem.*, 2011, **64**, 3661–3669.
279 W.-N. Li, F. Lin, X.-X. Li, L.-C. Zhang, W.-S. You and Z.-X. Jiang, *J. Coord. Chem.*, 2013, **66**, 2829–2842.
280 W.-Q. Kan, J.-M. Xu, Y.-H. Kan, J. Guo and S.-Z. Wen, *J. Coord. Chem.*, 2014, **67**, 195–214.
281 D. Shi, Z. Wang, J. Xing, Y. Li, J. Luo, L. Chen and J. Zhao, *Synth. React. Inorg. Met.-Org. Chem.*, 2012, **42**, 30–36.
282 Y. Zhong, H. Fu, J. Meng and E. Wang, *J. Coord. Chem.*, 2010, **63**, 26–35.
283 X. Wang, N. Han, H. Lin, J. Luan, A. Tian and D. Liu, *Inorg. Chem. Commun.*, 2014, **42**, 10–14.
284 H. Chen, H. An, X. Liu, H. Wang, Z. Chen, H. Zhang and Y. Hu, *Inorg. Chem. Commun.*, 2012, **21**, 65–68.
285 Y.-Q. Jiao, C. Qin, C.-Y. Sun, K.-Z. Shao, P.-J. Liu, P. Huang, K. Zhou and Z.-M. Su, *Inorg. Chem. Commun.*, 2012, **20**, 273–276.
286 H. Lin, C. Xu, X. Wang, Z. Chang, A. Tian, G. Liu and J. Zhang, *Inorg. Chem. Commun.*, 2013, **36**, 81–85.
287 N. Wu, Y. Qin, X.-L. Wang, C. Qin and E.-B. Wang, *Inorg. Chem. Commun.*, 2013, **37**, 174–177.
288 X. Meng, H.-N. Wang, G.-S. Yang, S. Wang, X.-L. Wang, K.-Z. Shao and Z.-M. Su, *Inorg. Chem. Commun.*, 2011, **14**, 1418–1421.
289 X.-L. Wang, Z.-H. Chang, H.-Y. Lin, G.-C. Liu, C. Xu, J. Luan, A.-X. Tian and J.-W. Zhang, *Inorg. Chim. Acta*, 2014, **413**, 16–22.
290 Y. Zhou, L. Zhang, X. Li and W. Ahmad, *J. Mol. Struct.*, 2013, **1049**, 212–219.
291 X.-L. Wang, N. Li, A.-X. Tian, J. Ying, D. Zhao and X.-J. Liu, *Inorg. Chem. Commun.*, 2012, **25**, 60–64.
292 X. Chen, S. Lin, L. Chen, X. Chen, C. Liu, J. Chen and L. Yang, *Inorg. Chem. Commun.*, 2007, **10**, 1285–1288.
293 X.-Y. Yu, X.-B. Cui, J. Lu, Y.-H. Luo, H. Zhang and W.-P. Gao, *J. Solid State Chem.*, 2014, **209**, 97–104.
294 X. Zhao, J. Yan, X. Xue, Z. Han, S. Cui, L. Zong, D. Zheng, C. Shen, H. Yu and X. Zhai, *Inorg. Chim. Acta*, 2014, **414**, 46–52.
295 J. Guo, J. Yang, Y.-Y. Liu and J.-F. Ma, *Inorg. Chim. Acta*, 2013, **400**, 51–58.
296 C.-H. Li, K.-L. Huang, Y.-N. Chi, X. Liu, Z.-G. Han, L. Shen and C.-W. Hu, *Inorg. Chem.*, 2009, **48**, 2010–2017.

297 Y. Guo and C. Hu, *J. Mol. Catal. A: Chem.*, 2007, **262**, 136–148.
298 Z. Zhang, J. Yang, Y.-Y. Liu and J.-F. Ma, *CrystEngComm*, 2013, **15**, 3843–3853.
299 M. A. AlDamen, J. M. Clemente-Juan, E. Coronado, C. Martí-Gastaldo and A. Gaita-Arino, *J. Am. Chem. Soc.*, 2008, **130**, 8874–8875.
300 J. Jing, B. P. Burton-Pye, L. C. Francesconi and M. R. Antonio, *Inorg. Chem.*, 2008, **47**, 6889–6899.
301 T. Devic, C. Serre, N. Audebrand, J. Marrot and G. Férey, *J. Am. Chem. Soc.*, 2005, **127**, 12788–12789.
302 S. Mahapatra, G. Madras and T. G. Row, *J. Phys. Chem. C*, 2007, **111**, 6505–6511.
303 G. Mele, E. Garcìa-Lòpez, L. Palmisano, G. Dyrda and R. Slota, *J. Phys. Chem. C*, 2007, **111**, 6581–6588.
304 J. Xu, Y. Ao, D. Fu and C. Yuan, *J. Hazard. Mater.*, 2009, **164**, 762–768.
305 A. L. Linsebigler, G. Lu and J. T. Yates Jr, *Chem. Rev.*, 1995, **95**, 735–758.
306 K. Wang, D. Zhang, J. Ma, P. Ma, J. Niu and J. Wang, *CrystEngComm*, 2012, **14**, 3205–3212.
307 J. Niu, S. Zhang, H. Chen, J. Zhao, P. Ma and J. Wang, *Cryst. Growth Des.*, 2011, **11**, 3769–3777.
308 T. Zhou, Y. Du, A. Borgna, J. Hong, Y. Wang, J. Han, W. Zhang and R. Xu, *Energy Environ. Sci.*, 2013, **6**, 3229–3234.
309 Y. Horiuchi, T. Toyao, M. Saito, K. Mochizuki, M. Iwata, H. Higashimura, M. Anpo and M. Matsuoka, *J. Phys. Chem. C*, 2012, **116**, 20848–20853.
310 K. G. Laurier, F. Vermoortele, R. Ameloot, D. E. De Vos, J. Hofkens and M. B. Roeffaers, *J. Am. Chem. Soc.*, 2013, **135**, 14488–14491.
311 T. T. Isimjan, H. Kazemian, S. Rohani and A. K. Ray, *J. Mater. Chem.*, 2010, **20**, 10241–10245.
312 C. Wang, D. Liu and W. Lin, *J. Am. Chem. Soc.*, 2013, **135**, 13222–13234.
313 F. X. Llabres i Xamena, A. Abad, A. Corma and H. Garcia, *J. Catal.*, 2007, **250**, 294–298.
314 H. A. Lopez, A. Dhakshinamoorthy, B. Ferrer, P. Atienzar, M. Alvaro and H. Garcia, *J. Phys. Chem. C*, 2011, **115**, 22200–22206.
315 A. Pichon, *Nature*, 2009, DOI: 10.1038/nchina.2009.1124.
316 C. G. Carson, K. Hardcastle, J. Schwartz, X. Liu, C. Hoffmann, R. A. Gerhardt and R. Tannenbaum, *Eur. J. Inorg. Chem.*, 2009, **2009**, 2338–2343.
317 J. J. Low, A. I. Benin, P. Jakubczak, J. F. Abrahamian, S. A. Faheem and R. R. Willis, *J. Am. Chem. Soc.*, 2009, **131**, 15834–15842.